



METHODS FOR PROGNOSTICS AND RELIABILITY IN COMPOSITE MATERIALS USING STRUCTURAL HEALTH MONITORING

BY:

Manuel Chiachío Ruano

A THESIS SUBMITTED IN PARTIAL FULFILLMENT OF THE REQUIREMENTS FOR
THE DEGREE OF
DOCTOR OF PHILOSOPHY

ADVISOR:

Dr. Guillermo Rus Carlborg

Department of Structural Mechanics & Hydraulic Engineering ,
University of Granada
Granada (Spain)

October 2014

Editor: Editorial de la Universidad de Granada
Autor: Manuel Chiachío Ruano
D.L.: GR 2221-2014
ISBN: 978-84-9083-294-3

**METHODS FOR PROGNOSTICS AND RELIABILITY IN COMPOSITE
MATERIALS USING STRUCTURAL HEALTH MONITORING**

Copyright © 2014 by Manuel Chiachío Ruano

El doctorando Manuel Chiachio Ruano y el director de la tesis Dr. Guillermo Rus Carlborg, garantizamos, al firmar esta tesis doctoral, que el trabajo ha sido realizado por el doctorando bajo la dirección del director de la tesis y hasta donde nuestro conocimiento alcanza, en la realización del trabajo, se han respetado los derechos de otros autores a ser citados, cuando se han utilizado sus resultados o publicaciones.

En Granada, a 19 de Septiembre de 2014,

Director de la Tesis

A handwritten signature in black ink, appearing to read 'Guillermo Rus Carlborg', with a long horizontal stroke extending to the right.

Fdo.: GUILLERMO RUS CARLBORG

El Doctorando

A handwritten signature in black ink, appearing to read 'Manuel Chiachio Ruano', with a long horizontal stroke extending to the right.

Fdo.: MANUEL CHIACHIO RUANO

Summary

The increasing use of composite materials in lightweight structures like aircraft or spacecraft structures, drastically increases their susceptibility to fatigue damage during their service life. Fatigue damage in composite materials is well-known to be hard to detect and difficult to predict mainly due to uncertainty that comes not only from modeling and measurement errors, but also from the lack of knowledge about the underlying physics of the damage process. This uncertainty can increase dramatically when dealing with full-scale composite structures in real environments, hence it becomes usually a critical issue for reliability and competitiveness of composite structures. Within this scenario, a prognostics system that is capable of assessing the structural integrity and predicting the remaining serviceability of critical components is of key importance for making composites competitive.

Prognostics is a core element in health management sciences, which aims to actively monitor and manage assets by predicting their lifetime through estimations of their future state of health based on knowledge about of the current state. Within the prognostics, damage prognosis has emerged over the recent years as a relevant research area which is increasingly gaining interest for its direct impact on safety and cost of high-responsibility structures and mechanisms. In this sense, damage prognosis is specially relevant for composite materials given that most of their applications are characterized by their difficulty, if not impossibility, of inspection and maintenance (e.g. spacecrafts, civil and industrial off-shore facilities, etc).

This thesis is aimed to report a new prognostics procedure to obtain predictive information about the *remaining useful life* and *end of life* of composite materials under fatigue degradation using real-world structural health monitoring data. To this end, degradation phenomena such as stiffness reduction and increase in matrix micro-cracks density are predicted by connecting micro-scale

and macro-scale damage models in a Bayesian filtering framework that allows the sequential assessment of the current damage state using damage data from structural health monitoring sensors. The estimated damage state is further propagated forward in time by simulating the models in absence of new data. The proposed framework allows incorporating various uncertainties in the prediction that are generally associated with material defects, unknown future inputs, sensing noise and modeling errors. The information stemming from the predictions is further used in an operational context to quantify the long-term reliability, and by extent, to predict the system failure probability. In this context, a new method is proposed for the estimation of the remaining useful life as a probability from the prediction of the long-term reliability, whose validity is formally proven using the axioms of Probability Logic.

This thesis also provides a novel prognostics algorithm, which achieves efficiency by employing Subset Simulation method as core engine for making simulations of future states. It has been named PFP-SubSim algorithm on behalf of the full denomination of the computational framework, namely, *particle-filter based prognostics based on Subset Simulation*. Following some theoretical development, it is demonstrated that PFP-SubSim algorithm is highly efficient for prognostics involving rare-events while maintaining a moderate computational cost.

The methodological contributions are demonstrated on run-to-failure data collected from a tension-tension fatigue experiment that includes measurements of the evolution of fatigue damage in carbon-fiber-reinforced polymer cross-ply laminates. Structural health monitoring is accomplished through Lamb wave-based active interrogation sensors together with a set of strain-gauges for measuring stiffness reduction. The data used in this thesis correspond to an open-access dataset distributed by the NASA Ames Prognostics Data Repository. Pseudocode implementations of the algorithms and methods developed for prognostics and reliability are specified and detailed to help the reader understand and implement these methods for further applications.

Throughout this thesis, the term *prediction* is used with the meaning of forecasting, i.e. anticipating any future outcome of the system using the most up-to-date information available. Since many other areas of science and engineering also adopt this term to actually denote *simulation or inference*, it is opportune to indicate this dissimilarity here for such an ubiquitous term for this work.

Resumen

El creciente uso de materiales compuestos en estructuras ligeras, como las estructuras aeroespaciales, ha propiciado que el daño por fatiga sea una de las fuentes de degradación a considerar durante la vida útil. El daño por fatiga en materiales compuestos es bien conocido por ser difícil de detectar y predecir, debido principalmente a la incertidumbre que proviene no sólo de los errores de medición y modelización, sino también de la falta de conocimiento sobre la física subyacente del proceso de daño por fatiga. Esta incertidumbre puede aumentar drásticamente cuando se trata de estructuras de materiales compuestos a escala real expuestas a cargas ambientales, lo que supone un asunto crítico para la fiabilidad y competitividad de dichas estructuras. En este escenario es de crucial importancia la disposición de un sistema de pronóstico que sea capaz de evaluar la integridad estructural y de predecir la vida remanente de los componentes críticos.

El pronóstico constituye un elemento central en las ciencias de gestión de la salud estructural teniendo como objetivo la gestión de activos mediante la predicción de su vida remanente. Esto es llevado a cabo mediante predicciones de los estados futuros de salud del sistema basadas en información actualizada de forma activa por la monitorización. Dentro de la materia de pronóstico, el pronóstico de daño está ganando cada vez mayores cuotas de interés por su impacto directo en la seguridad y viabilidad de estructuras de alta responsabilidad. En este sentido, el pronóstico de daño es especialmente relevante para estructuras de materiales compuestos debido a su dificultad, si no imposibilidad, de inspección y mantenimiento de dichas estructuras (por ejemplo, estructuras aeroespaciales, instalaciones off-shore, etc).

Esta tesis tiene como objetivo proporcionar un nuevo procedimiento de pronóstico para obtener información predictiva sobre la *vida remanente* y el *final de la vida útil* en materiales compuestos ante cargas de fatiga, utilizando datos reales procedentes de la monitorización de salud estructural. Con tal fin, fenómenos

de degradación tales como la reducción de la rigidez y el aumento de densidad de micro-fisuras en la matriz polimérica, son predichos mediante la conexión de modelos de daño a distinta escala dentro de un marco Bayesiano de filtrado de estados que permite la evaluación secuencial del daño actual utilizando datos procedentes de los sensores. La estimación del estado de daño es propagada en el tiempo mediante simulación en ausencia de nuevos datos. El marco propuesto permite la incorporación de diversas fuentes de incertidumbre en la predicción que generalmente se asocian a defectos del material, desconocimiento de valores futuros de variables aleatorias, ruido de sensores y errores de modelización. La información derivada de las predicciones se utiliza posteriormente en un contexto operacional para cuantificar la fiabilidad a largo plazo, y por extensión, para predecir la probabilidad de fallo del sistema. En este contexto, se propone un nuevo método para la estimación de la vida remanente como una probabilidad a partir de la predicción de la fiabilidad a largo plazo, y cuya validez se ha demostrado formalmente mediante el uso de los axiomas de la Probabilidad Lógica.

Esta tesis también proporciona un nuevo algoritmo de pronóstico, que consigue su eficiencia mediante el empleo del método de simulación "Subset". Este método es usado como motor principal de simulación para la obtención de los estados futuros de daño. El algoritmo ha sido denominado PFP-Subsim en base a su denominación completa, *pronóstico basado en filtros de partículas mediante simulación "Subset"*. Tras ciertos desarrollos teóricos, se demuestra que el algoritmo PFP-Subsim es altamente eficiente para pronóstico general de eventos raros, en el sentido de improbables, a la vez que mantiene un coste computacional moderado. Los ejemplos numéricos también corroboran la eficacia del algoritmo PFP-Subsim para el pronóstico de daño en materiales compuestos de fibra de carbono sometidos a cargas de fatiga.

Las contribuciones metodológicas reseñadas anteriormente son demostradas con datos de degradación hasta el fallo obtenidos mediante un experimento de fatiga de tipo tensión cíclica que incluye mediciones de series de evolución de daño por fatiga en composites tipo "cross-ply" de fibra de carbono. La monitorización de la salud estructural se obtiene a través de sensores de ondas Lamb, para medir el daño interno, junto con galgas extensométricas para medir la reducción de rigidez. Los datos de daño por fatiga utilizados en esta tesis provienen de un repositorio de libre acceso distribuido por la NASA. La implementación de los algoritmos así como los métodos desarrollados para pronóstico y fiabilidad

son especificados en detalle con objeto de facilitar su extensión a otras aplicaciones.

A lo largo de esta tesis, el término *predicción* es usado con el significado de previsión, es decir anticipar cualquier resultado futuro usando la información disponible más actualizada. Dado que este término es usado frecuentemente en otras áreas de la ciencia e ingeniería para referirse al concepto de *simulación* o *inferencia*, es oportuno indicar aquí esta puntualización en el contexto de este trabajo.

Acknowledgments

I would like to thank the responsible for the direction of my thesis, Dr. Guillermo Rus Carlborg, who is the head of the Nondestructive Evaluation Laboratory, Department of Structural Mechanics and Hydraulic Engineering. His philosophical thinking has influenced my work throughout this time. I couldn't forget to my friends and colleges of the Non Destructive Evaluation Laboratory. There have been a lot of enjoyable moments in the collaborations and I have learned much from them.

I would like to thank to the director of the Department of Structural Mechanics and Hydraulics Engineering, Dr. Fco. Javier Suárez for his help and advice and also thanks to all my colleges of the Department of Structural Mechanics for their generosity.

I need to express my sincere gratitude to my family. I'm in debt with them for the comprehension I receive for my Phd. work.

This work has been supported by the Ministry of Education of Spain through FPU grant no. P2009-2390. I would like to thank the Spanish Ministry of Economy for project DPI2010-17065, and Junta de Andalucía for project GGI3000IDIB, whose funding allowed me to take part into numerous international conferences.

Abbreviations

ANN	Artificial neuronal networks
CDF	Cumulative distribution function
CFRP	Carbon fiber reinforced polymers
COD	Crack opening displacement
CPU	Central processing unit
EDW	Edgeworth expansion method
EOL	End of life
ERR	Energy release rate
ESS	Effective sample size
FEA	Finite element analysis
FORM	First order reliability method
FPI	Fast probability integration
GD	Global delamination
IS	Importance sampling
LD	Local delamination
LSF	Limit state function
MC	Monte Carlo
MCMC	Markov Chain Monte Carlo
MH	Metropolis-Hastings
MMA	Modified Metropolis algorithm
MPP	Most probable point
PDF	Probability density function
PF	Particle filters
PFP-SubSim	Particle filter based prognostics based on Subset Simulation
PH	Prognostics horizon
PHM	Prognostics and Health Management
PMCMC	Particle Markov Chain Monte Carlo
PMIE	Principle of maximum information entropy

PRS	Pearson's semi-empirical distribution
PZT	Lead zirconate titanate
RSM	Response surface method
RUL	Remaining useful life
SFEM	Stochastic finite element modeling
SHM	Structural health monitoring
SIR	Systematic importance resampling
SIS	Sequential importance sampling
SORM	Second order reliability method
SS	Subset Simulation
SSFEM	Spectral stochastic finite element modeling
TC	Transverse cracking

List of Symbols

Symbol	Description
A	Modified Paris' Law constant
\mathbf{A}^*	Laminate stiffness matrix
\mathbf{A}^k	Stiffness matrix of k -th cracked ply (COD method)
\mathbf{a}^*	Laminate compliance matrix
\mathbf{a}_{ij}^*	(i, j) -th element of \mathbf{a}^*
b	Threshold level
b_j	Threshold level at j -th Subset simulation level
d	Dimension of \mathbf{z}
\mathbb{E}	Mathematical expectation
\mathbb{E}_{f_z}	Expectation using samples from $f_z(\mathbf{z})$
\mathbb{E}_{i_z}	Expectation using samples from $i_z(\mathbf{z})$
EOL_n	End of life predicted at time n
$f_z(\mathbf{z} \bar{\mathcal{U}})$	Probability density function of \mathbf{z} conditional on $\bar{\mathcal{U}}$
$f_z(\mathbf{z})$	Probability density function of \mathbf{z}
$F_z(\mathbf{z})$	Cumulative distribution function of \mathbf{z}
$F(g)$	Cumulative distribution function of $g(\mathbf{z}) \leq 0$
$FRUL_n$	Distribution of RUL predicted at time n
$f_{\chi_{n-1}^2}$	chi-square density function with n degrees of freedom
$g_z(\mathbf{z})$	Probability density function of \mathbf{z}
$g(\mathbf{z})$	Performance function
$h(\mathbf{z})$	Quantity of interest as a function of \mathbf{z}
\bar{h}	Sample mean of h
$i_z(\mathbf{z})$	Importance density of \mathbf{z}
$\mathbb{I}_{\bar{\mathcal{U}}}(\mathbf{z})$	Indicator function for \mathbf{z}
J	Result of the probability integral of $h(\mathbf{z})$
\tilde{J}_{IS}	Importance sampling estimator for J
\tilde{J}_{MC}	Monte Carlo estimator for J
\tilde{J}_{MCMC}	Markov Chain Monte Carlo estimator for J
\tilde{J}_{SS}	Subset simulation estimator for J
l	Half-crack spacing
\bar{l}	Normalized half-crack spacing
ℓ	Additive step index for prognostics
n	Sample index
n_u	Length of \mathbf{u}
n_v	Length of \mathbf{v}

Symbol	Description
n_w	Length of \mathbf{w}
n_x	Dimension of \mathcal{X}
n_y	Length of \mathbf{y}
n_θ	Dimension of Θ
N	Total amount of samples
N_s	Length of Markov Chains used in Subset simulation
N_c	Number of Markov Chains used in Subset simulation
N_T	Total amount of samples in Subset simulation
P_j^*	Scaling constant to control convergence to RMAD_j^*
P_0	Conditional probability for Subset Simulation
P_f	Failure probability (general)
$\bar{P}(\bar{U})$	System failure probability (normalizing constant)
$q(\mathbf{z}^{(\xi)} \cdot)$	Proposal distribution for $\mathbf{z}^{(\xi)}$
$\bar{\mathbf{Q}}^{(\phi)}$	Stiffness matrix of the outer $\left[\phi \frac{n_\phi}{2}\right]$ -sub-laminates
$\bar{\mathbf{Q}}^{(90)}$	Stiffness matrix of the outer $90_{n_{90}}$ -sub-laminates
r	radius of curvature
R	Reliability
RMAD_j^*	Target RMAD for $p(\theta_{n,j} y_{0:n})$
$R_{n+\ell n}$	ℓ -step ahead predicted reliability given information up to time n
$R_{n n}$	Updated estimation of reliability up to time n
$R^{(\tau)}$	Autocovariance of $h(\mathbf{z})$ at lag τ
$R_j^{(\tau)}$	Autocovariance of $h(\mathbf{z}_j)$ at lag τ for j th Subset simulation level
RUL_n	Remaining useful life predicted at time n
RUL_n^*	True remaining useful life at time n
\mathbf{S}^k	Cracked-ply compliance matrix (COD method)
\mathbf{u}	Random vector into-standard non-correlated space
\mathcal{U}	Useful domain in \mathbf{z} -space
\bar{U}_j	Failure region in \mathbf{z} -space at j th Subset simulation level, $j = 1, \dots, m$
\bar{U}	Failure region in \mathbf{z} -space
U_i	Ply invariants, $i = 1, \dots, 5$
\mathbf{v}	Random vector of process noise
\mathbf{v}_n	Process noise at time $n \in \mathbb{N}$
\mathbb{V}	Variance
\mathbb{V}_{f_z}	Variance using samples from $f_z(\mathbf{z})$
\mathbf{w}	Random vector of measurements noise
\mathbf{w}_n	Measurements noise at time $n \in \mathbb{N}$

Symbol	Description
\mathbf{x}	Hidden state predicted according to Υ
\mathbf{x}_n	Realization of \mathbf{x} at time $n \in \mathbb{N}$
\mathbf{y}	Measurements
\mathbf{y}_n	Measurements at time $n \in \mathbb{N}$
\mathcal{X}	Region of \mathbf{x} -outcomes
\mathcal{Z}	\mathbf{z} -space
\mathbf{z}	Random vector in \mathbf{z} -space
$\mathbf{z}^{(n)}$	Sample realization of random vector \mathbf{z}
$\mathbf{z}^{(\xi)}$	Candidate random vector
α	Modified Paris' Law exponent
β	Reliability index
β^{ik}	k -th ply diagonal matrix of crack openings (COD method)
β_i^k	i th element of β^{ik} , $i = 1, \dots, 3$. (COD method)
κ	curvature
μ_k	k -moment of the performance function $g(\mathbf{z})$
Φ	Normal standard cumulative distribution function
γ	Autocorrelation coefficient
γ_j	Autocorrelation coefficient for j th Subset simulation level
ω	Particle weight
ω_n	Particle weight at time $n \in \mathbb{N}$
$\hat{\omega}$	Unnormalized particle weight
$\hat{\omega}_n$	Unnormalized particle weight at time $n \in \mathbb{N}$
Σ_{ξ_n}	Covariance matrix of proposal density q
$\Sigma_{\mathbf{v}_n}$	Covariance matrix of model error \mathbf{v} at time n
$\Sigma_{\mathbf{w}_n}$	Covariance matrix of measurement error \mathbf{w} at time n
$\sigma_{\xi_n, k}^2$	k th element from the diagonal of matrix Σ_{ξ_n}
$\sigma_{\mathbf{v}_n, k}^2$	k th element from the diagonal of matrix $\Sigma_{\mathbf{v}_n}$
$\sigma_{\mathbf{w}_n, k}^2$	k th element from the diagonal of matrix $\Sigma_{\mathbf{w}_n}$
λ	Ply-thickness ratio
τ	Index-lag
ξ	Shear-lag parameter
δ	Delamination half-length
ϵ_0	Maximum applied strain
$\chi(\bar{l})$	Perturbation function (variational approach)

Symbol	SI	Description
D_n	[-]	Predicted normalized effective stiffness
\hat{D}_n	[-]	Measured normalized effective stiffness
$E_{x,0}$	[Pa]	Intact longitudinal Young's modulus
$E_x^{(\phi)}$	[Pa]	Laminate longitudinal Young's modulus
$E_x^{*(\phi)}$	[Pa]	Laminate effective longitudinal Young's modulus
$E_x^{(\phi)}$	[Pa]	Sublaminar longitudinal Young's modulus
$E_y^{(\phi)}$	[Pa]	Sublaminar transverse Young's modulus
$\nu_{xy}^{(\phi)}$	[-]	Sublaminar in-plane Poisson ratio
$G_{xy}^{(\phi)}$	[Pa]	Sublaminar in-plane shear modulus
$G_{yz}^{(\phi)}$	[Pa]	Sublaminar out-of-plane shear modulus
h	[m]	Laminate half-thickness
t_{90}	[m]	$[90_{n_{90}}]$ -sublaminar half-thickness
t_{90}	[m]	$[90_{n_{90}}]$ -sublaminar half-thickness
t_ϕ	[m]	$[\phi_{n_\phi}]$ -sublaminar thickness
E_1	[Pa]	Ply longitudinal Young's modulus
E_2	[Pa]	Ply transverse Young's modulus
$\nu_{12}^{(\phi)}$	[-]	Ply in-plane Poisson ratio
$\nu_3^{(\phi)}$	[-]	Ply out-of-plane Poisson ratio
$G_{12}^{(\phi)}$	[Pa]	Ply in-plane shear modulus
$G_{23}^{(\phi)}$	[Pa]	Ply out-of-plane shear modulus
ρ_n	$\frac{\# \text{ cracks}}{m}$	Predicted normalized effective stiffness
σ_x	[Pa]	Applied axial tension
$\hat{\rho}_n$	$\frac{\# \text{ cracks}}{m}$	Measured normalized effective stiffness

Contents

Summary	i
Resumen	iii
Acknowledgments	vii
Abbreviations	ix
List of Symbols	xii
I INTRODUCTION	5
Chapter 1 Context and motivation	7
Chapter 2 Objectives	11
Chapter 3 Outline of contributions	15
Chapter 4 Theoretical fundamentals	19
4.1 Basic concepts of composites	20
4.2 Overview of stochastic simulation methods	21
4.2.1 Monte Carlo Method	22
4.2.2 Importance sampling	23
4.2.3 Markov Chain Monte Carlo	25
4.2.4 Subset Simulation	28
4.3 Basis of reliability calculation	35
4.3.1 Fast probability integration (FPI) methods	35
4.3.2 Reliability assessment in composite laminates.	38
4.4 Stochastic system modeling	41

4.4.1	Bayesian state estimation	41
4.4.2	Sequential Monte Carlo for state and parameter estimation	44
4.4.3	ℓ -step ahead prediction	45
4.5	Prognostics problem formulation	48
4.5.1	Prognostics and SHM	48
4.5.2	Calculation of EOL and RUL	49
4.5.3	Filtering-based prognostics	50
4.5.4	Overview of prognostics metrics	53

II METHODOLOGICAL CONTRIBUTIONS 57

Chapter 5	A prognostics framework for composites	59
5.1	Introduction and state-of-the-art	60
5.2	Energy-based forward model of damage evolution	61
5.3	Micro-to-macro scale modeling of fatigue damage	62
5.4	Selecting prognostics targets for fatigue in composites	65
5.4.1	Competing damage modes	66
5.4.2	Interaction of cracks and (local) delamination	67
5.4.3	Global delamination	68
5.4.4	Balance of energy among damage modes	69
5.5	Model-based damage prognostics in composites	71
5.5.1	Stochastic system embedding	71
5.5.2	Stochastic system modeling	71
5.5.3	Particle filters for RUL and EOL estimations in composites	74
Chapter 6	Prognostics of reliability: reliability assessment along lifespan	77
6.1	Up-to-date review of reliability assessment in composites	78
6.1.1	Concept of failure.	79
6.1.2	Analytical approaches for reliability in composites	81
6.1.3	Recent numerical methods	82
6.1.4	Comparative review between reliability methods	83
6.1.5	Overview of recent computational techniques	85
6.2	Long-term reliability assessment of composites	90
6.2.1	Formulation of long-term reliability	90
6.2.2	Computation of RUL based on long-term reliability	91
6.2.3	Derivation of RUL as a probability using Probability Logic	92
6.2.4	Prognostics based on long-term reliability	94

Chapter 7	New efficient algorithm for prognostics involving rare-events	97
7.1	Introduction	98
7.2	Prediction of system failure	99
7.3	Prognostics involving rare-events.	100
7.3.1	Subset Simulation for prognostics	101
7.3.2	The PFP-SubSim algorithm	103

III EXPERIMENTAL AND NUMERICAL VALIDATIONS 107

Chapter 8	Fatigue damage dataset	109
8.1	Material and SHM system	110
8.1.1	Data acquisition for micro-cracks	110
8.1.2	Data organization	112
8.2	Damage feature extraction	113
8.2.1	SHM-PHM connection	114
8.2.2	Summary of damage data used for calculations	114
Chapter 9	Case study of prognostics and long-term reliability assessment	117
9.1	Results for EOL and RUL prediction	118
9.2	Results for long-term reliability prediction	126
9.3	Prognostics in composites using PFP-SubSim	126
9.4	Discussion of efficiency gained by PFP-SubSim	127
9.5	Numerical proofs for the computational efficiency gained	129

IV CONCLUSIONS AND FUTURE WORKS 137

Chapter 10	Conclusions and future works	139
Chapter 11	Conclusiones y trabajos futuros	145

V APPENDICES 151

Appendix A	Basic relations for ERR term formulation in composites	153
A.1	Shear-lag model nomenclature and basic relations of classical laminate theory	153
A.2	Energy release rate for micro-cracks interaction with local and global delamination (variational approach)	156

A.3 Energy release rate for micro-cracks interaction with local and global delamination (COD approach)	157
Appendix B Contributions	159
References	164

List of Figures

1.1	Picture of sustainable development in composite materials	9
4.1	Illustration of laminated FRP composite material	22
4.2	Conceptual two-dimensional example of IS	24
4.3	Conceptual two-dimensional example of Subset Simulation	31
4.4	Schematic representation of FORM/SORM approximations	36
4.5	Schematic representation of RUL calculation	50
4.6	Conceptual illustration of calculation of EOL using PF	52
4.7	Conceptual scheme of the particle-filter based prognostics framework	52
4.8	Illustrations of PH and $\alpha - \lambda$ prognostics metrics	54
5.1	Illustration for microscopic damage in $\left[\phi_{\frac{n_\phi}{2}} / 90_{n_{90}} / \phi_{\frac{n_\phi}{2}} \right]$ laminate along with basic geometrical parameters.	65
5.2	Energy release rate term as a function of the matrix crack density.	70
5.3	Filtering-based prognostics scheme proposed for composites.	76
6.1	Schematic representation of a reliability problem in composites.	79
6.2	Illustration of the proposed framework for prognostics based on long-term reliability. Top panel: samples of \mathbf{z} -states along with their idealized sample trajectories represented against different time steps. Bottom panel: long-term reliability predicted from cycle n to $n + \ell$, where $\ell > 1 \in \mathbb{N}$	95
6.3	Conceptual scheme for prognostics based on time-dependent reliability.	96
7.1	Schematic representation of a multi-step ahead prediction of an asymptotic process	99
7.2	Schematic representation of two-dimensional samples produced by PFP-SubSim algorithm	102
7.3	PFP-SubSim algorithm flowchart.	105

8.1	View of SMART® Layers location and coupon specimen. Both images are taken from [1], courtesy of NASA PCoE.	111
8.2	Plot of Lamb wave signals from PZT sensors	112
8.3	Schematical view of the new data structure from the Composite dataset, NASA Ames Prognostics Data Repository [1].	113
8.4	SHM-PHM connection in the context of the prognostics framework proposed.	116
9.1	Sequential state estimation for both matrix micro-crack density and normalized effective stiffness, along with multi-step ahead predictions.	119
9.2	Trace of the mean values of model parameters θ against time	120
9.3	Normalized histograms for EOL (part 1)	123
9.4	Normalized histograms for different PDFs of EOL (part 2)	124
9.5	RUL vs. cycles α - λ accuracy plot to assess lifetime prediction performance	125
9.6	Reliability updation and long-term prediction at different cycles along the process.	131
9.7	RUL vs. fatigue cycles plot obtained using the reliability-based prognostics framework. As in Figure 9.5, two cones of accuracy at 10% and 20% of true RUL, are represented using dashed lines (darker one corresponds to the cone at 10% of accuracy).	132
9.8	PFP-SubSim output for predicting matrix micro-cracks density and normalized effective stiffness. The triangles represent the experimental cycles for which matrix micro-cracks density and stiffness loss reach their respective thresholds, as observed from the data. . .	133
9.9	PFP-SubSim results for remaining useful life (RUL) predictions together with their quantified uncertainty by the 25% – 75% band. . .	134
9.10	Plot for $P(\vec{U})$ estimation using PFP-SubSim algorithm in comparison to the standard PF-based prognostics algorithm used as benchmark.	135
9.11	Results for the unit c.o.v. of $P(\vec{U})$ obtained using PFP-SubSim algorithm as compared to that obtained using Algorithm 6.	135
9.12	Results for the measures of accuracy and uncertainty of the RUL estimate using comparatively PFP-SubSim algorithm and Algorithm 6.	136

List of Tables

5.1	Nomenclature table for the terms used in shear-lag analysis	64
5.2	Selection of models for energy release rate due to microcrack-induced delamination	67
5.3	Models of energy release rate for edge delamination	69
6.1	Reliability bibliography Synoptic Table. Papers increasingly ordered by date of publication	89
8.1	Structure of the variable "path.data" from the Composite dataset, NASA Ames Prognostics Data Repository.	113
8.2	Experimental sequence of damage for cross-ply Torayca T700 CFRP laminate.	114
8.3	Ply properties used in the calculations (nominal values).	115
9.1	Nominal values and prior uncertainty of model parameters used in calculations	121

List of Algorithms

1	MH algorithm	26
2	Subset Simulation algorithm	32
3	PF with on-line parameter updating	46
4	PF-based prognostics algorithm	53
5	Pseudocode implementation for PFP-SubSim	104
6	PF-based prognostics algorithm used for calculations	121

Part I

INTRODUCTION

1

Context and motivation

Composites are high-performance materials used extensively in the construction of engineering structures and mechanisms for the aerospace, naval and construction industries, among others. As an emerging field, such as biotechnology today, the composite technology has seen a boost in research and development in the seventies. As a result, important advances were attained in the fields of mechanics of laminates, failure criteria, simulation methods, etc., most of them are well established topics for composites designers today.

Influenced by the metals' tradition, some aspects of the composites behavior, like fatigue degradation and failure, were initially treated as though they were metals [2], and as a consequence, numerous models were formulated as an extension of metals theories [3]. Later, experimental observations put in question this approach showing that, in composites materials, the evolution of several micro-scale patterns of damage led to failure events that were unpredictable by available theories [4]. The progression of such patterns of damage became instead the focus of the fatigue approaches since the 80s [5] and nowadays, a significant number of fatigue damage approaches are available in the composites literature, all of them apparently valid within their range of application [3]. However, the

fatigue behavior in composite materials still remains as an open question due to the *uncertainty* of the underlying damage process, even more in those applications combining long-term behavior and difficulty or absence of maintenance [5].

For example, in the aerospace industry, fatigue is overcome by adopting conservative designs that make use of high quality materials (fibers and matrices) produced by carefully designed manufacturing processes. This aims to reduce the variability in constituent properties which ultimately contributes to reduce the uncertainty in the fatigue behavior of composite materials. However, this is a costly solution that cannot be easily extrapolated for applications other than those from the aerospace industry. Moreover, as stated by [5], the emerging challenges of the 21st century lie in assuring the sustainability of technological developments by minimizing the impact of products and processes, which requires the adoption of new engineering paradigms different from those that merely adopt conservative designs by employing high quality materials and manufacturing processes. Instead, the continuous assessment of the design requirements for an expected performance during an estimated operational lifetime, seems to be a reasonable approach (not unique) to sustainability. In such a sustainable scheme, prognostics plays an important role since it allows us to make predictions of the expected behavior of engineering components and systems, and based on such predictions, to estimate the *remaining useful life* (RUL) of the system [6]. Furthermore, timely decisions can be made to optimize the global cost while reducing risks along the predicted lifetime. This can be viewed as a part of a bigger picture that entails the life cycle consideration for the materials and the energy inputs, as function of the required functionality and operativeness given a prescribed reliability level, as shown in Figure 1.1. Since prognostics deals with future predictions in absence of new data, several sources of uncertainty arise that influence the prediction behavior. Therefore, an effective design for prognostics requires a statistical framework to effectively account for the uncertainty. In the recent past, several works have contributed to the field of uncertainty quantification in damage prognostics. For example, the Damage Prognosis project [6, 7] at Los Alamos National Laboratory discussed uncertainty in fatigue crack growth in the context of structural health monitoring. Sankararaman *et al.* [8] developed a computational approach to account for unknown inputs, data uncertainty, and model uncertainty in crack growth prognosis. However, many of these methods are based on offline testing, i.e., testing before and after system operation, and not for *condition-based* monitoring prognostics, which aims to predict during system operation.

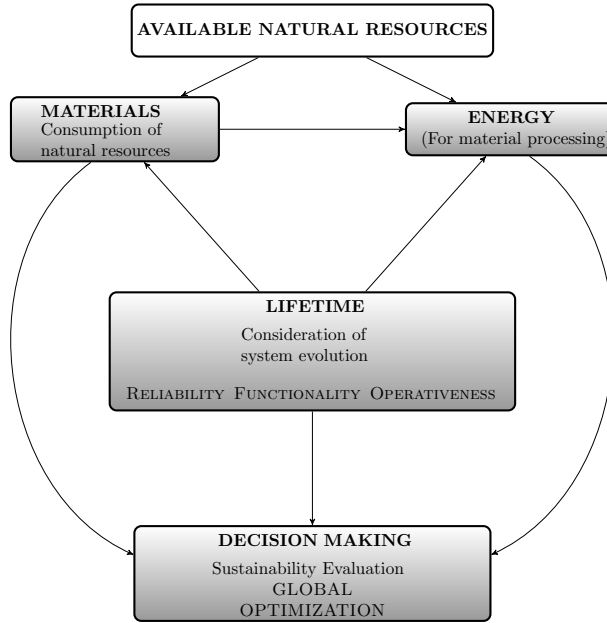


Figure 1.1: Sustainable development of composite materials by consideration of health management over the lifetime.

Developing methods for uncertainty quantification in the context of condition-based monitoring is challenging because uncertainty methods are generally computationally expensive, whereas condition-based monitoring and prognostics require real time computational power and results for decision-making. In this context, model-based prognostics frameworks have attracted significant attention of the PHM community since they improve predictability by capturing the underlying first principles behind the evolution of the fault indicator [9]. Several examples are found in the literature dealing with model-based prognostics for a widespread range of applications like fatigue crack growth in metals [10, 11], battery aging [12, 13] and failure of electronic components [14–17], just to name but a few.

In this thesis, a model-based filtering-based prognostics framework is presented for fatigue degradation of composite materials. Predictions of *end of life* (EOL) and *remaining useful life* (RUL) are obtained with high accuracy using structural health monitoring data. As a by-product, the output of the proposed prognostics framework is used to derive long-term reliability and correspondingly, system failure probability.

Note that numerical approximations by sampling-based algorithms (e.g. particle filters (PF)) [18, 19] are conventionally required in prognostics [20–22] since optimal closed-form solutions for model-based prognostics are very limited and often intractable in real life applications [23]. Multi-step ahead state estimation is a prerequisite to prognostics, hence the statistical uncertainty that arises from the approximation error is propagated in time leading to an artificial increase of the final uncertainty for the predictions of EOL/RUL [24], as well as for the estimation of system failure probability. When the faulty behavior is highly unprovable (as typically happens in many engineering systems like failure in nuclear plants, degradation under asymptotic behaviors, etc.), the increase in uncertainty might be exacerbated leading to a dramatical loss of accuracy. Higher-density sampling-based methods can be employed achieving higher resolution for the estimations, however it is at the expense of a high computational effort. Although various algorithms have been proposed in recent years to improve predictability [25], it is still an open-issue for the prognostics science which requires further research. In this thesis, a novel prognostics algorithm, called *PPF-SubSim algorithm*, is proposed to achieve high efficiency for rare-event prognostics while maintaining a moderate computational cost, resulting in an especially suited algorithm for the prognostics of matrix micro-cracks density saturation for carbon-epoxy laminates under fatigue loads.

2

Objectives

Anticipating the serviceability of composite materials under fatigue degradation is a challenge mainly due to the uncertainty in the physics of the damage process [26]. The integration of measurements from SHM sensors with theoretical knowledge about damage progression within a filtering-based prognostics framework emerges as a rational way to predict the evolution of damage in composites, while accounting for the uncertainty of the process. The latter along with the need to further explore the relationship between RUL and reliability in composites, is the main research objective of this thesis. The procedure to reach this research objective of this thesis is determined by means of a set of particular research questions to be investigated, which are presented below following an inductive reasoning:

1. Fatigue in composite materials is a complex multi-scale damage cumulative process, generally perceived as macro-scale reduction in stiffness and strength as a consequence of several fracture modes that evolve at the micro-scale along the lifespan of the structure [27]. Numerous modeling approaches have been proposed in the literature [3] however they usually

do not have predictive capabilities (in the sense of anticipation in absence of new data) and also they hardly account for the inherent uncertainty of the fatigue damage process. To partially overcome this drawback, fatigue damage prognostics emerges as a suitable approach to predict the fatigue damage progression under uncertainty while incorporating up-to-date information from measurements. Previous studies have reported about the fatigue damage prognostics [7, 10, 11, 21, 28, 29], but most of them in the context of metals. However, the application of a rigorous damage prognostics framework for composite materials still remains unexplored (except for some recent contributions by the author and co-workers, specified in Appendix B), precisely where the benefits of a probability-based prognostic approach can be fully exploited to deal with the well-known variability and complexity of the damage accumulation process.

Hypothesis 1: Damage prognostics is a suitable technique to deal with the complexity of the fatigue damage process in composites while using information from physics-based models and SHM measurements.

• **Research objective 1:** *Propose a model-based filtering-based prognostics framework to estimate the RUL/EOL of composite materials under fatigue conditions using data from SHM sensors.*

2. In composites, fatigue degradation progressively diminishes the material functionality to which it was primarily conceived. The reliability, which can be understood as a unified health indicator for the material, is influenced by the presence of damage scenarios caused by fatigue [30, 31]. The prediction forward in time of such fatigue degradation and the associated reliability of the composite structure is of paramount importance for safety and cost reasons [32], however it is still a partially understood problem. Several works deal with the problem of reliability in composites, but only few of them by considering the actual fatigue damage within the reliability formulation [33, 34]. As pointed out by the author in [34], more research effort is needed to consider the progressive failure of composite laminates within the reliability formulation, which would help to derive the connection between reliability and lifetime estimation in composites.

Hypothesis 2: The long-term evolution of damage modes in composites is expected to decrease the reliability. Predictive information about a component or sub-system damage can be a valuable resource in determining an appropriate course of action to avoid prospective failures, thus re-scheduling functionality and update reliability [35].

- Research objective 2:** *Explore the relationship between long-term reliability and RUL, and propose a reliability-based prognostics framework in application to fatigue in composite materials.*
3. In practice, different sources of uncertainty are present in the prediction [36, 37], which can be roughly classified into (a) modeling uncertainty, (b) uncertainty in the future inputs to the system, (c) measurements noise [37]. There is an additional source of error attributable to the prognostics algorithm itself, which is due to the lack of confidence in dealing with the RUL/EOL estimate, and it is especially representative of systems whose evolving dynamic exhibit an asymptotic behavior in approaching towards the thresholds (like the case of predicting matrix micro-crack saturation in composites) or when the damage threshold is very unprovable under the model. In this situation, prediction accuracy can vary significantly unless higher-density sampling-based methods are employed to characterize damage propagation trajectories achieving higher resolutions in the vicinity of the threshold, which considerably increases the computational cost. On the other hand, choosing a conservative threshold, such that it meets a propagation trajectory prior to the asymptotic region, is one approach but it results in throwing away potentially useful component life. Different algorithms have been proposed in recent years to improve predictability [25, 38] however it is evident the absence of efficient algorithms to deal with asymptotic processes as well as for rare-event process.

Hypothesis 3: The use of Subset Simulation method is expected to improve the predictability of asymptotic processes and rare-event process while significantly reducing the computational cost.

- Research objective 3:** *Develop a novel prognostic algorithm to efficiently estimate the RUL/EOL as well as the long-term reliability in those cases where simulations involve rare-events.*

In the next section, the scientific contributions of this thesis are presented in the context of the research objectives described here.

3

Outline of contributions

This thesis grew out of the desire to present a coherent story of a set of contributions made over the course of my graduate career. The references to the methodological and experimental contributions developed to investigate the research questions described in **Chapter 2**, are outlined here along with indication where they appear in the text.

Research objective 1: *Propose a model-based filtering-based prognostics framework to estimate the RUL/EOL of composite materials under fatigue conditions using data from SHM sensors.*

To deal with this research objective, a state-space formulation for the sequential estimation and updating of the fatigue damage propagation in composites is proposed and presented in **Chapter 5**. Fatigue degradation phenomena is predicted by connecting micro-scale and macro-scale damage models in a Bayesian filtering framework which uses periodical data from SHM sensors. The key contribution is the inclusion of micro-scale damage evolution models acting as state transition equation for the dynamical system, which are further hierarchically connected to a macro-scale stiffness reduction model into the Bayesian filtering algorithm.

The proposed method allows incorporating various uncertainties in the prediction that are generally associated with material defects, sensing noise and modeling errors. Multi-step ahead predictions of damage are possible by evaluating multiple times the prediction equation whereby RUL/EOL estimates are derived by computing the times indexes when damage reaches a set of thresholds. Since multiple fracture modes may co-exist during fatigue degradation in composites [4], the proposed model-based prognostics framework allows dynamically assessing the dominant damage mode and establishing the thresholds of each of the competing damage modes by means of a comparison of the energy spent by each single mode.

The approach is demonstrated in **Chapter 9**, Section 9.1 on data collected from a run-to-failure tension-tension fatigue experiment measuring the evolution of fatigue damage in CRFP cross-ply laminates, whose details are reported separately in **Chapter 8**. Results are presented for the prediction of expected end of life for a given panel with the associated uncertainty estimates.

Research objective 2: *Explore the relationship between long-term reliability and RUL, and propose a reliability-based prognostics framework in application to fatigue in composite materials.*

As an extension of the prognostics framework developed for the *Research Objective 1*, a reliability-based prognostic framework is proposed in **Chapter 6** to make long-term predictions of reliability of composite materials under fatigue degradation. It is shown that the prediction of the RUL is presented as a probability from the computation of the long-term reliability.

The approach broadly consists in a two-step recursive method: first, propagate forward in time the current damage state using the most up-to-date information from SHM data, and second, obtain the probability of the predicted states for belonging to the non-failure region (the region inside the damage thresholds), that defines the long-term reliability. As a by-product, the CDF of the RUL is obtained as the complementary of the long-term reliability. The results presented in Section 9.2 show that it is possible to make long-term reliability predictions with high accuracy since early stages of the fatigue damage process.

As a preliminary step before to proceed with the long-term reliability methodology proposed in **Chapter 6**, a state-of-art introductory section about reliability in composites is presented, which is motivated by the

lack of consensual framework for the use of reliability methods in composites. These, together with new trends to confer efficiency in reliability calculations, suggested the need for a thorough and up-to-date review of the literature in this area under unified notation. The review identifies the need for connections between reliability and lifetime calculation, and highlights the methods to confer high efficiency to the reliability calculation in composites.

Research objective 3: *Develop a novel prognostics algorithm to efficiently estimate the RUL/EOL as well as the long-term reliability in those cases where prognostics involve rare-events.*

A novel algorithm for estimating the RUL/EOL by combining the particle filter (PF)-based prognostics with the technique of Subset simulation is presented in **Chapter 7**. It has been named PFP-SubSim on behalf of the full denomination of the computational framework, namely, *PF-based prognostics based on Subset Simulation*. By Subset Simulation, a small failure probability simulation can be transformed into a sequence of more probable simulations by choosing a nested sequence of intermediate failure regions that correspond to increasingly closer approximations to the final region (failure region). It is shown that this scheme is especially useful when dealing with the prognostics of evolving processes with asymptotic behaviors, as observed in practice for many degradation processes like matrix micro-cracks saturation in composites [4].

Following some theoretical development in **Chapter 7**, the performance of the algorithm for forecasting of the system failure probability as well as for making predictions of the EOL and RUL of composites under fatigue damage propagation is reported in **Chapter 9**, Section 9.3.

Although PFP-SubSim algorithm was originally inspired by an attempt to obtain higher accuracy for the predictions of the matrix-micro crack saturation stage in composites, the numerical experiments showed that PFP-SubSim can be considered as general purpose prognostics algorithm, which is specially efficient when prognostics involves rare-event simulation.

4

Theoretical fundamentals

The aim of this chapter is to supply the theoretical basis on the methods used for the thesis. The focus is not to provide an exhaustive literature review on methods but on the theoretical and computational aspects of those methods that are extensively used or discussed in this thesis, which are presented here under unified notation. This chapter begins with an initial section dedicated to provide key definitions for several concepts regarding composite materials.

Throughout, it is assumed basic familiarity with Bayesian statistics, Bayesian state estimation algorithms and in general, Monte Carlo theory. For this relevant background information, the reader is referred to the many useful articles cited in this thesis.

4.1 Basic concepts of composites

Strictly speaking, a *composite material* consists of two or more different materials specifically arranged such that together they produce desirable properties that cannot be achieved with any of the constituents by their own [39]. In structural engineering, composite materials (which are mostly referred to as *composites*) make reference to a class of materials made through the conjunction of high-modulus and high-strength fibers and a matrix material [40]. The load-carrying function is attached to the fibers whilst the matrix is devoted to maintain the fibers together, to transfer the loads between them, and also to provide environment protection [41]. There are many possible types of fibers and matrices that can be employed, each one defining a different class of composite material. Synthetic long fibers and polymeric matrices are mostly used for structural applications, and they are referred to as *fiber reinforced polymers* (FRP) composite materials. An exhaustive overview and tutorial of constitutive materials for composites is provided by Kim [42]. The next is a list of key definitions of ubiquitous terms for this thesis regarding composites. Figure 4.1 provides graphical support to some of the concepts defined below.

Laminate: A laminate is a thin layer of composite material, which is considered as the macro unit for mechanical response. Its mechanical properties are accomplished through laboratory tests and they are typically provided by the supplier [39]. Its mechanical properties can also be obtained by simulation using the theory of micromechanics [2, 40].

Ply: The minimal unit of composite material characterized by a homogeneous orientation of the fibers [40]. Each of the plies of the laminate is typically denoted using the angle (expressed in degree units) of orientation of the fibers using any specified longitudinal axis as reference. For example, the expression "the 45° ply" is to denote the ply whose fibers are oriented at 45° with respect to any reference axis.

Sublaminate: Combination of adjacent plies with same orientation. As in the plies, sublaminates are denoted using the angle of orientation of their fibers.

Stacking sequence: The stacking-sequence refers to the arrangement of plies within the laminate. The rule $[\phi_1^o/\phi_2^o/.../\phi_n^o]_S$ is adopted in composites to indicate that the laminate has two sublaminates arranged symmetrically (by the "S" indication) whose plies are oriented (from outer to inner plies) as $\phi_1^o, \phi_2^o, \dots, \phi_n^o$, respectively [43]. See Figure 4.1a for further details.

Lay-up: Lay-up is used with the same meaning as stacking-sequence.

Cross-ply: Type of laminate whose plies are symmetrically arranged at orthogonal directions. To serve as an example, the stacking sequence $[0^\circ/90^\circ]_{KS}$ denotes a cross-ply of $2K$ plies, where K is an integer number to indicate the amount of repetitions of the $0^\circ/90^\circ$ pattern. Plies of same orientation may be grouped together, i.e., $[0_n^\circ/90_m^\circ]_{KS}$, being m, n the amount of plies corresponding to each direction, respectively.

Angle-ply: An angle-ply laminate can be considered as the general type of cross-ply laminates where direction 90° is replaced by any other angle in the interval $[0^\circ, 90^\circ]$. For example, $[0^\circ/15^\circ]_{KS}$, $[0^\circ/30^\circ]_{KS}$, $[0^\circ/45^\circ]_{KS}$ are possible arrangements for angle-ply laminates.

Quasi-isotropic: Type of laminate whose plies are symmetrically oriented at increments of 45° , i.e., $[0^\circ/45^\circ/90^\circ/-45^\circ/0^\circ]_{KS}$. As in cross-ply and angle-ply, plies of same orientation may be grouped together dealing to arrangements like $[0_n^\circ/45_m^\circ/90_p^\circ/-45_q^\circ/0_r^\circ]_{KS}$, where n, m, p, q, r are integer numbers to indicate the amount of plies in the $0^\circ, 45^\circ, 90^\circ, -45^\circ, 0^\circ$ direction, respectively.

On-axis: Regarding to any specific ply, on-axis makes reference to the orientation to adopt for a reference system so that principal stresses of the ply coincide with the axis directions of the reference system. By

Off-axis: Any direction which cannot be considered as on-axis.

Matrix-cracking: Damage mode of composites consisting of series of cracks arising at the matrix constituent, which are generally distributed following a specific geometric pattern characterized by equidistant parallel cracks. They initiate from the locations of defects such as voids, abnormally fiber concentrations or resin rich areas [44]. Matrix-cracking induced by impacts exhibit more complex geometrical pattern of cracks. See Chapter 5 for further insight.

Delamination: Damage mode in composites consisting of interlaminar cracks arising at the interfaces between consecutive plies. Generally, these interlaminar cracks merge into concentrated regions leading to what is typically called delamination [44]. Further insight is provided in Chapter 5.

4.2 Overview of stochastic simulation methods

In this section, stochastic simulation methods are presented as effective techniques to numerically solve probability integrals. Theoretical background of the

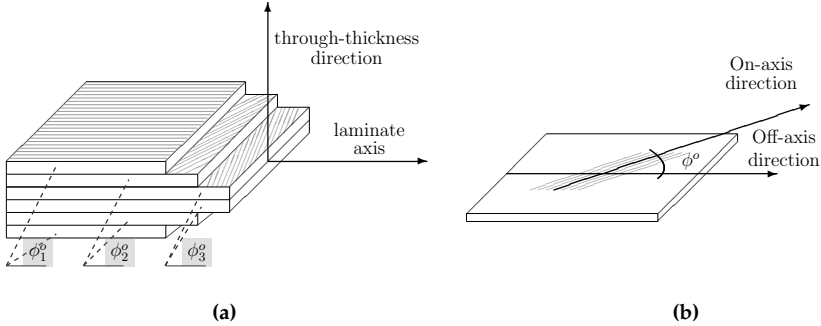


Figure 4.1: Panel a): schematic view of a FRP composite laminate of 6 plies and stacking sequence given by $[\phi_1^0/\phi_2^0/\phi_3^0]_S$. Panel b): Illustration of one of the plies with indication of fiber and laminate directions.

stochastic simulation methods used for this thesis is presented along with computational issues and details of implementation. Other stochastic simulation methods different from those overviewed here can be found in the literature, for example, stratified resampling, Latin Hypercube Sampling, Unscented Transform Sampling, to name but a few. The reader is referred to [45, 46] for further insight.

4.2.1 Monte Carlo Method

Let $\mathbf{z} = [z_1, \dots, z_d] \in \mathcal{Z} \subset \mathbb{R}^d$ be a vector of uncertain variables distributed according to the probability density function (PDF) $f_z(\mathbf{z})$, and let $h : \mathcal{Z} \rightarrow \mathbb{R}$ be a quantity of interest expressed as a function of \mathbf{z} . Let us now consider the following probability integral:

$$J = \int h(\mathbf{z})f_z(\mathbf{z})d\mathbf{z} \quad (4.1)$$

In practical cases, the Equation 4.1 may involve a multidimensional integral which cannot be easily evaluated by analytical methods nor by numerical schemes. Observe that the last integral can also be expressed as a mathematical expectation of $h(\mathbf{z})$ with $\mathbf{z} \sim f_z(\mathbf{z})$, i.e., $J = \mathbb{E}_{f_z}[h(\mathbf{z})]$, provided that $\mathbb{E}_{f_z}[h(\mathbf{z})] < \infty$. The standard Monte Carlo (MC) method [47] provides an effective procedure for obtaining an approximation for J by simulated samples from $f_z(\mathbf{z})$, as follows:

$$J \approx \tilde{J}_{\text{MC}} = \frac{1}{N} \sum_{n=1}^N h(\mathbf{z}^{(n)}) \quad (4.2)$$

where $\mathbf{z}^{(n)}$ are samples independent identically distributed i.i.d. as $f_z(\mathbf{z})$, $n = 1, \dots, N$. The error of this method is $\mathcal{O}(1/\sqrt{N})$ regardless of the dimension d , hence

it confers high versatility with respect to applications. However, a large amount of samples is required to achieve an acceptable accuracy when h takes its significant values at the tail regions of $f_z(\mathbf{z})$. Alternatively, other efficient stochastic simulation techniques different from MC method can be adopted to increase the computational efficiency while achieving good measure of accuracy in the estimations. They are presented further below in this chapter.

Statistical properties of estimators

Let us evaluate the variance for the Monte Carlo estimator \tilde{J}_{MC} as follows:

$$\begin{aligned}\mathbb{V}(\tilde{J}_{MC}) &= \mathbb{E} \left[(\tilde{J}_{MC} - J)^2 \right] = \frac{1}{N} \frac{1}{N} \sum_{n,m=1}^N \mathbb{E}_{f_z} \left[\left(h(\mathbf{z}^{(n)}) - J \right) \left(h(\mathbf{z}^{(m)}) - J \right) \right] \\ &= \frac{1}{N^2} \sum_{n,m=1}^N \text{cov} \left(h(\mathbf{z}^{(n)}) h(\mathbf{z}^{(m)}) \right)\end{aligned}\quad (4.3)$$

where $\text{cov} \left(h(\mathbf{z}^{(n)}) h(\mathbf{z}^{(m)}) \right)$ are the n - m -covariances between the pairs of samples $\left(h(\mathbf{z}^{(n)}), h(\mathbf{z}^{(m)}) \right)$, $n, m = 1, \dots, N$. Note that MC method uses i.i.d. samples, hence $\text{cov} \left(h(\mathbf{z}^{(n)}) h(\mathbf{z}^{(m)}) \right) = 0$ for indexes $n \neq m$. Therefore the last equation reduces to:

$$\mathbb{V}(\tilde{J}_{MC}) = \frac{1}{N^2} \sum_{n=1}^N \mathbb{E}_{f_z} \left(h(\mathbf{z}^{(n)}) - J \right)^2 = \frac{\mathbb{V}_{f_z}(h(\mathbf{z}))}{N} \quad (4.4)$$

where \mathbb{V}_{f_z} is the sample variance of h . The last result shows that \tilde{J}_{MC} will converge to J provided that N is large enough and $\mathbb{V}_{f_z}[h(\mathbf{z})] < \infty$.

4.2.2 Importance sampling

The importance sampling (IS) method aims to obtain better estimates by sampling more frequently from inside the "importance region", the region where function h reaches its higher values. This is achieved by replacing the original PDF $f_z(\mathbf{z})$ in Equation 4.1 by an importance sampling density $i_z(\mathbf{z})$ which is appropriately selected so as to generate a large amount of samples close to the importance region as follows:

$$J = \int h(\mathbf{z}) f_z(\mathbf{z}) d\mathbf{z} = \int \underbrace{\frac{h(\mathbf{z}) f_z(\mathbf{z})}{i_z(\mathbf{z})}}_{g_z(\mathbf{z})} i_z(\mathbf{z}) d(\mathbf{z}) \quad (4.5)$$

Following the same conceptual idea cited in the last section about expressing J as a mathematical expectation, Equation 4.5 may be also written as $J = \mathbb{E}_{i_z} [g_z(\mathbf{z})]$, which can be approximated by simulation as follows:

$$J \approx \tilde{J}_{\text{IS}} = \frac{1}{N} \sum_{n=1}^N g_z(\mathbf{z}^{(n)}) \quad (4.6)$$

where $\mathbf{z}^{(n)}$ are N samples i.i.d. as $i_z(\mathbf{z})$. Figure 4.2 shows an illustration of the performance of IS method for drawing samples using an importance density $i_z(\mathbf{z})$. For ease of representation, the \mathbf{z} -samples have dimension two. The left panel (a) shows the case where the crude density $f_z(\mathbf{z})$ is used. Observe the efficiency that can be gained with IS for drawing samples within the importance region, which in this example is represented as the region in the vicinity of a performance function $g(\mathbf{z}) : \mathcal{Z} \rightarrow \mathbb{R}$. When the performance function g serves to delimit a failure region in \mathcal{Z} (denoted by \bar{U}), then it is shown that IS is also an efficient method to deal with an estimation of failure probability as the amount of samples that lie within \bar{U} (darker circles in panel (b)) in relation to the total amount of samples. Note that if samples from the crude density $f_z(\mathbf{z})$ were used, a larger amount of samples should have been employed to reach a good approximation of failure probability. This will be further explained in later sections in the context of reliability calculations.

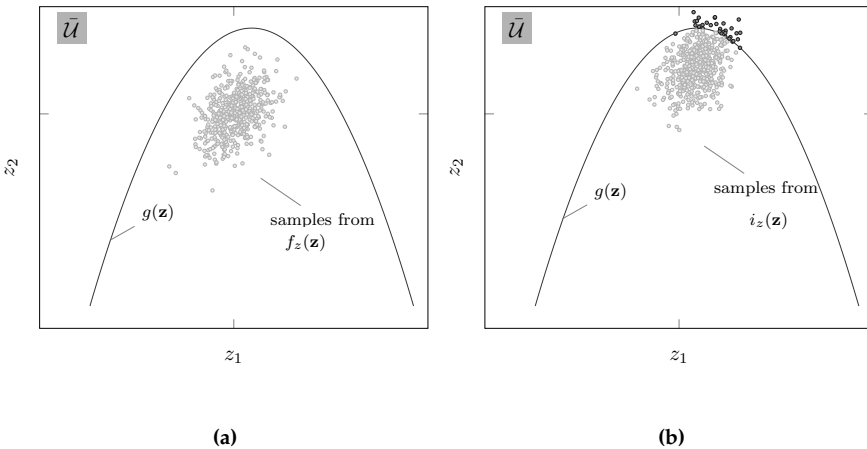


Figure 4.2: Conceptual two-dimensional example about obtaining the estimator \tilde{J} using samples from (a) the crude density $f_z(\mathbf{z})$ and (b) the importance density $i_z(\mathbf{z})$

Since \tilde{J}_{IS} is an average of i.i.d. samples from $i_z(\mathbf{z})$, the formulation for the approximation error as well as for the statistical properties coincide with those from the standard MC method explained before. It is important to remark that the latter is true when $i_z(\mathbf{z})$ has been appropriately chosen such that $g_z(\mathbf{z})$ has finite variance under $i_z(\mathbf{z})$. Guidelines on how to best select $i_z(\mathbf{z})$ are well-known in the literature [18, 48] and they are not repeated here. Further recommendations are specifically provided in those chapters where the IS method is used.

In the literature one can find various improved versions to the IS method. One of the most relevant for reliability and prognostics is the *adaptive sampling* [48–50], where the efficiency of IS is continuously improved by updating the importance density $i_z(\mathbf{z})$ based on the information obtained after evaluating the estimator \tilde{J}_{IS} for an initial set of few samples, often called as pre-samples. It has been reported in several works, e.g. [51], the gain in efficiency as compared to the standard MC method. However, it is important to remark that this efficiency is obtained in those cases where the dimension of the \mathbf{z} -space is not too large and the performance function h is relatively simple to describe. For time-dependent problems such as stochastic processes of damage evolution, first-excursion reliability problems, etc., the dimension of the uncertain parameter space is often large and the performance function may be highly complex. Therefore, the construction of the importance sampling density using information numerically extracted from the pre-samples becomes much more difficult [52].

4.2.3 Markov Chain Monte Carlo

Markov Chain Monte Carlo (MCMC) methods are stochastic simulation methods which aim to generate samples distributed according to an arbitrary probability distribution, which can be known only up to scaling constant. The samples are obtained from a specially constructed Markov chain¹ which has as stationary probability density the *target PDF*, provided that chain is ergodic and a large amount of samples are used [54]. Under the assumption of ergodicity, the Markov chain samples will converge to the target PDF even if the initial samples are simulated from a PDF different from the target. The theoretical treatment of ergodicity and stationarity for MCMC methods is out of the scope of this work and well-known in the specialized literature (e.g. [46, 54]), hence it is not repeated here.

¹A Markov chain is a sequence of random variables of length N , i.e. $\mathbf{z}^{(1)}, \mathbf{z}^{(2)}, \dots, \mathbf{z}^{(N)}$, that satisfies the *Markov property* which states that the future of the process is conditionally independent of the past states, given the present [53]. In mathematical terms $P(\mathbf{z}^{(N)} | \mathbf{z}^{(N-1)}, \mathbf{z}^{(N-2)}, \dots, \mathbf{z}^{(1)}) = P(\mathbf{z}^{(N)} | \mathbf{z}^{(N-1)})$, where $P(\cdot)$ denotes probability.

The simplest and original algorithm from the family of MCMC methods is the Metropolis algorithm, after the celebrated paper *Equation of State Calculations by Fast Computing Machines* by Nicholas Metropolis *et al.* in 1953 [55], that was further extended to the Metropolis-Hastings (MH) algorithm [55, 56]. Several other algorithms of the class of MCMC methods are found in the literature such as the Gibbs Sampler, Modified Metropolis algorithm (MMA), Auxiliary variable MCMC algorithms, population-based MCMC algorithms (PMCMC), just to name but a few [46, 57–59]. However, the MH algorithm is typically adopted for its versatility and implementation simplicity.

By sampling a *candidate vector* $\mathbf{z}^{(\xi)}$ from a *proposal PDF* $q(\mathbf{z}^{(\xi)}|\mathbf{z})$, the MH algorithm obtains the state of the chain at n , given the state at $n - 1$, specified by $\mathbf{z}^{(n-1)}$. The candidate $\mathbf{z}^{(\xi)}$ is accepted as the next state of the chain (i.e. $\mathbf{z}^{(n)} = \mathbf{z}^{(\xi)}$) with probability $\min\{1, r\}$, and rejected ($\mathbf{z}^{(n)} = \mathbf{z}^{(n-1)}$) with the remaining probability $1 - \min\{1, r\}$, where

$$r = \frac{f_{\mathbf{z}}(\mathbf{z}^{(\xi)}|\bar{\mathcal{U}})q(\mathbf{z}^{(n-1)}|\mathbf{z}^{(\xi)})}{f_{\mathbf{z}}(\mathbf{z}^{(n-1)}|\bar{\mathcal{U}})q(\mathbf{z}^{(\xi)}|\mathbf{z}^{(n-1)})} \quad (4.7)$$

The process is repeated until a sufficient amount of samples are generated. A pseudocode implementation of the MH algorithm is provided as Algorithm 1. When the proposal PDF q is symmetric, then $q(\mathbf{z}^{(\xi)}|\mathbf{z}^{(n-1)}) = q(\mathbf{z}^{(n-1)}|\mathbf{z}^{(\xi)})$, and

Algorithm 1 MH algorithm

```

1. Initialize  $\mathbf{z}^{(0)}$ 
for  $n = 1$  to  $N$  do
    2. Generate  $\mathbf{z}^{(\xi)} \sim q(\mathbf{z}^{(\xi)}|\mathbf{z}^{(n-1)})$ 
    3. Accept/reject  $\mathbf{z}^{(\xi)}$  as  $\mathbf{z}^{(n)}$  with probability  $r$ 
        $r = \min\left\{1, \frac{f_{\mathbf{z}}(\mathbf{z}^{(\xi)}|\bar{\mathcal{U}})q(\mathbf{z}^{(n-1)}|\mathbf{z}^{(\xi)})}{f_{\mathbf{z}}(\mathbf{z}^{(n-1)}|\bar{\mathcal{U}})q(\mathbf{z}^{(\xi)}|\mathbf{z}^{(n-1)})}\right\}$ 
end for

```

the MH algorithm reduces to the Metropolis algorithm, also referred to as *random walk Metropolis*.

The relation between the number of accepted samples over the total amount of candidate samples is the *acceptance rate* of the algorithm \bar{r} , which can be straightforwardly evaluated as an average of the r -values over the N samples. A recommended interval for \bar{r} to ensure an adequate speed of convergence for the MH algorithm is 0.2 – 0.4 for low dimensional spaces (say, $d \leq 10$), which can be

achieved by appropriately scaling the variance of the proposal PDF $q(\mathbf{z}^{(\xi)}|\mathbf{z})$ via some pilot runs [60, 61].

One of the most practical applications of MCMC methods is to sample from conditional distributions, or directly, to generate *conditional samples*, which is of especial relevance for this thesis. In a general sense, let $f_z(\mathbf{z}|\bar{\mathcal{U}})$ be the PDF of \mathbf{z} conditional on the event $\{\mathbf{z} \in \bar{\mathcal{U}}\}$, where $\bar{\mathcal{U}} \in \mathbb{R}^d$ is a specific subset of \mathcal{Z} . In mathematical terms:

$$f_z(\mathbf{z}|\bar{\mathcal{U}}) = \frac{\mathbb{I}_{\bar{\mathcal{U}}}(\mathbf{z})f_z(\mathbf{z})}{P(\bar{\mathcal{U}})} \quad (4.8)$$

where $\mathbb{I}_{\bar{\mathcal{U}}}(\mathbf{z})$ is an indicator function for \mathbf{z} that assigns a value of 1 when $\mathbf{z} \in \bar{\mathcal{U}}$ and 0 otherwise. Observe that, it is possible to evaluate the numerator for any valid sample for \mathbf{z} but not $P(\bar{\mathcal{U}})$, which acts here as a normalizing constant. However, MCMC methods can effectively generate samples of a specially constructed Markov chain whose stationary distribution is $f_z(\mathbf{z}|\bar{\mathcal{U}})$ without the need to evaluate $P(\bar{\mathcal{U}})$.

Statistical properties of estimators

Under the assumption of ergodicity and $\mathbb{E}_{f_z}[h(\mathbf{z})] < \infty$ [46], the MCMC samples can be used for statistical averaging as if they were i.i.d. samples although with some reduction in efficiency. The MCMC estimator for the expectation of h over the Markov chain samples is expressed as follows:

$$J \approx \tilde{J}_{\text{MCMC}} = \frac{1}{N} \sum_{n=1}^N h(\mathbf{z}^{(n)}) \quad (4.9)$$

where $\mathbf{z}^{(n)} \sim f_z(\mathbf{z}|\bar{\mathcal{U}})$ for any $\bar{\mathcal{U}} \subset \mathcal{Z}$. The variance of \tilde{J}_{MCMC} is examined below:

$$\begin{aligned} \mathbb{V}(\tilde{J}_{\text{MCMC}}) &= \mathbb{E} \left[(\tilde{J}_{\text{MCMC}} - J)^2 \right] = \frac{1}{N} \frac{1}{N} \sum_{n,m=1}^N \mathbb{E}_{f_z} \left[\left(h(\mathbf{z}^{(n)}) - J \right) \left(h(\mathbf{z}^{(m)}) - J \right) \right] \\ &= \frac{1}{N^2} \sum_{n,m=1}^N \text{cov} \left(h(\mathbf{z}^{(n)}) h(\mathbf{z}^{(m)}) \right), \end{aligned} \quad (4.10)$$

where the term $\text{cov} \left(h(\mathbf{z}^{(n)}) h(\mathbf{z}^{(m)}) \right)$ are the n - m -covariances between the pairs $\left(h(\mathbf{z}^{(n)}), h(\mathbf{z}^{(m)}) \right)$, $n, m = 1, \dots, N$, as a measure of their correlation. Given that the covariances have the symmetry property, the summative of Equation 4.10

can be evaluated more efficiently by avoiding repeating indexes such that:

$$\begin{aligned}\mathbb{V}(\tilde{J}_{\text{MCMC}}) &= \frac{1}{N^2} \sum_{n=1}^N \mathbb{V}_{f_z}(h(\mathbf{z}^{(n)})) + \frac{1}{N^2} \sum_{\tau=1}^{N-1} \sum_{n=1}^{N-\tau} \text{cov} \left(h(\mathbf{z}^{(n)}) h(\mathbf{z}^{(n+\tau)}) \right) \\ &= \frac{\mathbb{V}_{f_z}(h(\mathbf{z}))}{N} + \frac{1}{N^2} \sum_{\tau=1}^{N-1} \sum_{n=1}^{N-\tau} \text{cov} \left(h(\mathbf{z}^{(n)}) h(\mathbf{z}^{(n+\tau)}) \right)\end{aligned}\quad (4.11)$$

By the ergodicity condition, the Markov chain $\{h(\mathbf{z}^{(n)}), h(\mathbf{z}^{(n+1)}), \dots, h(\mathbf{z}^{(\tau+n)})\}$ is stationary and hence the correlation depends only on the lag-distance τ between the pairs but not on their n, m positions, i.e. $\text{cov} \left(h(\mathbf{z}^{(n)}) h(\mathbf{z}^{(\tau+n)}) \right) = \text{cov} \left(h(\mathbf{z}^{(1)}) h(\mathbf{z}^{(\tau+1)}) \right)$, $n = 1, \dots, N - \tau$. Thus, Equation 4.10 can be written as:

$$\mathbb{V}(\tilde{J}_{\text{MCMC}}) = \frac{\mathbb{V}_{f_z}(h(\mathbf{z}))}{N} + \frac{1}{N^2} \sum_{\tau=1}^{N-1} (N - \tau) \overbrace{\text{cov} \left(h(\mathbf{z}^{(1)}) h(\mathbf{z}^{(\tau+1)}) \right)}^{R^{(\tau)}} \quad (4.12)$$

In the literature, the covariances $\text{cov} \left(h(\mathbf{z}^{(1)}) h(\mathbf{z}^{(\tau+1)}) \right)$, $\tau = 1, \dots, N - 1$ are commonly expressed using $R^{(\tau)}$, the *autocovariance* sequence of $h(\mathbf{z})$ at lag τ defined as $R^{(\tau)} = \mathbb{E} \left[h(\mathbf{z}^{(1)}) h(\mathbf{z}^{(\tau+1)}) \right] - \bar{h}^2$, $\tau = 1, \dots, N - 1$, where \bar{h} is the sample mean of h using samples from the stationary chain. Next, the variance for the estimator \tilde{J}_{MCMC} can be finally expressed as follows:

$$\mathbb{V}(\tilde{J}_{\text{MCMC}}) = \frac{\text{Var}(h(\mathbf{z}))}{N} (1 + \gamma), \quad (4.13)$$

where:

$$\gamma = 2 \sum_{\tau=1}^{N-1} \left(\frac{N - \tau}{N} \right) \frac{R^{(\tau)}}{R^{(0)}} \quad (4.14)$$

defined at lag $\tau = 1, \dots, N - 1$. In the last expression $R^{(0)} \equiv \mathbb{V}(\tilde{J}_{\text{MCMC}})$.

4.2.4 Subset Simulation

Subset Simulation (SS) is a method for efficiently generating conditional samples that correspond to specified levels of a performance function $g : \mathcal{Z} \subset \mathbb{R}^d \rightarrow \mathbb{R}$ in a progressive manner, converting a problem involving rare-event simulation into a sequence of problems involving higher probability events [62]. It was originally proposed to compute small failure probabilities encountered in reliability analysis of engineering systems (e.g. [63, 64]).

Let us consider that $\bar{\mathcal{U}}$ is a failure region in the \mathbf{z} -space, corresponding to exceedance of the performance function g above some specified threshold level b :

$$\bar{\mathcal{U}} = \{\mathbf{z} \in \mathcal{Z} : g(\mathbf{z}) > b\} \quad (4.15)$$

Let us now assume that $\bar{\mathcal{U}}$ is defined as the intersection of m regions $\bar{\mathcal{U}} = \bigcap_{j=1}^m \bar{\mathcal{U}}_j$, such that they are arranged as a nested sequence $\bar{\mathcal{U}}_1 \supset \bar{\mathcal{U}}_2 \dots \supset \bar{\mathcal{U}}_{m-1} \supset \bar{\mathcal{U}}_m = \bar{\mathcal{U}}$, where $\bar{\mathcal{U}}_j = \{\mathbf{z} \in \mathcal{Z} : g(\mathbf{z}) > b_j\}$, with $b_{j+1} > b_j$, such that $f_{\mathbf{z}}(\mathbf{z}|\bar{\mathcal{U}}_j) \propto f_{\mathbf{z}}(\mathbf{z})\mathbb{I}_{\bar{\mathcal{U}}_j}(\mathbf{z})$, $j = 1, \dots, m$. The term $f_{\mathbf{z}}(\mathbf{z})$ is to denote the probability model for \mathbf{z} . When the event $\bar{\mathcal{U}}_j$ holds, then $\{\bar{\mathcal{U}}_{j-1}, \dots, \bar{\mathcal{U}}_1\}$ also hold, and hence $P(\bar{\mathcal{U}}_j|\bar{\mathcal{U}}_{j-1}, \dots, \bar{\mathcal{U}}_1) = P(\bar{\mathcal{U}}_j|\bar{\mathcal{U}}_{j-1})$, so it follows that:

$$P(\bar{\mathcal{U}}) = P\left(\bigcap_{j=1}^m \bar{\mathcal{U}}_j\right) = P(\bar{\mathcal{U}}_1) \prod_{j=2}^m P(\bar{\mathcal{U}}_j|\bar{\mathcal{U}}_{j-1}) \quad (4.16)$$

where, for simpler notation, we use $P(\bar{\mathcal{U}}) \equiv P(\mathbf{z} \in \bar{\mathcal{U}})$ and $P(\bar{\mathcal{U}}_j|\bar{\mathcal{U}}_{j-1}) \equiv P(\mathbf{z} \in \bar{\mathcal{U}}_j|\mathbf{z} \in \bar{\mathcal{U}}_{j-1})$. In the last equation, $P(\bar{\mathcal{U}}_j|\bar{\mathcal{U}}_{j-1})$ is the conditional failure probability at the $(j-1)$ th conditional level. Observe that the probability $P(\bar{\mathcal{U}})$ may be relatively small, however it can be approximated by Subset Simulation as the product of larger conditional probabilities, thus avoiding simulation of rare events.

In the last equation, apart from $P(\bar{\mathcal{U}}_1)$ which can be readily estimated by the standard Monte Carlo method (MC), the remaining factors cannot be efficiently estimated because of the conditional sampling involved. However, MCMC methods can be used for sampling from the PDF $p(\mathbf{z}_{j-1}|\bar{\mathcal{U}}_{j-1})$ when $j \geq 2$, although it is at the expense of generating N dependent samples, giving:

$$P(\bar{\mathcal{U}}_j|\bar{\mathcal{U}}_{j-1}) \approx \bar{P}_j = \frac{1}{N} \sum_{n=1}^N \mathbb{I}_{\bar{\mathcal{U}}_j}(\mathbf{z}_{j-1}^{(n)}), \quad \mathbf{z}_{j-1}^{(n)} \sim f_{\mathbf{z}}(\mathbf{z}_{j-1}|\bar{\mathcal{U}}_{j-1}) \quad (4.17)$$

where $\mathbb{I}_{\bar{\mathcal{U}}_j}(\mathbf{z}_{j-1}^{(n)})$ is the indicator function for the region $\bar{\mathcal{U}}_j$, $j = 1, \dots, m$, such that $\mathbb{I}_{\bar{\mathcal{U}}_j}(\mathbf{z}_{j-1}^{(n)}) = 1$ when $g(\mathbf{z}_{j-1}^{(n)}) > b_j$, and 0 otherwise.

Observe that it is possible to obtain Markov chain samples that are generated at the $(j-1)$ th level which lie in $\bar{\mathcal{U}}_j$, so that they are distributed as $f_{\mathbf{z}}(\cdot|\bar{\mathcal{U}}_j)$. Hence they provide "seeds" for generating more samples according to $f_{\mathbf{z}}(\mathbf{z}|\bar{\mathcal{U}}_j)$ by using MCMC sampling. Because of the way the seeds are chosen, SS exhibits the benefits of *perfect sampling* [54, 65] which is an important feature to avoid wasting samples during a burn-in period, in contrast to other MCMC algorithms like MH algorithm.

As described further below, \bar{U}_j is actually chosen adaptively based on the samples $\{\mathbf{z}_{j-1}^{(n)}, n = 1, \dots, N\}$ from $f_z(\mathbf{z}|\bar{U}_{j-1})$ in such a way that there are exactly NP_0 of these seed samples in \bar{U}_j (so $\bar{P}_j = P_0$ in Equation 4.17). Then, a further $(1/P_0 - 1)$ samples are generated from $f_z(\mathbf{z}_j|\bar{U}_j)$ by MCMC starting at each seed, giving a total of N samples in \bar{U}_j . Repeating this process, one can compute the conditional probabilities of the higher-conditional levels until the final region $\bar{U}_m = \bar{U}$ has been reached. Note that the intermediate threshold value b_j defining \bar{U}_j is obtained in an adaptive manner as the $[(1 - N)P_0]$ th largest value among the values $g(\mathbf{z}_{j-1}^{(n)})$, $n = 1, \dots, N$, in such a way that the sample estimate of $P(\bar{U}_j|\bar{U}_{j-1})$ in Eq. (4.17) is equal to P_0 . See Figure 4.3 where the Subset Simulation method is illustrated using a toy example of dimension two. Panel (a) shows the initial set of samples which are i.i.d according to any specified PDF $f_z(\mathbf{z})$. Panels (b) and (c) show conditional samples distributed according to $f_z(\mathbf{z}|\bar{U}_j)$, $j = 1, 2$, respectively, using for representation increasing gray tones for the rings.

In Subset Simulation, the choice of an adequate P_0 has a significant impact on the efficiency of the algorithm. Indeed, a small value for the conditional probability ($P_0 \rightarrow 0$) makes that the distance between consecutive intermediate levels $b_j - b_{j-1}$ becomes too large, which leads to a rare-event simulation problem. If, on the contrary, the intermediate threshold values were chosen too close ($P_0 \rightarrow 1$), the algorithm would require more simulation levels m (and hence large computational effort) to progress towards \bar{U} . In the literature of Subset Simulation, several works have reported about the scaling strategies for P_0 . In the original presentation of Subset Simulation in [62], $P_0 = 0.1$ was recommended, and more recently in [65], the range $0.1 \leq P_0 \leq 0.3$ was found to be near optimal after a rigorous sensitivity study of Subset Simulation. In this thesis, $P_0 = 0.2$ is adopted following the recommendation in [66] by the author. For convenience of implementation, P_0 is chosen so that NP_0 and $1/P_0$ are positive integers.

As stated before, to draw samples from the conditional PDF $f_z(\mathbf{z}_j|\bar{U}_j)$, MCMC methods like Metropolis-Hastings [55] are adequate. In the original version of Subset Simulation [62], the modified Metropolis algorithm (MMA) was proposed that worked well for very high dimensions (e.g. 10^3 - 10^4), because the MH algorithm fails in this case [62]. Further insights for SS using MMA as conditional sampler are provided by Zuev *et al.* [65] where an exhaustive sensitivity study of MMA is presented along with enhancements for SS method, and more recently by Chiachio *et al.* [66], although the context there is about the use of SS for Approximate Bayesian Computation [67, 68].

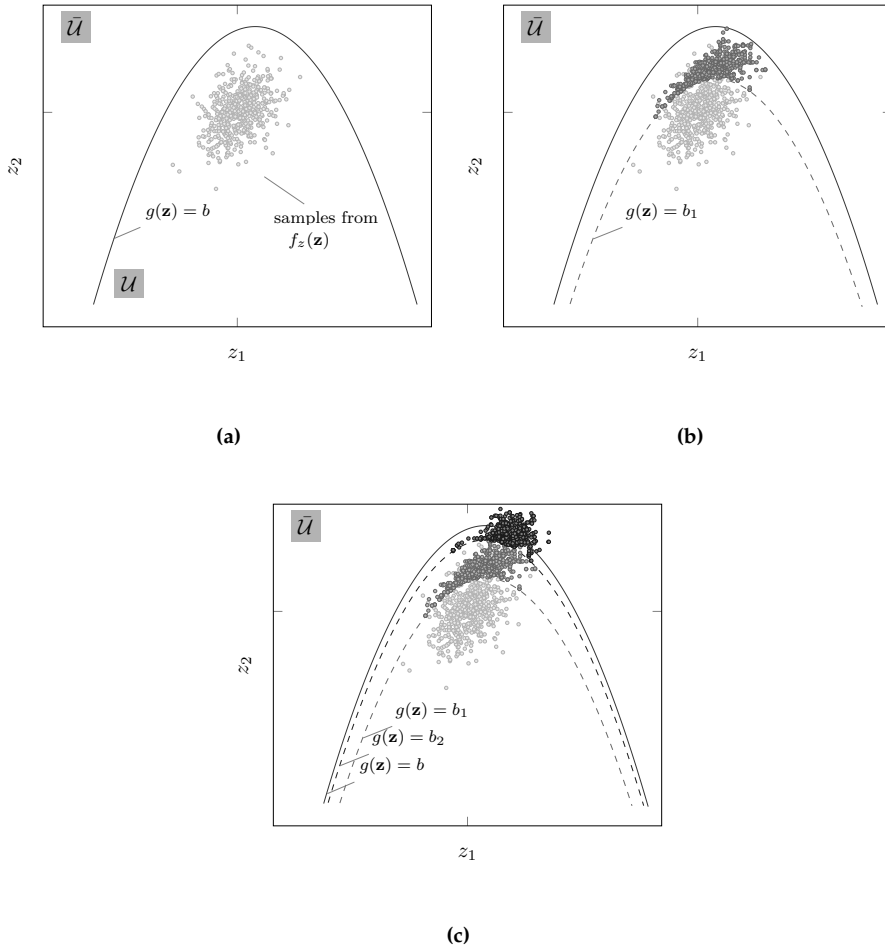


Figure 4.3: Conceptual two-dimensional example of Subset Simulation. Panel (a) shows the case where the \mathbf{z} -samples are drawn using the raw density $f_{\mathbf{z}}(\mathbf{z})$. In (b) & (c), samples are increasingly distributed in subsets according to $f_{\mathbf{z}}(\mathbf{z}|\bar{\mathcal{U}}_j)$, $j = 1, 2$, until the final region is reached. Note that each subset is represented using the same total amount of samples.

See Algorithm 2 for a pseudocode implementation, which is intended to be sufficient for most cases of application. The algorithm is implemented such that a fixed amount of N samples are drawn per simulation level $\bar{\mathcal{U}}_j$, so that $N_T = mN$, being N_T the total amount of model evaluations required by the algorithm to reach the final threshold. It is important to remark that the last does not imply any restriction but it allows controlling the computational burden.

Algorithm 2 Subset Simulation algorithm

Inputs:

$P_0 \in [0, 1]$ {gives percentile selection, chosen so $NP_0, 1/P_0 \in \mathbb{Z}^+$; $P_0 = 0.2$ is recommended}.

N , {number of samples per intermediate level}; m , {maximum number of simulation levels allowed}

Algorithm:

Sample $[\mathbf{z}_0^{(1)}, \dots, \mathbf{z}_0^{(n)}, \dots, \mathbf{z}_0^{(N)}]$, where $\mathbf{z} \stackrel{\text{i.i.d.}}{\sim} f_z(\mathbf{z})$

for $j : 1, \dots, m$ **do**

for $n : 1, \dots, N$ **do**

 Evaluate $g_j^{(n)} = g(\mathbf{z}_{j-1}^{(n)})$

end for

Sort $[\mathbf{z}_{j-1}^{(n)}, n : 1, \dots, N]$ so that $g_j^{(1)} \leq g_j^{(2)} \leq \dots \leq g_j^{(N)}$

Fix $b_j = \frac{1}{2} (g_j^{(NP_0)} + g_j^{(NP_0+1)})$

for $k = 1, \dots, NP_0$ **do**

 Select as a seed $\mathbf{z}_j^{(k),1} = \mathbf{z}_{j-1}^{(k)} \sim f_z(\mathbf{z}_j | \bar{\mathcal{U}}_j)$

 Run MMA [62] to generate $1/P_0$ states of a Markov chain lying in $\bar{\mathcal{U}}_j$:

$[\mathbf{z}_j^{(k),1}, \dots, \mathbf{z}_j^{(k),1/P_0}]$

end for

Renumber $[\mathbf{z}_j^{(k),i} : k = 1, \dots, NP_0; i = 1, \dots, 1/P_0]$ as $[\mathbf{z}_j^{(1)}, \dots, \mathbf{z}_j^{(N)}]$

if $b_j \leq b$ **then**

 End algorithm

end if

end for

In Subset Simulation, the variance of the local proposal PDF for a MCMC sampler has a significant impact on the speed of convergence of the algorithm [60, 61]. Optimal adaptive scaling strategies in Subset Simulation have been previously reported (e.g. [65]). To avoid duplication of literature for this technique, the method for the optimal choice of the variance along with the statistical properties of estimators are presented in a brief manner in the next section.

Statistical properties of estimators

Let denote by $\tilde{J}_{j,SS}$ an estimator for a quantity of interest $h : \mathcal{Z} \rightarrow \mathbb{R}$, which is obtained by simulated samples from the j th simulation level of Subset Simulation algorithm. Since each simulation level is compounded by MCMC samples, an

expression for the variance of the estimator can be written as follows [62]:

$$\mathbb{V}(\tilde{J}_{j,SS}) = \frac{R_j^{(0)}}{N} (1 + \gamma_j), \quad (4.18)$$

where

$$\gamma_j = 2 \sum_{\tau=1}^{N_s-1} \left(\frac{N_s - \tau}{N_s} \right) \frac{R_j^{(\tau)}}{R_j^{(0)}} \quad (4.19)$$

In the last equation, $R_j^{(0)} = \text{Var}(h(\mathbf{z}_j))$ and $N_s = 1/p_0$, the length of each of the Markov chains which are considered probabilistically equivalents [62]. The term $R_j^{(\tau)}$, $\tau = 0, 1, \dots, N_s - 1$ is the autocovariance of $h(\mathbf{z}_j)$ at lag τ , $R_j^{(\tau)} = \mathbb{E} \left[h(\mathbf{z}_j^{(1)}) h(\mathbf{z}_j^{(\tau+1)}) \right] - \bar{h}_j^2$, which can be estimated using the Markov chain samples $\{\mathbf{z}_j^{(k),i} : k = 1, \dots, N_c; i = 1, \dots, N_s\}$ as²:

$$R_j^{(\tau)} \approx \tilde{R}_j^{(\tau)} = \left[\frac{1}{N - \tau N_c} \sum_{k=1}^{N_c} \sum_{i=1}^{N_s-\tau} h(\mathbf{z}_j^{(k),i}) h(\mathbf{z}_j^{(k),\tau+i}) \right] - \bar{h}_j^2 \quad (4.20)$$

where $N_c = NP_0$, so that $N = N_c N_s$.

In view of Equation 4.18 the efficiency of the estimator \bar{h}_j is reduced when γ_j is high, therefore the optimal proposal variance σ_j^2 for simulation level j^{th} should be chosen so that to minimize γ_j . This configuration typically gives an acceptance rate \bar{r} for each simulation level in the range of 0.2-0.4 [65]. This is supported by the numerical experiments performed with the example in Section 9.3 and also in [66].

On the other hand, the choice of the conditional probability P_0 has also a significant influence on the number of intermediate simulation levels required by Subset Simulation, as mentioned in the last section. The higher the conditional probability P_0 is, the higher the number of simulation levels employed by the algorithm to reach the probability $P(\bar{U})$ for a fixed number of model evaluations (N) per simulation level. This necessarily increases the computational cost of the algorithm. At the same time, the smaller P_0 is, the higher the correlation between simulated trajectories, that is, the larger the values of γ_j in Equation

²It is assumed for simplicity in the analysis that the samples generated by the different N_c chains are uncorrelated under the quantity of interest h , although the samples are actually dependent because the seeds may be correlated. See further details in [62], Section 6.2.

4.18. Therefore, the choice of P_0 reflects a trade-off between computational efficiency and efficacy, in the sense of quality of the $\tilde{J}_{j,SS}$ estimator. This fact is examined below by adopting a fixed total number of samples, i.e. $N_T = mN$, where m is the number of conditional levels $m = \log P_{\tilde{u}} / \log P_0$. An optimal choice of P_0 is by minimizing the variance of the estimator $\tilde{J}_{j,SS}$ for the last simulation level:

$$\mathbb{V}(\tilde{J}_{j,SS}) = \frac{R_m^{(0)}}{N_T/m} (1 + \gamma_m) \propto m(1 + \gamma_m) = \frac{\log P(\tilde{U})}{\log P_0} (1 + \gamma_m) \quad (4.21)$$

Notice that for a fixed value of N_T , γ_m depends upon P_0 as it will be shown later for the numerical contributions. The value $P_0 = 0.2$ for Subset Simulation is also supported by [66] and by the numerical experiments performed in the examples in Chapter 9.

4.3 Basis of reliability calculation

To characterize the failure behavior of a component, subsystem or system in quantitative terms, it is necessary to evaluate the probability that the random variable \mathbf{z} lies within the failure region, formally defined as the subset of the outcome space where failure occurs, denoted as $\tilde{U} \subset \mathcal{Z}$. The following probability integral is defined:

$$P_f = P(\mathbf{z} \in \tilde{U}) = \int f_z(\mathbf{z}) \mathbb{I}_{\tilde{U}}(\mathbf{z}) d\mathbf{z} = \int_{\tilde{U}} f_z(\mathbf{z}) d(\mathbf{z}) \quad (4.22)$$

where $\mathbb{I}_{\tilde{U}}(\mathbf{z})$ is an indicator function that assigns 1 when $\mathbf{z} \in \tilde{U}$ and 0 otherwise. The failure region \tilde{U} can be defined by means of a performance function g as in Equation 4.46:

$$\tilde{U} = \{\mathbf{z} \in \mathcal{Z} : g(\mathbf{z}) > b\} \quad (4.23)$$

where $b \in \mathbb{R}$. In the reliability literature, the function $g(\mathbf{z})$ is widely termed as limit state function (LSF).

The evaluation of Equation 4.22 is difficult, especially if the dimension of \mathcal{Z} is large and the failure region \tilde{U} is far from the region of high probability content of $f_z(\mathbf{z})$. Numerical solutions are typically employed for its evaluation, among others, MC method, IS method, SS method [69]. The idea is to replace the generic quantity of interest $h(\mathbf{z})$ from the integrand of Equation 4.1 by the indicator function $\mathbb{I}_{\tilde{U}}(\mathbf{z})$. Observe that the estimator J in this case is just the failure probability estimate, i.e., P_f is estimated as a sample average of $\mathbb{I}_{\tilde{U}}(\mathbf{z})$ over samples of \mathbf{z} drawn from the PDF $f_z(\mathbf{z})$. All the concepts about quality and convergence of a sample estimate for P_f obtained using any of the methods explained in the last section, also apply here so they are not repeated again.

Other approaches have been proposed [69] in the literature that provide methods to analytically evaluate the Equation 4.1 under certain conditions, typically attributable to the random variables \mathbf{z} . These are presented in the next section in a concise way. There are additional reliability methods of special interest for composite applications which are covered in Chapter 5 under the format of a state-of-the-art.

4.3.1 Fast probability integration (FPI) methods

FPI methods rely on approximating the failure surface by a predetermined geometric form whereby the evaluation of the integral in the Equation 4.22 is practical [69]. The most probable point (MPP) is searched during the evaluation, over which the failure surface is approximated by such geometric form. The distance

between the origin and the MPP corresponds to the radius β of a hypersphere of dimension d beside the failure domain and tangent with it in the MPP. In the literature, this β value is referred to as *Reliability index* and it is equivalent to the distance from MPP to the origin in units of standard deviation, as shown in Figure 4.4. Within FPI methods, first order reliability methods (FORM) and second order reliability methods (SORM) are included.

First order reliability methods.

The first order reliability methods (FORM) use a linear approximation of the LSF in the vicinity of the MPP to obtain the β -index [70]. This method requires standard normal non-correlated variables, so that the vector of random variables \mathbf{z} should be transformed into standard non-correlated variables vector $\mathbf{u} \sim f_u(\mathbf{u})$ as,

$$\mathbf{u} = \phi^{-1}(F_z(\mathbf{z})) \quad (4.24)$$

where $F_z(\mathbf{z})$ is the CDF of \mathbf{z} and ϕ^{-1} is the inverse of the normal standard CDF. The reliability index β is then calculated as:

$$\beta = \min(\mathbf{u} \cdot \mathbf{u}^T)^{\frac{1}{2}} \quad (4.25)$$

which represents the Euclidean distance between the origin and the failure function $g(\mathbf{u})$ in the non-correlated normal standard space, as shown in Figure 4.4.

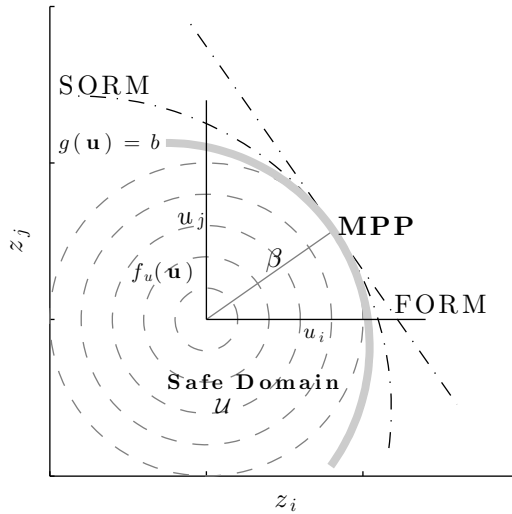


Figure 4.4: Schematic representation of FORM/SORM approximations.

If any correlation exists in the random variables, the Cholesky decomposition of the covariance matrix [71] may be used to transform from the real space to the non-correlated standard space. In case of non-normal variables, Rackwitz-Fiessler Method [72] can be employed. In case of correlated and non-normal variables, the Rosenblatt transformation is recommend [73, 74].

The PDF $f_u(\mathbf{u})$ integrated over the safe domain is found to be equal to the standard normal integral (distribution function) at β , therefore, the reliability R can be expressed as:

$$R = \Phi(\beta) \quad (4.26)$$

where the probability of failure is the complement,

$$P_f = 1 - R = 1 - \Phi(\beta) = \Phi(-\beta) \quad (4.27)$$

Second order reliability methods

To improve the accuracy of the β -index calculation beyond the approximation level achieved by FORM, additional information about the failure surface is required [69]. The second order reliability methods (SORM) use the β -index in conjunction with the second derivatives of $g(\mathbf{z})$ at MPP. The method is based on a general quadratic expansion of the failure hyper-plane $g(\mathbf{z})$ into a second order Taylor series over the MPP. Since the hyper-plane curvatures can be positive, negative or zero; parabolic, elliptic, or hyperbolic forms may result. This methodology requires complicated integrations that may restrict the applicability of SORM for certain reliability calculations [75]. Two simpler forms are extensively used in the literature for the quadratic approximation that are relatively simple for use: the rotational paraboloid and non-central hypersphere forms [72].

The rotational paraboloid approximation gives,

$$P_f \approx \int_0^\infty \Phi \left[\beta - \frac{t}{2r} \right] f_{\chi_{n-1}^2}(t) dt \quad (4.28)$$

where $f_{\chi_{n-1}^2}$ is the chi-square density function with n degrees of freedom and r is the radius of curvature, $r = 1/\kappa$. Analogously, the non-central hypersphere approximation gives,

$$P_f \approx 1 - \chi_{n,\delta}^2(r^2) \quad (4.29)$$

where $\chi_{n,\delta}^2(r^2)$ is the non-central Chi-Squared distribution with non-centrality parameter $\delta = [r - \beta]^2$.

First Order Second Moment Method

In this method only the mean and variance of uncertain variables \mathbf{z} along with the first-order Taylor's series expansion of $g(\mathbf{z})$ are used to calculate two moments (mean and variance) of the failure probability [76].

4.3.2 Reliability assessment in composite laminates.

Since a laminate can be viewed as a mechanical set of plies, whole laminate reliability may consider systems reliability. An accurate evaluation of laminate reliability is essential, overall all in those areas where reliability determines the final design of the composite structure.

In composites, Soares [77] presented an overview of system reliability methods used for laminates, and pointed out two main approaches: *the bounding and system reliability formulation* [78]. The former establishes an interval where the actual reliability value relies, whilst in system reliability, the progressive failure process of the full laminate is considered. The vast majority of authors use the bounding formulation for reliability calculation in composite laminates. Most of them, for simplification in a safe position, propose lower bound reliability using *first-ply-failure* (FPF) as LSF, which implies that the ply is considered as failure unit. To provide a basis for a discussion about this claim, its timely to consider the subject again in the form of fundamental concepts.

Bounding formulation

The starting point for such bounding formulation is the definition of the unit of failure as the unit statistically homogeneous for the failure. Two such units have been proposed: the ply units and modal units [78]. The former assumes that the individual plies are the failure units whereas in modal units, three potential modes of failure are recognized within each ply: longitudinal, transverse and shear, thus resulting in $3n$ individual units of failure for a laminate compounded by n plies.

The upper bound reliability limit considers that ultimate failure of the laminate will not occur until every individual unit had failed. Thus, the failure probability for the laminate is given by the product of failure probabilities corresponding to the individual units. This can be expressed in terms of reliability as follows:

$$R_{Uply} = 1 - \prod_{i=1}^n (1 - R_i) \quad \text{Non-Interactive} \quad (4.30a)$$

$$R_{Umodal} = 1 - \prod_{i=1}^n \prod_{j=1,2,6} R_{ij} \quad \text{Interactive} \quad (4.30b)$$

where R_i is the reliability of i th ply, and R_{ij} is the reliability of the j th mode failure of ply i .

As lower bound reliability, a series system formulation is proposed, so that the failure of the whole laminate is subject to the failure of the weakest unit. In reliability terms,

$$R_{Lply} = \prod_{i=1}^n R_i \quad \text{Non-Interactive} \quad (4.31a)$$

$$R_{Lmodal} = \prod_{i=1}^n \prod_{j=1,2,6} R_{ij} \quad \text{Interactive} \quad (4.31b)$$

with the same meaning for R_i and R_{ij} as described above. The most representative works that belong to the bounding approach are reviewed by Soares in [77]. Those up to [77] are introduced in the following paragraphs where some concluding remarks are extracted.

Kam *et al.* [79] used experimental distributions of FPF load for validation of different types of baseline PDFs over centrally loaded graphite-epoxy laminated composite plates with different stacking sequence. The failure data were compared with those obtained analytically using FEA for stress calculations, in both interactive and non interactive failure criteria. Results showed that, in general, differences between the experimental and theoretical distributions of FPF are small (less than 12%) irrespective of the types of PDFs used for modeling the lamina strength and FPF load.

More recently, Frangopol [80] presented a benchmark study of laminate failure probability by MC method considering the loads as random variables and FPF as failure criterion. Two main cases were studied: a single-layer laminate plate of graphite-epoxy and two-layers laminate plate of glass-epoxy, each one subjected to uniaxial and biaxial tension. In such cases, the material strength parameters were considered as deterministic, and the stresses as lognormal distributed random variables since no information on the type of distribution for

principal stresses was available for this study. An interesting conclusion was pointed out about the influence of additional plies on the reliability of composite laminates. In presence of new plies, the laminate does not necessarily increase its reliability but it depends on the fiber orientation and its thickness ratios. The special case of two orthogonal layers was studied, showing that the weakest more stressed lamina approximately determines the whole reliability, which implicitly supports the weakest link hypothesis (bounding formulation) in this specific case. Other results encountered up to Soares review [77] also use the bounding approach for system reliability calculation in composites [81–86].

System reliability formulation

In system reliability formulation, the step-by-step failure process of the laminate is considered. Note that the bounding formulation described above does not attempt to represent the whole failure process of the laminate, but just an interval where the desired reliability value relies. Although an attempt to precisely describe probabilistic failure of a laminate would be really impacting and necessary, the methodology of system reliability has been shortly explored in the literature.

In Yang *et al.* [87], a reliability analysis of a composite structural system was derived with consideration of stiffness degradation for a set of plies. Gurvich *et al.* [88] utilized a mesoscale approach for progressive failure of composite laminates with both in plane and bending loads, which call attention the search for computational efficiency by agreeing individual plies into sublaminates as whole failure units for the step-by-step process of failure. This author also made a comparative study to evaluate the differences between the bounding and system reliability formulation using data as benchmark for failure, and concluded that the bounding reliability formulation leads to lower failure probability values as the scatter in the strength parameters increases.

Wu *et al.* [89] proposed a micromechanical approach and accounted local load sharing and sizing effects. It was settled that the scale considered for the study conditions may influence the final result of reliability. Henceforth, exploring multiscale probabilistic failure seems to be an interesting way to derive a robust framework for progressive failure of composites.

4.4 Stochastic system modeling

Let us consider a generic component or subsystem whose state evolution³ can be modeled as:

$$\frac{dz}{dt} = \Upsilon(t, \mathbf{z}, \mathbf{u}, \mathbf{v}) \quad (4.32)$$

where Υ is a generic function of the time t , that establishes a deterministic relationship between a set of system inputs \mathbf{u} (e.g. loading and environmental conditions), the process noise \mathbf{v} (used to represent unmodeled uncertain variations in the system) and the own state \mathbf{z} . The function Υ should rigorously account for the uncertainty and accurately computes their effect on the state estimate, so that the state values can be represented using probability distributions.

Typically, state estimation is accomplished by periodical measurements of output variables through sensors, as essential part of the system health tracking. Then, in addition to the above state prediction model, the following measurement equation is adscribed:

$$\mathbf{y} = \psi(t, \mathbf{z}, \mathbf{u}, \mathbf{w}) \quad (4.33)$$

where ψ represents the mismatch between the model output Υ and measurements \mathbf{y} at time t as a function the states \mathbf{z} predicted from Equation 4.32, system inputs \mathbf{u} and measurement errors \mathbf{w} . By using recursively Equations 4.32 and 5.15a, the state estimate at time t can be obtained as shown below in the next section.

4.4.1 Bayesian state estimation

Many problems in a variety of areas of science like computational statistics, time series, signal processing, etcetera, can be stated as a discrete-time state-space model as follows:

$$\mathbf{x}_n = \Upsilon_n(\mathbf{x}_{n-1}, \mathbf{u}_n, \mathbf{v}_n, \theta) \quad (4.34a)$$

$$\mathbf{y}_n = \psi_n(\mathbf{x}_n, \mathbf{u}_n, \mathbf{w}_n, \theta) \quad (4.34b)$$

These difference equations are the discrete versions of Equations 4.32 and 4.33, respectively, by considering a sufficiently small time step $\Delta t \in \mathbb{R}$. The states $\mathbf{x}_n = \mathbf{x}(n \cdot \Delta t) \in \mathbb{R}^{n_x}$, $n \in \mathbb{N}$, are assumed to follow a hidden Markov process whilst the observations $\mathbf{y}_n = \mathbf{y}(n \cdot \Delta t) \in \mathbb{R}^{n_y}$ are assumed conditionally independent

³At this point, state-evolution refers to the variation-not necessarily monotonic-of any feature of interest, which can be monitored.

given the states \mathbf{x}_n . The discrete-time state-space model is accomplished with the uncertain variables $\mathbf{v}_n = \mathbf{v}(n \cdot \Delta t) \in \mathbb{R}^{n_v}$ and $\mathbf{w}_n = \mathbf{w}(n \cdot \Delta t) \in \mathbb{R}^{n_w}$ to account for model error and measurement error, respectively.

The function $\Upsilon_n : \mathbb{R}^{n_x} \times \mathbb{R}^{n_u} \times \mathbb{R}^{n_v} \times \mathbb{R}^{n_\theta} \rightarrow \mathbb{R}^{n_x}$ represents the transition equation for the sequence of states $\{\mathbf{x}_n, n \in \mathbb{N}\}$, $\mathbf{x}_n \in \mathcal{X} \subset \mathbb{R}^{n_x}$, whose initial distribution is known and equal to $p(\mathbf{x}_0)$. Here \mathcal{X} is the region of all possible state outcomes predicted according to Υ_n . The function $\psi_n : \mathbb{R}^{n_x} \times \mathbb{R}^{n_u} \times \mathbb{R}^{n_w} \times \mathbb{R}^{n_\theta} \rightarrow \mathbb{R}^{n_y}$ is the likelihood of the observations. Both Υ_n and ψ_n are possibly nonlinear functions that may depend on a set of model parameters $\boldsymbol{\theta} \in \Theta \subset \mathbb{R}^{n_\theta}$ along with input parameters to the system at time n , $\mathbf{u}_n = \mathbf{u}(n \cdot \Delta t) \in \mathbb{R}^{n_u}$. Hereinafter, time index will be denoted by $n \in \mathbb{N}$.

Let us now define the augmented state $\mathbf{z}_n = (\mathbf{x}_n, \boldsymbol{\theta})$ in the joint state-parameter space $\mathcal{Z} = \Theta \times \mathcal{X} \subset \mathbb{R}^{n_\theta + n_x}$, so that $p(\mathbf{z}_n) = p(\mathbf{x}_n|\boldsymbol{\theta})p(\boldsymbol{\theta})$.

The main goal of Bayesian state estimation is to recursively estimate the PDF of the state \mathbf{z}_n given the measurements up to time n , $\mathbf{y}_{0:n} = \{\mathbf{y}_0, \dots, \mathbf{y}_{n-1}, \mathbf{y}_n\}$, which is expressed as $p(\mathbf{z}_n|\mathbf{y}_{0:n})$. Two steps are required for the Bayesian state estimation: the *prediction* of $p(\mathbf{z}_n|\mathbf{y}_{0:n-1})$ and *updating* to $p(\mathbf{z}_n|\mathbf{y}_{0:n})$, that follow the Total Probability Theorem and Bayes' Theorem, respectively⁴:

$$p(\mathbf{z}_n|\mathbf{y}_{0:n-1}) = \int_{\mathcal{Z}} p(\mathbf{x}_n|\mathbf{x}_{n-1}, \boldsymbol{\theta}) \underbrace{p(\mathbf{x}_{n-1}|\boldsymbol{\theta}, \mathbf{y}_{0:n-1})p(\boldsymbol{\theta}|\mathbf{y}_{0:n-1})}_{p(\mathbf{x}_{n-1}, \boldsymbol{\theta}|\mathbf{y}_{0:n-1})} d\mathbf{x}_n d\boldsymbol{\theta} \quad (4.35a)$$

$$\begin{aligned} p(\mathbf{z}_n|\mathbf{y}_{0:n}) &= \frac{p(\mathbf{y}_n|\mathbf{z}_n)p(\mathbf{z}_n|\mathbf{y}_{0:n-1})}{\int_{\mathcal{Z}} p(\mathbf{y}_n|\mathbf{z}_n)p(\mathbf{z}_n|\mathbf{y}_{0:n-1})d\mathbf{z}_n} \\ &= \frac{p(\mathbf{y}_n|\mathbf{z}_n)p(\mathbf{z}_n|\mathbf{y}_{0:n-1})}{p(\mathbf{y}_n|\mathbf{y}_{0:n-1})} \end{aligned} \quad (4.35b)$$

In the last equations, it is assumed that the PDFs for \mathbf{v}_n and \mathbf{w}_n are prescribed and also that the PDF of the initial state is known in advance $p(\mathbf{z}_0|\mathbf{y}_0) \equiv p(\mathbf{z}_0)$ (note that \mathbf{y}_0 is not a measurement). When the interest is instead in obtaining the PDF of the history of states up to time n , $\mathbf{z}_{0:n}$, Bayes' Theorem can be used to deal with the posterior PDF as:

$$p(\mathbf{z}_{0:n}|\mathbf{y}_{0:n}) = p(\mathbf{z}_{0:n}|\mathbf{y}_n, \mathbf{y}_{0:n-1}) \quad (4.36a)$$

$$\propto p(\mathbf{y}_n|\mathbf{z}_{0:n}, \mathbf{y}_{0:n-1})p(\mathbf{z}_{0:n}|\mathbf{y}_{0:n-1}) \quad (4.36b)$$

$$\propto p(\mathbf{y}_n|\mathbf{z}_n)p(\mathbf{z}_n|\mathbf{z}_{n-1})p(\mathbf{z}_{0:n-1}|\mathbf{y}_{0:n-1}) \quad (4.36c)$$

⁴For simpler notation the conditioning on the model input \mathbf{u}_n is dropped from Eq. (4.34).

In the equations 4.35 and 4.36, it is used the fact that $p(\mathbf{y}_n | \mathbf{z}_{0:n}, \mathbf{y}_{0:n-1}) = p(\mathbf{y}_n | \mathbf{z}_n)$ and that $p(\mathbf{z}_n | \mathbf{z}_{0:n-1}, \mathbf{y}_{0:n-1}) = p(\mathbf{z}_n | \mathbf{z}_{n-1})$, since Equation 4.34a describes a Markov model of order one.

A key problem that typically arises when sequentially updating the state vector $\mathbf{z}_{0:n} = (\mathbf{x}_{0:n}, \boldsymbol{\theta})$ as an augmented state is the non-dynamics nature of $\boldsymbol{\theta}$, which makes it difficult to explore the $\boldsymbol{\theta}$ -space except for the first time index. A common solution is to add small random perturbations to $\boldsymbol{\theta}$ (e.g., zero-mean Gaussian) under the last posterior PDF at time $n - 1$, before evolving to the next predicted state at time n :⁵

$$\boldsymbol{\theta}_n \sim p(\boldsymbol{\theta} | \boldsymbol{\theta}_{n-1}) = \mathcal{N}(\boldsymbol{\theta}_{n-1}, \Sigma_{\xi_n}) \quad (4.37)$$

where $\Sigma_{\xi_n} \in \mathbb{R}^{n_\theta \times n_\theta}$ is a specified covariance matrix. Observe that by this method, the model parameters are virtually time-evolving although they are essentially not dependent on time. This time-varying imposes a loss of information in $\boldsymbol{\theta}$ over time as additional uncertainties are artificially added to the parameters, which ultimately influences the precision of the filtering. There exist several works in the literature providing the basis to overcome this drawback, with the most popular being those that employ sufficient statistics [90, 91] and optimal kernel smoothing of particles [92, 93]. More recently, an efficient method of this class has been proposed by M. Daigle and K. Goebel [94], which consists in modifying the variance of the random walk by adding a negative scalar proportional to the relative distance between the actual and the target spread of the marginal posterior PDF of the j th component of model parameter $\boldsymbol{\theta}_n = [\theta_{n,1}, \dots, \theta_{n,j}, \dots, \theta_{n,n_\theta}]$, denoted by $p(\theta_{n,j} | y_{0:n})$, as follows:

$$\sigma_{\xi_{n,j}}^2 = \sigma_{\xi_{n-1,j}}^2 \left(1 - P_j^* \frac{\text{RMAD}(\theta_{n,j}) - \text{RMAD}_j^*}{\text{RMAD}(\theta_{n,j})} \right) \quad (4.38)$$

In the last equation, $\sigma_{\xi_{n,j}}^2$ is the variance of the proposal PDF for $\theta_{n,j}$. $\text{RMAD}(\theta_{n,j})$ is the *relative median absolute deviation* of $p(\theta_{n,j} | y_{0:n})$, RMAD_j^* is the target RMAD for $p(\theta_{n,j} | y_{0:n})$. The factor $P_j^* \in [0, 1]$ is a scaling constant to control the speed of convergence to RMAD_j^* . In [94] a comprehensive discussion to optimally

⁵Hereinafter, $\boldsymbol{\theta}_n$ denotes that the information for $\boldsymbol{\theta}$ is from the PDF at time n . Analogously, $\boldsymbol{\theta}_{0:n}$ is to denote the accumulated posterior information about $\boldsymbol{\theta}$ up to time n . Recall that $\boldsymbol{\theta}$ is not dependent on time.

choose P_j^* and $RMAD_j^*$ is provided. The term $RMAD(\theta_{n,j})$ can be readily calculated using K samples from the marginal posterior at current time n , $\tilde{\theta}_{n,j} = \{\theta_{n,j}^{(1)}, \dots, \theta_{n,j}^{(k)}, \dots, \theta_{n,j}^{(K)}\} \sim p(\theta_{n,j} | \mathbf{y}_{0:n})$, as follows:

$$RMAD(\theta_{n,j}) = \frac{\text{median} \left(\left\{ |\theta_{n,j}^{(k)} - \text{median}(\tilde{\theta}_{n,j})| \right\}_{k=1}^K \right)}{\text{median}(\tilde{\theta}_{n,j})} \quad (4.39)$$

4.4.2 Sequential Monte Carlo for state and parameter estimation

The filtering methodology exposed above requires the evaluation of multi-dimensional integrals of the type occurring in Equations 4.35, which are usually intractable except some especial linear cases with Gaussian uncertainties [95]. An alternative for the general case of both non-linear and non-Gaussian state-space models is to use particle methods, a set of sequential Monte-Carlo methods which provide samples approximately distributed according to the target PDF $p(\mathbf{x}_{0:n}, \theta_{0:n} | \mathbf{y}_{0:n})$, $n \in \mathbb{N}$, with a feasible computational burden [96, 97]. Particle filters (PF) [98] are one of the most common techniques among particle methods for filtering [18] and prognostics [22]. With PF, a set of N discrete particle paths, namely $\{\mathbf{z}_{0:n}^{(i)} = (\mathbf{x}_{0:n}^{(i)}, \theta_{0:n}^{(i)})\}_{i=1}^N$, are readily sampled from a convenient importance distribution $q(\mathbf{z}_{0:n} | \mathbf{y}_{0:n})$ and further used to obtain an approximation for the required posterior PDF as:

$$p(\mathbf{z}_{0:n} | \mathbf{y}_{0:n}) \approx \sum_{i=1}^N \hat{\omega}_n^{(i)} \delta(\mathbf{z}_{0:n} - \mathbf{z}_{0:n}^{(i)}) \quad (4.40)$$

where $\hat{\omega}_n^{(i)}$ is the unnormalized importance weight for the i th particle

$$\hat{\omega}_n^{(i)} = \frac{p(\mathbf{z}_{0:n}^{(i)} | \mathbf{y}_{0:n})}{q(\mathbf{z}_{0:n}^{(i)} | \mathbf{y}_{0:n})} \quad (4.41)$$

It is demonstrated that the approximation in Equation 4.40 is asymptotically unbiased if \mathcal{Z} , the support region for $p(\mathbf{z}_{0:n} | \mathbf{y}_{0:n})$, is a subset of that for $q(\mathbf{x}_{0:n} | \mathbf{y}_{0:n})$ [99]. In addition, for practical reasons, the PDF $q(\mathbf{z}_{0:n} | \mathbf{y}_{0:n})$ is chosen so that it admits a sampling procedure by choosing $q(\mathbf{z}_{0:n} | \mathbf{y}_{0:n}) = q(\mathbf{x}_{0:n} | \mathbf{y}_{0:n-1})$, hence it can be factorized in a form similar to that of the target posterior PDF, i.e., $q(\mathbf{z}_{0:n} | \mathbf{y}_{0:n}) = q(\mathbf{z}_{0:n-1} | \mathbf{y}_{0:n-1})q(\mathbf{z}_n | \mathbf{z}_{n-1})$. By substituting Equation 4.36 into Equation 4.41 and also by using the last cited condition for the importance PDF,

the unnormalized importance weight for the i th particle at time n can then be rewritten as:

$$\hat{\omega}_n^{(i)} \propto \frac{p(\mathbf{x}_{0:n-1}^{(i)}, \boldsymbol{\theta}_{0:n-1}^{(i)} | \mathbf{y}_{0:n-1})}{\underbrace{q(\mathbf{x}_{0:n-1}^{(i)}, \boldsymbol{\theta}_{0:n-1}^{(i)} | \mathbf{y}_{0:n-1})}_{\hat{\omega}_{n-1}^{(i)}}} \frac{p(\mathbf{x}_n^{(i)} | \mathbf{x}_{n-1}^{(i)}, \boldsymbol{\theta}_{n-1}^{(i)}) p(\mathbf{y}_n | \mathbf{x}_n^{(i)}, \boldsymbol{\theta}_n^{(i)})}{q(\mathbf{x}_n^{(i)} | \mathbf{x}_{n-1}^{(i)}, \boldsymbol{\theta}_n^{(i)})} \quad (4.42)$$

where the joint state \mathbf{z} is decomposed into its two components $(\mathbf{x}, \boldsymbol{\theta})$ for better comprehension of the weight calculation method. Guidelines on how to best select $q(\mathbf{x}_n | \mathbf{x}_{n-1}, \boldsymbol{\theta}_{n-1})$ are well known in the literature [18]. An often followed strategy is to use the conditional distribution $p(\mathbf{x}_n | \mathbf{x}_{n-1}, \boldsymbol{\theta}_{n-1})$ from the transition equation in 4.34a [19] since it is straightforward to evaluate. By means of this, the expression for the i th unnormalized particle weight yields:

$$\hat{\omega}_n^{(i)} = \hat{\omega}_{n-1}^{(i)} p(\mathbf{y}_n | \mathbf{z}_n^{(i)}) = \hat{\omega}_{n-1}^{(i)} p(\mathbf{y}_n | \mathbf{x}_n^{(i)}, \boldsymbol{\theta}_n^{(i)}) \quad (4.43)$$

Observe from last equation that the weight values are known only up to a scaling factor, which can be bypassed by normalization: $\omega_n^{(i)} = \hat{\omega}_n^{(i)} / \sum_{i=1}^N \hat{\omega}_n^{(i)}$, where $\omega_n^{(i)}$ denotes the normalized value of the i th particle at time n . A pseudocode implementation for the PF is given in Algorithm 3, which includes a systematic resampling step [100] to limit the well-known degeneracy problem⁶. The approach by M. Daigle and K. Goebel [94] is adopted for parameter regeneration.

4.4.3 ℓ -step ahead prediction

Using the most up-to-date information of the system, $p(\mathbf{z}_n | \mathbf{y}_{0:n})$, the PDF of the ℓ -step ahead prediction of states, namely $p(\mathbf{z}_{n+\ell} | \mathbf{y}_{0:n})$, can be obtained by Total Probability theorem as:

$$\begin{aligned} p(\mathbf{z}_{n+\ell} | \mathbf{y}_{0:n}) &= \int_{\mathcal{Z}} p(\mathbf{z}_{n+\ell} | \mathbf{z}_{n:n+\ell-1}) p(\mathbf{z}_{n:n+\ell-1} | \mathbf{y}_{0:n}) d\mathbf{z}_{n:n+\ell-1} \\ &= \int_{\mathcal{Z}} \left[\prod_{t=n+1}^{n+\ell} p(\mathbf{z}_t | \mathbf{z}_{t-1}) \right] p(\mathbf{z}_n | \mathbf{y}_{0:n}) d\mathbf{z}_{n:n+\ell-1} \end{aligned} \quad (4.44)$$

where we use the fact that the factors $p(\mathbf{z}_{n+\ell} | \mathbf{z}_{n:n+\ell-1}) = p(\mathbf{z}_{n+\ell} | \mathbf{z}_{n+\ell-1})$, $\ell \in \mathbb{N} > 1$, since Equation 4.34a defines a Markov model of order one and also by the assumption that the observations are conditionally independent given the

⁶During resampling, particles are either dropped or reproduced that may result in a loss of diversity of the particle paths [18]. If necessary, a control step of degeneracy by quantifying the effective sample size (ESS) [101] may be incorporated before the resampling.

Algorithm 3 PF with on-line parameter updating

inputs: N , {number of particles per time step} N_T , {threshold of effective sample size (ESS)} $\Sigma_{\xi_0} = \text{diag}(\sigma_{\xi_{0,1}}^2, \sigma_{\xi_{0,2}}^2, \dots, \sigma_{\xi_{0,n_\theta}}^2)$, {initial covariance for artificial dynamics} $RMAD_j^*$, {target RMAD for j th component of θ } P_j^* , {to control speed of convergence to $RMAD_j^*$ }**Algorithm:**Initialize $\left[(\theta_0^{(1)}, \mathbf{x}_0^{(1)}), \dots, (\theta_0^{(i)}, \mathbf{x}_0^{(i)}), \dots, (\theta_0^{(N)}, \mathbf{x}_0^{(N)}) \right]$, where $(\theta, \mathbf{x}) \sim p(\theta)p(\mathbf{x}|\theta)$ Assign the initial unnormalized weights: $\{\hat{\omega}_0^{(i)} = p(\mathbf{y}_0|\mathbf{x}_0^{(i)}, \theta^{(i)})\}_{i=1}^N$ At $n \geq 1$ {time n evolves as new data point arrives}**for** $i = 1$ to N **do**Sample $\theta_n^{(i)} \sim p(\theta_n|\theta_{n-1}^{(i)})$ and $\mathbf{x}_n^{(i)} \sim p(\mathbf{x}_n|\mathbf{x}_{n-1}^{(i)}, \theta_n^{(i)})$ Set $\mathbf{z}_n^{(i)} = (\mathbf{x}_n^{(i)}, \theta_n^{(i)})$ and $\mathbf{z}_{0:n}^{(i)} = (\mathbf{x}_{0:n}^{(i)}, \theta_{0:n}^{(i)})$.Update the weight $\hat{\omega}_n^{(i)} = \omega_{n-1}^{(i)} p(\mathbf{y}_n|\mathbf{z}_n^{(i)})$ **end for****for** $i = 1$ to N **do**Normalize weights $\omega_n^{(i)} = \frac{\hat{\omega}_n^{(i)}}{\sum_{i=1}^N \hat{\omega}_n^{(i)}}$ **end for****for** $j = 1$ to n_θ **do**Sample $\{\hat{\theta}_{n,j}^{(k)}\}_{k=1}^K \sim p(\theta_{n,j}|\mathbf{y}_{0:n}) \approx \sum_{k=1}^K \omega_n^{(k)} \delta(\theta_{n,j} - \hat{\theta}_{n,j}^{(k)})$ Compute $RMAD(\theta_{n,j})$ according to Eq. 4.39Update variance of random walk: $\sigma_{\xi_{n,j}}^2 = \sigma_{\xi_{n-1,j}}^2 \left(1 - P_j^* \frac{RMAD(\theta_{n,j}) - RMAD_j^*}{RMAD(\theta_{n,j})} \right)$ **end for**set $\Sigma_{\xi_n} = \text{diag}(\sigma_{\xi_{n,1}}^2, \dots, \sigma_{\xi_{n,n_\theta}}^2)$ **if** $EES < N_T$ **then**Resampling of N particles according to weights $\omega_n^{(i)}$, $i = 1, \dots, N$.Set $\omega_n^{(i)} = 1/N$, $i = 1, \dots, N$.**end if**

states. Replacing $p(\mathbf{z}_n | \mathbf{y}_{0:n})$ in the last equation by its PF approximation obtained from Equation 4.40, we obtain:

$$\begin{aligned}
p(\mathbf{z}_{n+\ell} | \mathbf{y}_{0:n}) &\approx \int_{\mathcal{Z}} \sum_{i=1}^N p(\mathbf{z}_{n+1} | \mathbf{z}_n^{(i)}) \hat{\omega}_n^{(i)} \delta(\mathbf{z}_n - \mathbf{z}_n^{(i)}) \prod_{t=n+2}^{n+\ell} p(\mathbf{z}_t | \mathbf{z}_{t-1}) d\mathbf{z}_{n+1:n+\ell-1} \\
&= \sum_{i=1}^N \hat{\omega}_n^{(i)} \int_{\mathcal{Z}} p(\mathbf{z}_{n+1} | \mathbf{z}_n^{(i)}) \prod_{t=n+2}^{n+\ell} p(\mathbf{z}_t | \mathbf{z}_{t-1}) d\mathbf{z}_{n+1:n+\ell-1}
\end{aligned} \tag{4.45}$$

which corresponds to a weighted sum of integrals. Note that each integral can be readily evaluated by extending the i th trajectory $\mathbf{z}_{0:n}^{(i)} \rightarrow \mathbf{z}_{n:n+\ell}^{(i)}$, $i = 1, \dots, N$ using recursively the transition equation in 4.34a i.e., $\mathbf{z}_t^{(i)} \sim p(\mathbf{z}_t | \mathbf{z}_{t-1}^{(i)})$ and $\mathbf{z}_{0:t}^{(i)} = (\mathbf{z}_{0:t-1}^{(i)}, \mathbf{z}_t^{(i)})$, $t = n+1, \dots, n+\ell \in \mathbb{N}$.

4.5 Prognostics problem formulation

Prognostics is the science of determining the *end of life* (EOL) and *remaining useful life* (RUL) predictions of components and subsystems given the information about the current state along with a set of inputs (loads and environmental conditions). In prognostics, the EOL is understood as the limiting time when an asset or property is expected to leave the serviceability conditions. The RUL is, though, the period of time remaining from the current time (or time of prediction) until the EOL.

Technically speaking, prognostics is a natural extension of structural health monitoring (SHM) in the sense that the decisions are made based on predictions that are timely updated using data from a sensing system. It is rather a continuous process of *updating-predicting-reassessment* where the user is not only concerned with detecting, isolating and sizing a fault mode but also (a) predicting the remaining time before the failure occurs; and (b) quantifying the uncertainty in the prediction to be further used for risk assessment and rational rescheduling. Henceforth, prognostics requires periodical measurement updates to increasingly improve the predictions of EOL and RUL. Consequently, suitable SHM sensors that can interrogate in real time the system and assess any change in fault severity are of paramount importance for prognostics. Ground-based non-destructive evaluation inspections can also provide valuable trending information, however, the focus on prognostics today is on automated technologies that make use of permanently installed sensors built into the component or subsystem [102].

It is important to remark that techniques and methodologies for prognostics are application-specific [103] and hence global solutions for specific problems are rarely available. In fact, designing a prognostics framework requires (in a broad sense): (a) the choice of an adequate sensing method capable to provide health information given the practical constraints of the specific application, (b) the development of an ad-hoc probabilistic formulation for prediction, uncertainty quantification and management in the context of condition-based monitoring to the system. The following sections overview both aspects of prognostics.

4.5.1 Prognostics and SHM

Since measurements are periodically incorporated into the prognostics framework, the higher the precision and accuracy expected from prognostics, the better the quality required for the information from the sensing system. However, this

information comes with a price for more targeted sensing and significant computational requirements. Complex systems subject to a variety of fault modes (cracks, voids, delamination, corrosion, etc.), often require dedicated sensors and sensor networks for detection as no one sensor type can cover all.

The choice of the sensing methods is typically guided by the feature or set of features to be tracked. For example weight loss or power demand sensors on-board airspace systems results in a different sensor choice than for monitoring vibrations in buildings or corrosion in bridge structures [102, 103]. Therefore, an adequate SHM project should be viewed as connected component for prognostics.

Sensor locations are chosen such that the feature being monitored contains statistically significant information, so that the better the quality of the information from measurements, the higher the precision and accuracy expected from prognostics, as will be seen further below. There are well-known methods for optimal placement of sensors that consider the uncertainty in both measurements and model response (see for example [104]).

In this thesis, the SHM method for on-line monitoring the health is predetermined, such that the methodological contributions of prognostics are proposed from this standpoint.

4.5.2 Calculation of EOL and RUL

For the estimation of EOL and RUL at a certain time-instant n , it is necessary to consider the following elements:

- I updated state estimate at the current time n using the information from most up-to date measurements;
- II forward model that might be parameterized by a set of model parameters to quantify model uncertainty;
- III estimation of inputs at future time instants $t \geq n$;
- IV estimation of process noise (including both model errors and measurement errors) for future instants $t \geq n$.

Figure 4.5 shows a conceptual scheme for prognostics, which is intended to provide a general viewpoint of the RUL calculation. Note that RUL becomes a functionally dependent estimation of the above quantities which are, in principle, uncertain. The consideration of uncertainty within the prognostics is not a trivial task even when the forward propagation models are linear and the uncertain variables follow Gaussian distributions [38, 105]. This is because the combination

of the cited uncertain quantities within a fault propagation model will generally render a non-linear function of the predicted states [106]. Hence analytical methods for prognostics are very limited and often intractable in real life applications [37, 107]. Sampling-based algorithms (e.g. *particle filters* (PF)) [18, 19] are best-suited in prognostics to efficiently approximate the information of predicted states (which is obtained in the form of a PDF) through a limited set of discrete particle paths representing random trajectories of system evolution in the state space [20–22]. The next section presents a PF-based prognostics framework, which is widely used in the literature for its versatility and ease of implementation. A pseudocode implementation of the PF-based algorithm for EOL/RUL calculation is presented in next section which uses as inputs the information from the Algorithm 3.

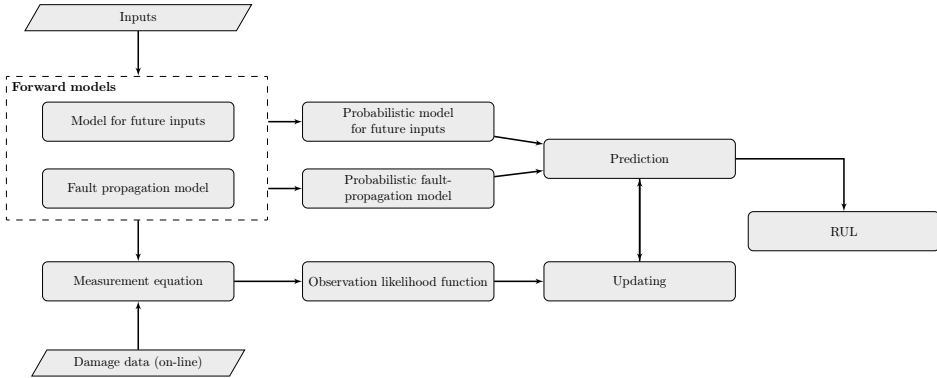


Figure 4.5: Schematic representation of RUL calculation.

4.5.3 Filtering-based prognostics

The role of prognostics algorithms is to efficiently apply the fault propagation model into future instants with consideration of future inputs as well as the overall uncertainty. With PF, it is possible to project in time the filtered state $p(\mathbf{z}_n | \mathbf{y}_{0:n})$ in absence of new observations, which is achieved by using the state transition equation 4.34a in a recursive manner. As final outcome, the ℓ -step ahead prediction of state PDF based on the information at current time n , namely $p(\mathbf{z}_{n+\ell} | \mathbf{y}_{0:n})$, is obtained [22].

To compute the RUL based on the predicted states $p(\mathbf{z}_{n+\ell} | \mathbf{y}_{0:n})$, the existence of a *useful domain* for the predicted states is first required. Let $\mathcal{U} \subset \mathcal{Z}$ be the non-empty subset of authorized states of our system, whereas the complementary subset $\bar{\mathcal{U}} = \mathcal{Z} \setminus \mathcal{U}$, is the subset of states where the system behavior becomes

unacceptable, or simply, where system failure occurs. With no loss of generality, we can alternatively define $\bar{\mathcal{U}}$ as the region of states where a performance function $g : \mathcal{Z} \rightarrow \mathbb{R}$ exceeds some specified threshold level b :

$$\bar{\mathcal{U}} \equiv \{\mathbf{z} \in \mathcal{Z} : g(\mathbf{z}) > b\} \quad (4.46)$$

Using the PF approach for prognostics defined above, the EOL predicted from time n can be obtained for the i th particle trajectory as the time index of the first-passage point into $\bar{\mathcal{U}}$, or in other words, the earliest time index t at which the event $\mathbf{z}_t^{(i)} \in \bar{\mathcal{U}}$ occurs. It can be computed as:

$$\text{EOL}_n^{(i)} = \inf\{t \in \mathbb{N} : t \geq n \wedge \mathbb{I}_{(\bar{\mathcal{U}})}(\mathbf{z}_t^{(i)}) = 1\} \quad (4.47)$$

where $\mathbb{I}_{(\bar{\mathcal{U}})} : \mathcal{Z} \rightarrow \{0, 1\}$ is an indicator function that maps a given point in \mathcal{Z} to the Boolean domain $\{0, 1\}$ as follows:

$$\mathbb{I}_{(\bar{\mathcal{U}})}(\mathbf{z}) = \begin{cases} 1, & \text{if } \mathbf{z} \in \bar{\mathcal{U}} \\ 0, & \text{if } \mathbf{z} \in \mathcal{U} \end{cases} \quad (4.48)$$

The RUL predicted from time n for the i th particle trajectory can be obtained using $\text{EOL}_n^{(i)}$ as:

$$\text{RUL}_n^{(i)} = \text{EOL}_n^{(i)} - n \quad (4.49)$$

Figure 4.6 provides an schematic illustration to exemplify the trajectory of the i th particle of a general \mathbf{z} -state of dimension two (for simplicity of representation) along with the indication of $\text{EOL}_n^{(i)}$ and $\text{RUL}_n^{(i)}$.

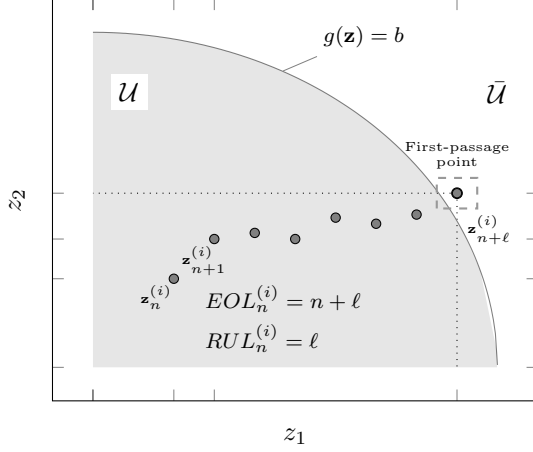


Figure 4.6: Conceptual illustration of a two-dimensional example of i th particle trajectory to EOL. Solid disks represent samples in \mathcal{Z} .

By repeating the process for each particle $i = 1, \dots, N$, an approximation to the PDF of EOL at time n can be obtained as:

$$p(\text{EOL}_n | \mathbf{y}_{0:n}) \approx \sum_{i=1}^N \omega_n^{(i)} \delta(\text{EOL}_n - \text{EOL}_n^{(i)}) \quad (4.50)$$

Similarly, the PDF of RUL_n can be approximated as:

$$p(\text{RUL}_n | \mathbf{y}_{0:n}) \approx \sum_{i=1}^N \omega_n^{(i)} \delta(\text{RUL}_n - \text{RUL}_n^{(i)}) \quad (4.51)$$

An algorithmic description of the prognostics procedure is provided as Algorithm 4. A companion conceptual scheme is provided in Figure 4.7 to better understand the PF-based prognostics framework.

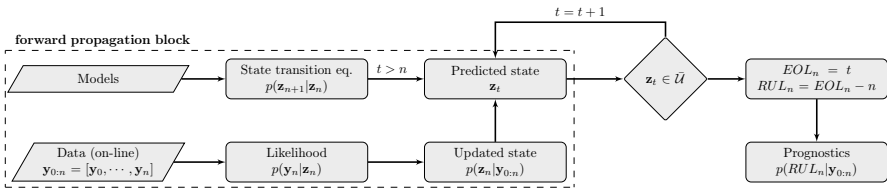


Figure 4.7: Conceptual scheme of a PF-based prognostics framework.

Algorithm 4 PF-based prognostics algorithm

```
1: inputs:  
    $\{ \mathbf{z}_n^{(i)} = (\mathbf{x}_n^{(i)}, \boldsymbol{\theta}_n^{(i)}), \omega_n^{(i)} \}_{i=1}^N$ , {updated particles at time  $n$ . Use e.g. Algorithm 3}  
2:  $\mathcal{U} \subset \mathcal{Z}$ , {useful domain}  
3: for  $i = 1$  to  $N$  do  
4:    $t \leftarrow n$   
5:    $\mathbf{z}_t^{(i)} \leftarrow \mathbf{z}_n^{(i)}$   
6:   Evaluate  $EOL_n^{(i)}(\mathbf{z}_t^{(i)})$   
7:   while  $\mathbb{I}_{(\mathcal{U})}(\mathbf{z}_t^{(i)}) = 0$  do  
8:     predict  $\mathbf{u}_t$   
9:     Sample  $\boldsymbol{\theta}_{t+1}^{(i)} \sim p(\boldsymbol{\theta}_{t+1} | \boldsymbol{\theta}_t^{(i)})$   
            $\mathbf{x}_{t+1}^{(i)} \sim p(\mathbf{x}_{t+1} | \mathbf{x}_t^{(i)}, \boldsymbol{\theta}_{t+1}^{(i)}, \mathbf{u}_t)$ .  
10:     $t \leftarrow t + 1$   
11:     $\mathbf{z}_t = (\mathbf{x}_t^{(i)}, \boldsymbol{\theta}_t^{(i)}) \leftarrow \mathbf{z}_{t+1} = (\mathbf{x}_{t+1}^{(i)}, \boldsymbol{\theta}_{t+1}^{(i)})$   
12:  end while  
13:   $EOL_n^{(i)} \leftarrow t$   
    $RUL_n^{(i)} = EOL_n^{(i)} - n$   
14: end for
```

4.5.4 Overview of prognostics metrics

As mentioned above, the key motivation for prognostics is increasing availability by improving safety whilst reducing costs. Once a component or subsystem is being monitored using an appropriate sensor network design which is integrated in a cost-effective manner, the next requirement for achieving success of a prognostics framework resides in prediction performance. Decisions based on poor and/or late predictions may increase the risk of system failure, whereas early predictions of failure (false positives) trigger unnecessary maintenance actions with unavoidable cost increase.

A detailed discussion into deriving prognostics requirements from top level system goals is proposed by [108]. These requirements are generally specified in terms of prediction performance that prognostics must satisfy for desired level of safety or cost benefit. A variety of prognostic performance evaluation metrics have been defined in the literature, like prediction horizon (PH), α - λ accuracy measure, and relative accuracy measures [109, 110]. As recently described in [111], prognostic performance can be summarized into three main attributes, namely:

correctness, which is related to the prediction accuracy when compared with observed (future) outcomes;

timeliness, which accounts for how fast an algorithm produces the output as compared to the rate of upcoming outcomes from the system;

confidence, which deals with the uncertainty in a prognostic output, typically from a prognostic algorithm.

Among the metrics proposed by Saxena *et al.* [109, 110], the PH and the α - λ accuracy measures are widely used in prognostics and also adopted for this thesis. The PH serves to determine the maximum early warning capability that a prediction algorithm can provide with a user-defined confidence level denoted by α . Typically, a graphical representation using a straight line with negative slope serves to illustrate the true RUL that decreases linearly as time progresses. Predicted RULs are plotted against time of prediction using error bars (e.g. by 5%-95% error bars) as Figure 4.8a shows. Ideally predictions should stay on the dotted line

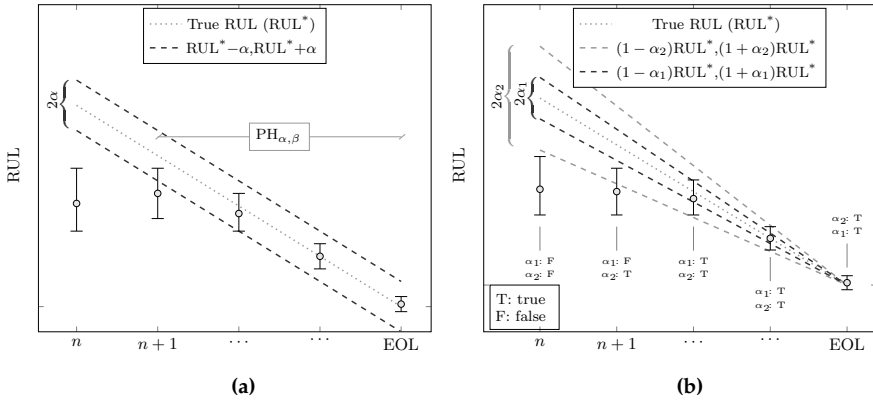


Figure 4.8: Illustrations of (a) PH and (b) $\alpha - \lambda$ prognostics metrics.

(RUL^*) as they get updated with time or, at least, stay within the accuracy zones specified by α . By means of this representation, the PH can be straightforwardly determined by graphical methods. The PH metric can be further parameterized by a parameter β (thus denoted by $PH_{\alpha, \beta}$) that specifies the minimum acceptable probability of overlap between the predicted RUL and the α accuracy bounds delimited by the dashed lines in Figure 4.8a. Both α and β are scaling parameters for the prognostics which should be fixed considering the application scenario.

In α - λ accuracy metric, it is also used a straight line with negative slope representing the true RUL. Predicted RULs are plotted against time of prediction

(which is termed as λ in the original paper by Saxena *et al.* [109]) using error bars. As in Figure 4.8a, accurate predictions should lie on this line as they get sequentially updated with time. In this case, the accuracy region is determined by parameter α , which represents a percentage of the true RUL, so that it captures the notion that accuracy of prediction becomes more critical as EOL approaches. See Figure 4.8b for an illustration of computation of α - λ accuracy metric. In this case, two confidence regions are employed by adopting $0 < \alpha_1 < \alpha_2 < 1$, so that each predicted RUL can be validated depending on whether or no it belongs to any the α_1 or α_2 regions.

Part II

METHODOLOGICAL CONTRIBUTIONS

5

A prognostics framework for composites

In this chapter, a model-based prognostics methodology is proposed to predict the remaining useful life (RUL) of composite materials under fatigue loads. Degradation phenomena such as stiffness reduction and increase in matrix micro-cracks density are predicted by connecting micro-scale and macro-scale damage models in a Bayesian framework. This framework also allows incorporating various uncertainties in the prediction that are generally associated with material defects, sensing noise, modeling errors, etc. It is shown that this approach confers an efficient way to make prognostics for damage evolution using data from SHM sensors. A detailed report and discussion about a Bayesian framework in application to fatigue in composites is given by Chiachio in [112] and also by the author and co-workers in [113, 114]. To avoid text duplication but conferring independence for this thesis, the relevant details from [112] are presented here in a concise way with special focus on the filtering process, which is required as a previous step before making prognosis.

5.1 Introduction and state-of-the-art

Unlike metals, fatigue damage degradation in composites is a complex multi-scale process driven by several internal fracture mechanisms such as matrix-cracks, local and global delaminations, fiber-breakage, etc, that ultimately lead to the alteration of the macro-scale mechanical properties [4]. The progression of these damage modes is a multi-scale process influenced by the material properties, stacking sequence, stress level and other loading conditions [4, 115, 116]. The inherent complexity of this process implies uncertainty that comes not only from the variability of loading conditions and material heterogeneity, but also from the incomplete knowledge of the underlying damage process. This uncertainty can increase dramatically when dealing with full-scale structures in real environments. Nevertheless, real time measurements of the structural performance are now available through state-of-art SHM techniques, and large amount of response data can be readily acquired, processed and further analyzed to assess various health-related properties of structures. Henceforth, a SHM-based prognostic approach is best suited to accurately predict the service life of a composite structure while accounting for uncertainty.

Damage prognostics is concerned with determining the health state of system components and predicting their RUL based on predefined thresholds, given a suitable model of damage evolution. In recent decades, a large number of articles have been reported to cover probabilistic approaches for damage evolution under the topic of stochastic modeling of damage growth for a number of applications [117–120]. First attempts involve modeling the damage evolution as a Markov process [121]. In [122–124] Markov chain models are proposed to describe the progression of fatigue degradation in composites from laminate compliance measurements, as an extension of the pioneering work of Bogdanoff and Kozin [125]. The author and co-workers have recently proposed in [126, 127] an enhancement of [122] by a model parameterization that allows accounting for the non-stationarity of the damage process, which is presented and discussed in more detail by Chiachio in [112], Chapter 5.

When the interest is focused on predicting future damage states from up-to-date measurements (which is the primary aim of fatigue prognostics), the damage models should be described in state-space form by stochastic embedding [128]. A dynamical system [96, 97] is then obtained so that it can be sequentially updated using information from sensors [128, 129].

In the last years, the topic of fatigue damage prognostics is slowly gaining interest [7, 10, 28, 29, 130] although the focus is predominantly on fatigue crack

growth in metals. Very few contributions can be encountered in the literature focusing on composite materials [131–133], the majority of them using deterministic approaches for lifetime calculation. However, a probabilistic-based prognostics approach can be fully beneficial since it can deal with the variability and complexity of the fatigue damage accumulation process [102, 132, 134, 135].

As with diagnostics, prognostics methods are typically categorized as either model-based or data-driven [136], depending on whether the considered damage model is based on physical first principles, or, alternatively uses run-to-failure data to capture trends of degradation [94]. Model-based approaches provide EOL estimates that are more accurate and precise than data-driven approaches, if good models are available [137]. Specifically, these models can be adapted to different conditions (specimen, materials, dimensions, etc.) without much training, they are more transparent to human understanding, and furthermore, they can incorporate monitoring data in a structural health monitoring context. Particularly in composites, where multiple fracture modes may co-exist, a model-based prognostics framework allows dynamically assessing the dominant damage mode and establishing the thresholds of each of the competing damage modes, by means of a comparison of the energy spent by each single mode [138], as will be explained further below.

In this chapter, a model-based prognostics framework is proposed to predict a sequence of damage states of composite laminates subjected to fatigue loadings. The damage states as well as the model parameters of the underlying damage model, are predicted and updated based on available SHM data. Damage thresholds are rationally assessed by means of a balance of energy among the competing damage modes, as a function of model parameters. A PF-based prognostics algorithm is proposed to jointly obtain state-parameter predictions.

To the author’s best knowledge, this thesis along with the companion papers (see Appendix B) are the first works dealing with a probabilistic-based prognostics framework for fatigue in composites using real-world data. Since the methodology presented here implies complex formulations with multiple connections and multiple parameters, this chapter concludes with a schematic description of the proposed framework.

5.2 Energy-based forward model of damage evolution

In this work, the longitudinal stiffness loss of the composite laminate is chosen as the macro-scale damage variable [140] since, in contrast to the strength, it can be measured non-destructively during operation. At the micro-scale level, matrix

micro-cracking [141] is selected as the dominant fracture mode for the early stage of damage accumulation. Both damage features can be measured using SHM sensors, which is of key importance for the proposed prognostics approach for this thesis.

There exists a closed connection between micro-scale damage propagation models and macro-scale manifestation through the *energy release rate* (ERR) term, which gives us a measure of the energy released by the formation of a new crack between two existing cracks. It can be calculated using the following expression [138, 142]:

$$G = \frac{\sigma_x^2 h}{2\rho t_{90}} \left(\frac{1}{E_x^*(2\rho)} - \frac{1}{E_x^*(\rho)} \right) \quad (5.1)$$

where σ_x is the applied axial tension, and h and t_{90} are the laminate and 90° sublaminates half-thickness, respectively. The term $E_x^*(\rho)$, as a function of crack density ρ , is the effective Young's modulus of the cracked laminate. Several families of models can be found in the literature of composites addressing the relation between the (macro-scale) effective stiffness E_x^* , and the (micro-scale) matrix micro-cracks density ρ , which essentially constitutes the basis for the underlying physics behind the damage evolution. They are presented in the next section.

The energy released calculated by Equation 5.1 can be further introduced into the modified Paris' law [143, 144] to obtain the evolution of matrix micro-cracks density as a function of fatigue cycle n , as shown below:

$$\frac{d\rho}{dn} = A(\Delta G)^\alpha \quad (5.2)$$

where A and α are fitting parameters, and ΔG is the increment in ERR for a specific stress amplitude, i.e., $\Delta G = G(\sigma_{x,max}) - G(\sigma_{x,min})$. Due to the complexity of the expression for ΔG , which involves the underlying micro-damage mechanics model for the evaluation of $E_x^*(\rho)$, a closed-form solution for Equation (5.2) is hard to obtain. To overcome this drawback, the resulting differential equation can be solved by approximating the derivative using "unit-cycle" finite differences by assuming that damage evolves cycle-to-cycle as:

$$\rho_n = \rho_{n-1} + A (\Delta G(\rho_{n-1}))^\alpha \quad (5.3)$$

5.3 Micro-to-macro scale modeling of fatigue damage

To accurately represent the relation between the internal damage and its manifestation through macro-scale properties, several families of *damage mechan-*

ics models have been proposed in the literature [145]. These models are based on first principles of admissible ply stress fields in presence of damage, and can be roughly classified into 1) analytical models, 2) semi-analytical models and 3) computational models. The last two families have been shown to be promising, however they are computationally prohibitive in a filtering-based prognostics approach, where repeated model evaluations are required. Therefore, the focus here is on the set of analytical models, which, depending on the level of assumptions adopted to model the stress field in presence of damage, they can be classified (from simpler to more complex) into *shear-lag* models [140, 146], *variational* models [147], and *crack opening displacement* (COD) based models [141, 148]. Among them, the shear-lag models have received most attention in the literature and, as a consequence, a vast number of modifications and extensions are found [145]. Shear-lag models use one-dimensional approximations of the equilibrium stress field after cracking to derive expressions for stiffness properties of the cracked laminate. The main modeling assumption of shear-lag models is basically that, in the position of matrix cracks, axial load is transferred to uncracked plies by the axial shear stresses at the interfaces. These models are usually restricted to cross-ply laminates or $\left[\phi_{\frac{n_\phi}{2}}/90_{n_{90}}/\phi_{\frac{n_\phi}{2}} \right]$ layups, where $\phi \in [-90^\circ, 90^\circ]$ is the ply-angle of the outer sublaminates (see Figure 5.1). For general laminates with arbitrary stacking sequence, COD-based models are best suited due to their versatility. These models are expected to better capture the various damage mechanisms since they involve more complex formulation of the mechanics of damage, but it might be at expense of more information extracted from the data [113, 114]. Then, if such models are utilized for future prediction, as arises in prognostics, the results are expected to significantly depend on the statistical details of the available data. In this thesis, the *classical* shear-lag model [146, 149] is chosen to represent the relation between matrix micro-cracks density and stiffness loss, as it provides reasonable accuracy results while it extracts less information from data. In addition, it is expected to be less sensitive to sensor noise, as has been shown recently for composites materials in [113]. An up-to date review on this matter along with a detailed discussion is provided in the doctoral thesis by Chiachio [112] and by the author in [113, 114]. Therefore, to avoid unnecessary text duplication, it is not repeated here. Finally, it is remarked that the prognostics method proposed in this thesis is not restricted but opened to other damage modeling options.

Stiffness reduction model

Following the unifying formulation by [150] for shear-lag models, the effective longitudinal Young's modulus E_x^* can be calculated as a function of the crack-spacing in the 90° plies as:

$$E_x^* = \frac{E_{x,0}}{1 + a \frac{1}{2\bar{l}} R(\bar{l})} \quad (5.4)$$

where $E_{x,0}$ is the initial longitudinal Young's modulus of the undamaged laminate and $\bar{l} = \frac{l}{t_{90}}$ is the half crack-spacing normalized by the 90° sub-laminate thickness. The normalized half-crack spacing \bar{l} can be expressed as a function of ρ , the matrix crack density, as: $\bar{l} = \frac{1}{2\rho t_{90}}$. The term a in Equation 5.4 is a function of mechanical properties of the laminate and it is defined in the Appendix A. The function $R(\bar{l})$, known as the *average stress perturbation function*, is defined as:

$$R(\bar{l}) = \frac{2}{\xi} \tanh(\xi \bar{l}) \quad (5.5)$$

where ξ is the *shear-lag parameter*, that can be obtained for the "classical" shear-lag model [146, 149] as follows:

$$\xi = \sqrt{G_{23} \left(\frac{1}{E_2} + \frac{t_{90}}{t_\phi E_x^{(\phi)}} \right)} \quad (5.6)$$

The superscript (ϕ) in last equation denotes "property referred to the $\left[\phi \frac{n_\phi}{2} \right]$ -sublaminate" (see Figure 5.1 for clarification). For the sake of clearness, the terms involved in Equations 5.4 to 5.6 are grouped in Table 5.1. The sub-laminate and laminate properties can be obtained from the ply properties using classical laminate theory, as states in Appendix A.

Laminate				
E_x	Longitudinal Young's modulus		t_ϕ	$\left[\phi \frac{n_\phi}{2} \right]$ -sublaminate thickness
E_x^*	Effective long. Young's modulus		t	Ply thickness
h	Laminate half-thickness			
Sublaminate			Ply	
$E_x^{(\phi)}$	Longitudinal Young's modulus		E_1	Longitudinal Young's modulus
$E_y^{(\phi)}$	Transverse Young's modulus		E_2	Transverse Young's modulus
$\nu_{xy}^{(\phi)}$	In-plane Poisson ratio		ν_{12}	In-plane Poisson ratio
$G_{xy}^{(\phi)}$	In-plane shear modulus		ν_{23}	Out-of-plane Poisson ratio
$G_{xz}^{(\phi)}$	Out-of-plane shear modulus		G_{12}	In-plane shear modulus
t_{90}	$[90_{n_{90}}]$ -sublaminate half-thickness		G_{23}	Out-of-plane shear modulus

Table 5.1: Nomenclature table for the terms used in shear-lag analysis.

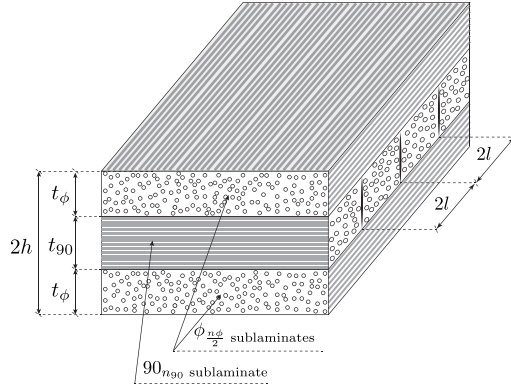


Figure 5.1: Illustration for microscopic damage in $\left[\phi_{\frac{n_{\phi}}{2}} / 90_{n_{90}} / \phi_{\frac{n_{\phi}}{2}} \right]$ laminate along with basic geometrical parameters.

5.4 Selecting prognostics targets for fatigue in composites

Structures are subjected to a variety of fault modes (cracks, corrosion, etc.), which often require dedicated sensors and sensor networks for better observability as no single sensor can cover all. Composite structures present even more challenges due to multiple simultaneous fault modes arising at different mechanical scales. Therefore, it may be prohibitively expensive, if not impossible, to cover all fault modes in real cases. Well-designed health management solutions typically identify potential targets for diagnostics and prognostics to optimize costs while maintaining the system carefully monitored. In this sense, it is a common practice to identify "hot spot" locations and critical fault modes in order to prioritize targets for prognostics. For instance, from a design perspective, it may be decided that all identified hot spots are monitored for fault detection but only some critical ones are considered as targets for prognostics.

A natural way to select a target for fatigue in composites would be by focusing on the evolution of effective strength along the lifecycle, so that failure would occur when it decreases below to the maximum applied stress. Given that strength can not be measured non-destructively, other suitable targets based on measurable properties, such as modulus-degradation and damage-tolerance approaches, can be encountered in the literature [3] which are better aligned for prognostics.

When considering the Young's modulus as target, fatigue failure is assumed to occur when the modulus degrades up to a certain level. For example, Hahn

and Kim [151] and O'Brien [152] stated that fatigue failure occurs when the secant modulus is reduced to the range of static secant modulus. Hwang and Han [132] proposed a strain failure criterion based on the concept of "fatigue modulus", defined as $F_n = \sigma_{max}/\epsilon_n$, where ϵ_n is the cumulative strain up to cycle n . The fatigue failure is assumed to occur when $\epsilon_n = \frac{\sigma_{max}}{F_n} \geq \epsilon_u$, where ϵ_u is the static ultimate strain. This strain failure criterion is later assumed by Post *et al.* [153]. In [152], deterministic methods for fatigue analysis of damaged laminates were developed, whereby fatigue failure was considered to occur when the maximum global strain reaches the effective failure strain in presence of delaminations. This approach combines both residual-strength degradation and modulus degradation, through a strain-energy-release rate and a delamination-growth law. Since then, it is observed in the literature that energy-based methods are preferably used in most of the contributions [138]. One conclusion that can be extracted is that, as happens when studying static failure in composites [34], there is not a consensual framework about what to consider as fatigue failure target in composites. The aim of this thesis is not to address this question in deep, however, a rational way to select a suitable fatigue damage threshold is presented in next sub-sections for the purpose of prognostics.

5.4.1 Competing damage modes

In composites, the evolution of fatigue damage involves a progressive or sudden change of the macro-scale mechanical properties, such as stiffness or strength, as a consequence of different fracture modes that evolve at the micro-scale along the lifespan of the structure [4]. Among them, transverse matrix cracking¹ holds a central position as a precursor of other damage modes in adjacent plies, such as local delaminations² [138] and fiber breakage [116, 154]. It is generally accepted that the matrix micro-cracks density in off-axis plies tends asymptotically to an upper bounded value corresponding to a spacing of aspect ratio unity³, termed as *characteristic damage state* [115]. This state is usually concomitant with more severe damage scenarios that may lead to a subsequent catastrophic failure.

In addition to the characteristic damage state, damage progression may exceed other "subcritical damage states" before ultimate failure, corresponding for

¹The terms matrix micro-cracks, transverse cracks or intralaminar cracks can be invariably used to refer to the cracks growing along fiber directions in off-axis plies.

²Local delaminations are small inter-laminar fractures growing from the tips of matrix cracks.

³Ratio between average crack spacing ($2l$) and ply thickness, t .

instance with the onset of local delaminations or global delaminations respectively [4]. These damage states define tolerance limits that can be used as thresholds for prognostics. However, establishing a deterministic damage progression path to these subcritical states is not an easy task because of the uncertainties in the growth and interactions of internal fracture modes from different scales. Before going in deep with the procedure for establishing prognostics thresholds for fatigue in composites, an overview of main contributions addressing the interaction between damage modes is shown below.

5.4.2 Interaction of cracks and (local) delamination

In this section it is considered the case where a delamination with length 2δ has developed from each tip of any matrix crack. The effects of local delamination vary depending on the stacking sequence considered for the laminate. It is shown by [155] that local delamination slightly influences the fatigue damage manifestation for the case of CFRP cross-ply laminates, particularly, at the macro-scale level. The last is not true when stacking sequences different than cross-ply are considered. In special, when quasi-isotropic and angle-ply laminates are considered, the local delaminations progress until reaching some edge, producing global delaminations of considerable extension [4]. In this thesis, the focus is on cross-ply laminates since this is the laminate type considered in the numerical examples, and also, because it is widely used by the industry. The Young's modulus reduction can be derived as a function of the matrix cracks and delamination at tips of the cracks through the ERR term [138].

Author	Classification	Energy release rate G_{LD}
N. Takeda <i>et al.</i> [155]	1D (shear lag)	$\frac{t_{90} E_x^{(90)} (f_3 E_x^{(S)} + t_{90} E_x^{(90)}) \epsilon_0^2}{2t_3 E_x^{(S)} \xi} \left(1 - \frac{4}{(\exp[\frac{\delta}{2l}(1-\delta)] + \exp[-\frac{\delta}{2l}(1-\delta)])^2} \right)$
J.A. Nairn & S. Hu [138]	2D (Variational)	$C_3 t_{90} \left(\frac{E_x^{(90)}}{E_x^{(\phi)}} \Delta \sigma_x \right)^2 \left(\frac{\chi'(0) - \chi'(l-\delta)}{2} \right)$
P. Gudmundson & Z. Weilin [148]	3D (COD)	$\frac{a^2 l}{2\rho t_{90}} \left(\frac{1}{E_x^*(2\rho)} - \frac{1}{E_x^*(\rho)} \right)$

Table 5.2: Selection of models for energy release rate due to microcrack-induced delamination.

There is disperse literature addressing the formulation of ERR under mixed-mode crack-delamination for fatigue. Table 5.2 highlights the main contributions to this field for cross-ply laminates. The function χ' as well as the terms C_1 and C_3 are given in Appendix A.2. The normalized effective stiffness $E_x^*(\rho)$ for the COD model by P. Gudmundson & Z. Weilin is provided in Appendix A.3. The term ξ is given in Equation 5.6 and ϵ_0 is the unitary deformation of the laminate subject to

the increase in tension $\Delta\sigma_x = \sigma_{x,max} - \sigma_{x,min}$. Since the interactions of cracks and local delaminations are far from being one-dimensional, the two-dimensional approach by J. A. Nairn & S. Hu [138] is preferred.

It is important to remark that nowadays, there are not efficient methods available to measure non-destructively the local delaminations, overall when they are dispersed along the composite laminate although some partial information can be obtained by edge replicas [26]. A promising technique has been recently proposed by Schmutzler *et al.* [156] which utilizes pulse-phase thermography to detect, locate, and measure the delamination crack openings for cross-ply laminates. However, it still requires more research effort to make this method extensible for different laminate configurations, and also to achieve good sensitivity for detecting local delaminations from their incipient stage. Moreover, a prognostics procedure by considering local delaminations still needs further research on SHM technology able to efficiently measure local delaminations in real-time.

5.4.3 Global delamination

Global delamination is a special case of cracks arising between plies. In composites, global delaminations can occur at cut-free edges, such as holes and notches. Global delamination may also occur as consequence of impacts, even with low-energy impacts [156]. The presence of global delamination in composites implies complex phenomena of interaction with matrix cracks (ply cracks), and vice-versa. In the literature, numerous experimental studies report these interactions for different stacking sequences [26, 138, 155]. For the case of cross-ply laminates, global delamination may only be expected at the final stage of the damage process, coinciding when local-delaminations induce a damage so severe that the catastrophic failure can occur at anytime (even before the global delamination on-set) [155]. However, as already mentioned in last sub-section, matrix cracks in quasi-isotropic and angle-ply laminates induce global delamination areas located at the free-edges of the specimen, and this process usually begins since the early stages of the fatigue process. So, in these cases, delamination on-set and growth should also be predicted in parallel to matrix micro-cracks. To account for the global delamination within the formulation of ERR, several models are also available in the literature. Table 5.3 gives an overview of two of the most referred models for the ERR for global delamination. The reader is also referred to the recent work of Hosoi *et al.* [157, 158] for detailed studies of interaction between cracks and edge delamination, based on the energy model of Nairn *et al.* [159].

Author	Classification	Energy release rate G_{GD}
T.K. O'Brien <i>et al.</i> [152]	No interaction with cracks	$\epsilon_0^2 h (E_{x,0} - E_x^*)$
J.A. Nairn [160]	Interaction with cracks	$h \left(\frac{\Delta\sigma_x}{E_x^*} \right)^2 \left(E_x^{(\text{center})} - E_x^{(\text{edge})} \right)$

Table 5.3: Models of energy release rate for edge delamination.

The terms, $E_x^{(\text{center})}$ and $E_x^{(\text{edge})}$ are the effective stiffness measured at the centre and edge of the laminate, respectively. The description of the rest of terms involved in these equations are described in the list of symbols at the beginning of the document and also grouped in Table 5.1.

5.4.4 Balance of energy among damage modes

Due to the dependency upon the laminate stacking sequence, ply properties and experimental conditions for the damage progression, an energy-based framework is used here to establish thresholds of fatigue damage without much previous experimental evidences. Based on a balance of energies between different plausible damage modes (namely, transverse cracks, local delamination and global delamination) one can address the question of whether the next increment in fatigue damage will be through another transverse crack, local delamination or global delamination induced by the existing micro-cracks [138]. Figure 5.2 illustrates this concept through a case study for a cross-ply laminate, whose mechanical properties are further presented in Tables 8.3 and 9.1. In Figure 5.2, the terms TC, LD and GD refer to transverse cracks, local delamination and global delamination, respectively. The two square markers correspond to the points where a change in the dominant fracture mode is expected. Observe that, initially, the energy release for transverse cracks is larger than that of the rest of damage modes. Therefore, matrix micro-cracks are expected to accumulate at a faster rate at earlier cycles. Results also show that until the final stage of the process, the local delamination mode of damage releases more strain energy than the global delamination mode. Therefore, local delamination onset is expected much earlier than global delaminations along the fatigue damage process. These conclusions agree well with the experimental evidence obtained for cross-ply laminates reported in [26] and also with the dataset from NASA Ames Prognostics Data Repository [1]. Observe also that the point where TC and LD curves intersect, defines a critical value for the matrix micro-cracks density. At this point, local delaminations are more likely to appear than another matrix crack. This point can be computed

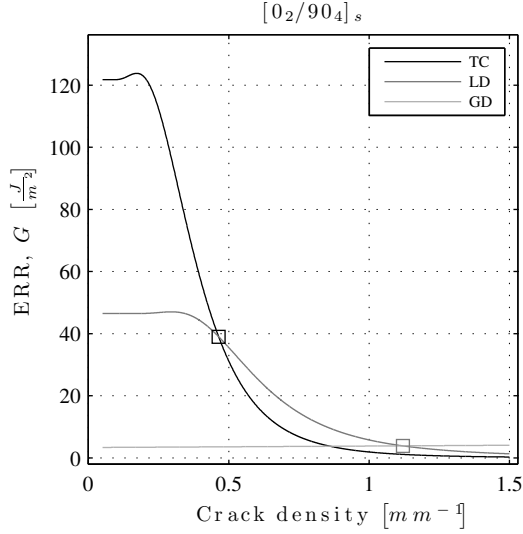


Figure 5.2: Energy release rate term as a function of the matrix crack density. The square markers delimit the points where a change in the dominant fracture mode is expected.

from any of the expressions for G_{TC} in Table 5.2 by using $\delta = 0$. Another important reference-point is the intersection of the LD and GD curves, where local delaminations are supposed to cease starting a global delamination process. Notice that global delamination is unlikely to appear since the energy release rate associated to its onset and growth is too small. Therefore, the required damage for global delamination onset is so severe, that the specimen usually fail before that point.

Based on this reasoning, prognostics thresholds can be established by predicting the position of these reference points as the fatigue process continues. It is seen that matrix micro-cracking is the most plausible damage mode in the first stage of fatigue damage for angle-ply, quasi-isotropic and cross-ply laminates [26]. Hence, the selected critical threshold in this thesis is the saturation of matrix micro-cracks (together with its associated stiffness loss), which is a priori unknown.

It is important to remark that the ERR term depends on model parameters which are sequentially updated as new data arrive. Hence, the intersection-points defining the thresholds dynamically shift their position until a convergence stage. All these aspects will be covered using a numerical example in Chapter 9.

5.5 Model-based damage prognostics in composites

In this section, the PF-based prognostics framework presented in Section 4.5 is exploited for prognostics by just specializing the framework to the fatigue damage modeling in composites.

5.5.1 Stochastic system embedding

Having defined the forward problem about fatigue damage propagation, the next step is to develop a prediction methodology by integrating the damage propagation modeling within the Bayesian filtering framework, whereby the simulations and measurements are coupled to predict future damage states with quantified uncertainty. To this end, a probability-based description of the deterministic models previously described in Section 5.2 is firstly required. This procedure will make extensive use of the concept of damage state, as a damage event predicted at a certain time, as shown below.

5.5.2 Stochastic system modeling

Let us consider a generic damage progression model defined in state space form using the following discrete *state transition equation*:

$$\mathbf{x}_n = \mathbf{f}(\mathbf{x}_{n-1}, \mathbf{u}_n, \boldsymbol{\theta}) + \mathbf{v}_n \quad (5.7)$$

where $\mathbf{f}(\mathbf{x}_{n-1}, \mathbf{u}_n, \boldsymbol{\theta}) : \mathbb{R}^{n_x} \times \mathbb{R}^{n_u} \times \mathbb{R}^{n_\theta} \rightarrow \mathbb{R}^{n_x}$ is a possibly nonlinear function of the latent damage state \mathbf{x}_n that may depend on a set of n_θ model parameters $\boldsymbol{\theta} \in \Theta \subset \mathbb{R}^{n_\theta}$ along with a set of input parameters to the system $\mathbf{u}_n \in \mathbb{R}^{n_u}$. Here $\mathbf{v}_n \in \mathbb{R}^{n_x}$ is a model-error term that represents the difference between the actual system response \mathbf{x}_n and the model output \mathbf{f} . It is assumed to be modeled as a zero-mean Gaussian distribution, which is supported by the Principle of Maximum Information Entropy (PMIE)⁴ [161, 162]. It follows that the entire state transition equation is also modeled as a Gaussian distribution, as:

$$p(\mathbf{x}_n | \mathbf{x}_{n-1}, \mathbf{u}_n, \boldsymbol{\theta}) = ((2\pi)^{n_x} |\Sigma_{\mathbf{v}_n}|)^{-\frac{1}{2}} \exp\left(-\frac{1}{2} (\mathbf{x}_n - \tilde{\mathbf{x}}_n)^T \Sigma_{\mathbf{v}_n}^{-1} (\mathbf{x}_n - \tilde{\mathbf{x}}_n)\right) \quad (5.8)$$

where $\tilde{\mathbf{x}}_n = \mathbf{f}(\mathbf{x}_{n-1}, \mathbf{u}_n, \boldsymbol{\theta})$ and $\Sigma_{\mathbf{v}_n} \in \mathbb{R}^{n_x \times n_x}$ is the covariance matrix of the model error \mathbf{v}_n . Observe that the state transition equation defined in Equation 5.8, satisfies the Markov property [163], i.e., the process is conditional dependent on the

⁴It states that the probability model should be selected so as to produce the most uncertainty (largest Shannon entropy) subject to parameterized constraints that we wish to impose. Any other probability model would lead to an unjustified reduction of modeling uncertainty.

past sequence only through the last state. Thus, the state transition equation describes a Markovian process of order one.

As discussed in Section 5.2, the progression of damage is studied in this thesis by focusing on the matrix-cracks density ρ_n , and the normalized effective stiffness $D_n = \frac{E_x^*}{E_{x,0}}$, so that the following joint state transition equation of two components $\mathbf{f} = [f_1, f_2]$ is defined as follows:

$$x_{1_n} = \rho_n = \underbrace{f_1(\rho_{n-1}, \mathbf{u}_n, \boldsymbol{\theta})}_{\text{Eq. 5.3}} + v_{1_n} \quad (5.9a)$$

$$x_{2_n} = D_n = \underbrace{f_2(\rho_n, \mathbf{u}_n, \boldsymbol{\theta})}_{\text{Eq. 5.4}} + v_{2_n} \quad (5.9b)$$

where $\mathbf{x}_n = [x_{1_n}, x_{2_n}] \in \mathbb{R}^2$ is the system response at time n . Subscripts 1 and 2 correspond to the damage subsystems, namely, matrix-crack density and normalized effective stiffness, respectively. The vector $\mathbf{v}_n = [v_{1_n}, v_{2_n}] \in \mathbb{R}^2$ corresponds to the model error vector of the overall system.

A key concept here is the consideration of model errors v_{1_n} and v_{2_n} as stochastically independent, even though the models corresponding to the damage subsystems, f_1 and f_2 , are mathematically related, as shown in Section 5.2. It follows that the covariance operator $\Sigma_{\mathbf{v}_n}$ is a diagonal matrix, i.e. $\Sigma_{\mathbf{v}_n} = \begin{bmatrix} \sigma_{v_{1,n}}^2 & 0 \\ 0 & \sigma_{v_{2,n}}^2 \end{bmatrix} \mathbf{I}_2$, where \mathbf{I}_2 is the identity matrix of order 2, and $\sigma_{v_{1,n}}$ and $\sigma_{v_{2,n}}$ the corresponding standard deviation of the errors v_{1_n} and v_{2_n} , respectively. Therefore, the state transition equation of the overall system can be readily expressed as a product of univariate Gaussians, as⁵:

$$p(\mathbf{x}_n | \mathbf{x}_{n-1}, \boldsymbol{\theta}) = p(D_n | \rho_n, \boldsymbol{\theta}) p(\rho_n | \rho_{n-1}, \boldsymbol{\theta}) \quad (5.10)$$

where

$$p(\rho_n | \rho_{n-1}, \boldsymbol{\theta}) = \frac{1}{\sqrt{2\pi}\sigma_{v_{1,n}}} \exp\left(-\frac{(\rho_n - f_1(\rho_{n-1}, \boldsymbol{\theta}))^2}{2\sigma_{v_{1,n}}^2}\right) \quad (5.11a)$$

$$p(D_n | \rho_n, \boldsymbol{\theta}) = \frac{1}{\sqrt{2\pi}\sigma_{v_{2,n}}} \exp\left(-\frac{(D_n - f_2(\rho_n, \boldsymbol{\theta}))^2}{2\sigma_{v_{2,n}}^2}\right) \quad (5.11b)$$

Let us now suppose that the system response can be measured during operation and that, at a certain fatigue cycle n , the measured system response can be

⁵For simpler notation the conditioning on the model input \mathbf{u}_n is dropped from Eq. (5.9).

studied through a function of the latent state \mathbf{x}_n , as follows:

$$\mathbf{y}_n = \mathbf{x}_n + \mathbf{w}_n \quad (5.12)$$

where $\mathbf{y}_n = [y_{1_n}, y_{2_n}] \equiv [\hat{\rho}_n, \hat{D}_n] \in \mathbb{R}^2$ are the measurements for both, matrix micro-cracks density and normalized effective stiffness respectively, and $\mathbf{w}_n = [w_{1_n}, w_{2_n}] \in \mathbb{R}^2$ is the vector of measurement errors. As stated before, we use the PMIE to choose \mathbf{w}_n to be distributed as zero mean Gaussian PDF with covariance matrix $\Sigma_{\mathbf{w}_n}$. Thus, the *measurement equation* defined in Equation 5.12 can be expressed in probabilistic terms as:

$$p(\mathbf{y}_n | \mathbf{x}_n, \theta) = \left((2\pi)^2 |\Sigma_{\mathbf{w}_n}| \right)^{-\frac{1}{2}} \exp \left(-\frac{1}{2} (\mathbf{y}_n - \mathbf{x}_n)^T \Sigma_{\mathbf{w}_n}^{-1} (\mathbf{y}_n - \mathbf{x}_n) \right) \quad (5.13)$$

Since the measurements of each subsystem (micro-cracks and stiffness loss) are considered as stochastically independent, then $\Sigma_{\mathbf{w}_n} = \begin{bmatrix} \sigma_{w_{1_n}}^2 & 0 \\ 0 & \sigma_{w_{2_n}}^2 \end{bmatrix} \mathbf{I}_2$. Here $\sigma_{w_{1_n}}$ and $\sigma_{w_{2_n}}$ are the standard deviation of the corresponding measurement errors w_{1_n} and w_{2_n} , respectively. Thus, the measurement equation defined in Equation 5.12 can be readily expressed as:

$$p(\mathbf{y}_n | \mathbf{x}_n, \theta) = p(\hat{\rho}_n | \rho_n) p(\hat{D}_n | D_n) \quad (5.14)$$

where

$$p(\hat{\rho}_n | \rho_n) = \frac{1}{\sqrt{2\pi}\sigma_{w_{1_n}}} \exp \left(-\frac{(\hat{\rho}_n - \rho_n)^2}{2\sigma_{w_{1_n}}^2} \right) \quad (5.15a)$$

$$p(\hat{D}_n | D_n) = \frac{1}{\sqrt{2\pi}\sigma_{w_{2_n}}} \exp \left(-\frac{(\hat{D}_n - D_n)^2}{2\sigma_{w_{2_n}}^2} \right) \quad (5.15b)$$

The PDF of the initial damage state \mathbf{x}_0 together with the PDFs for the state transition equation and the measurement equation, defined in Equations 5.10 and 5.14, provide a complete statistical description of the overall system and play a major role in the filtering-based prognostics methodology explained below.

In the last equations the model parameters θ are selected among the complete set of mechanical and geometrical parameters describing Equations 5.2 to 5.6 through a Global Sensitivity Analysis based on variances and following the methodology proposed by Saltelli [164]. The ply properties $\{E_1, E_2, t\}$ along with the fitting constant $\{\alpha\}$ emerged as sensitive parameters to model

output uncertainty [113]. To the last cited selection is added the variances of the model error function \mathbf{v}_n since they are uncertain a priori, resulting in $\theta = \{\alpha, E_1, E_2, t, \sigma_{v_{1,n}}, \sigma_{v_{2,n}}\} \in \mathbb{R}^6$. The rest of parameters are fixed at any point within their range of variation, (e.g. the mean value) without significantly influencing the output uncertainty. The probabilistic information of parameters are given in Chapter 9 in the context of a numerical example.

5.5.3 Particle filters for RUL and EOL estimations in composites

In this section, the PF procedure is specialized for the state-space model previously defined in last section for the study of fatigue prognosis in composites. As already mentioned, data $\mathbf{y}_{0:n}$ are compounded by simultaneous measurements of both, micro-cracks density $\hat{\rho}_n$ and normalized effective stiffness \hat{D}_n . Thus, by substituting the Equation 5.14 into 4.43, the formula for updating the particle weights leads to the next expression:

$$\omega_n^{(i)} \propto \omega_{n-1}^{(i)} p(\hat{\rho}_n | \rho_n^{(i)}) p(\hat{D}_n | D_n^{(i)}) \quad (5.16)$$

Observe that when data are available over a set of non-regularly scheduled cycles $\{n, n+k, \dots, n+\ell\} \in \mathbb{N}$, with $\ell > k+1, k > 1$, samples from the state transition equation $p(\mathbf{z}_{n+1} | \mathbf{z}_n)$ cannot be directly drawn. This is due to the "one-step" description of the matrix-cracks evolution model, as is defined in Equation 5.9a. To overcome this drawback, which is usual in fatigue testing, the Total Probability Theorem can be applied to bridge the missing path of damage states between two non-subsequent measurements. For example, for general cycles n and $n+\ell$, with $\ell \in \mathbb{N} \geq 1$, the PDF $p(\mathbf{z}_{n+\ell} | \mathbf{z}_n)$ for the ℓ -step-ahead states distribution can be obtained as:

$$p(\mathbf{z}_{n+\ell} | \mathbf{z}_n) = \int_{\mathcal{Z}} p(\mathbf{z}_{n+\ell} | \mathbf{z}_{n+1:n+\ell-1}, \mathbf{z}_n) p(\mathbf{z}_{n+1:n+\ell-1} | \mathbf{z}_n) d\mathbf{z}_{n+1:n+\ell-1} \quad (5.17)$$

where $\mathbf{z}_{n+1:n+\ell-1} = \{\mathbf{z}_{n+1}, \mathbf{z}_{n+2}, \dots, \mathbf{z}_{n+\ell-1}\} \in \mathcal{Z}$ is the sequence of "missing" states between the measuring times n and $n+\ell$. Making use of the Markov property of state transition equation, Equation 5.18 can be rewritten as:

$$p(\mathbf{z}_{n+\ell} | \mathbf{z}_n) = \int_{\mathcal{Z}} \prod_{t=n+1}^{n+\ell} p(\mathbf{z}_t | \mathbf{z}_{t-1}) d\mathbf{z}_{n+1:n+\ell-1} \quad (5.18)$$

To numerically solve this multi-dimensional integral, a sample approximation can be readily obtained by *conditional sampling*, using recursively the "one-step"

transition equation defined in 5.10, i.e.: first sample $\tilde{\mathbf{z}}_{n+1}^{(i)}$ using the aforementioned one-step transition equation conditional on the initial state \mathbf{z}_n , i.e., $\tilde{\mathbf{z}}_{n+1}^{(i)} \sim p(\mathbf{z}_{n+1}|\mathbf{z}_n)$; then sample the succeeding state conditional on the previous sample, i.e., $\tilde{\mathbf{z}}_{n+2}^{(i)} \sim p(\cdot|\mathbf{z}_{n+1}^{(i)})$; finally, repeat the same process until the target time $n + \ell$ is reached. For the filtering of the damage states, Algorithm 3 can be used by just employing Equations 5.10 and 5.10 as transition equations, and Equation 5.16 for particle updating. The artificial dynamics of model parameters $p(\boldsymbol{\theta}_n|\boldsymbol{\theta}_{n-1})$ is carried-out by using the method proposed by M. Daigle and K. Goebel in [94], whose details of implementation and scaling constants are specified in Section 9.1 in the context of the experimental example. Using the most-up-to date information of damage state from the PF algorithm, multi-step ahead predictions can be obtained by evaluating recursively the state transition equation as states in Equation 4.44. EOL and RUL estimates can be readily computed using Algorithm 4.

Figure 5.3 provides a schematic description of the stochastic embedding of the Modified Pari's law along with then connection with the rest of the PF-based prognostics framework until RUL and EOL calculation.

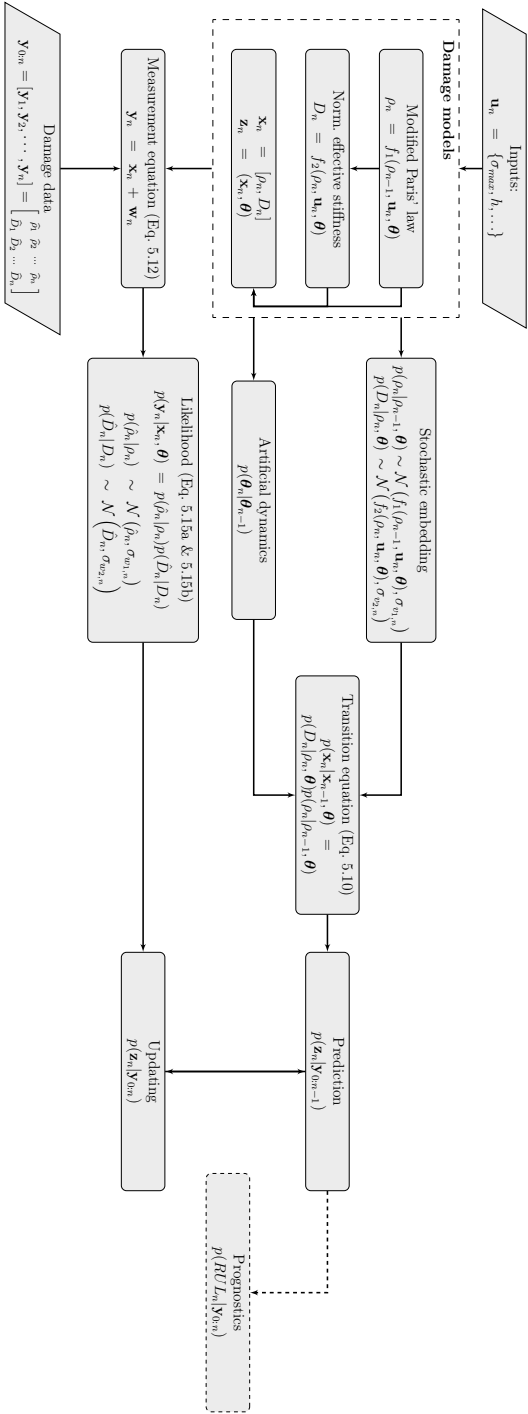


Figure 5.3: Filtering-based prognostics scheme proposed for composites.

6

Prognostics of reliability: reliability assessment along lifespan

In addition to predict the remaining useful life of a component or sub-system, it is also of much interest to obtain the probability of the system to fulfill the design requirements in the future. Reliability emerges as a suitable unified indicator for prognostics since it encapsulates information of the system health state within a probabilistic formulation. In this chapter, a reliability-based prognostics framework is presented. The key contribution is the estimation of the RUL as a by-product from the prediction of the time-dependent reliability at future times.

As a previous step before to proceed with the proposed reliability-based prognostics framework, a selective review of the reliability literature of composites is provided in the introductory section of this chapter. The content of this review has been partially covered in a publication by the author in 2012 [34], henceforth those references up to [34] are reviewed in this thesis. Following the structure of contents of this thesis, the basis of reliability methods are presented and referenced in Chapter 4.

6.1 Up-to-date review of reliability assessment in composites

As a response to the rampant increase in research activity within reliability in the past few decades, and to the lack of a conclusive framework for composite applications, this section attempts to identify the most relevant reliability topics to composite materials and provide a selective review.

Variability in the performance of composite materials arises mainly from the variability in constituent properties, fiber distribution, structural geometry, loading conditions and also manufacturing process. As an orthotropic material, this variability may lead to a catastrophic failure mainly when inaccuracy arises in loading direction or fiber orientation, while the traditional approach of safety factors could result in a costly and unnecessary conservatism [166], which is a serious drawback for making composites competitive and sustainable.

In the recent decades, a large number of articles have been reported to cover probabilistic failure and reliability in composites. The first contributions were in the form of probabilistic strength over aircraft applications [87, 167]. Shortly later, the β -index method (recall Section 4.3) [70] was applied to laminated plates [168]. Wetherhold *et al.* [169] evaluated reliability methods used in composites through an example and Soares [77] made an overview and gave a perspective about deriving reliability from ply to laminate level.

However, due to the inherent variability in the material behavior, reliability in composites requires that several decisions are adopted. The reasons for that are multiple: 1) there are a wide range of possible failure functions to adopt, 2) numerous influencing random variables need being incorporated, 3) several reliability methods arise and 4) there are different ways to consider reliability for a laminate, as shown in Figure 6.1.

According to Soares [77], several results have been reported, but unfortunately, a lack of consensual framework is observed from the literature for the use of methods, failure criteria, statistical description of mechanical variables, and even for conclusions. These, together with new trends to confer efficiency in reliability calculations, require the need for a thorough and up-to-date review of the literature in this area.

As a first step to provide a basis for a discussion about this claim, the present chapter reviews some fundamental concepts of reliability from an orthotropic material perspective. This work highlights the results where connections between reliability and failure criteria in composites are most striking. It also gives a concise background of reliability methods for applications in composite materials (since the more general methods for reliability are presented in Section 4.3), and

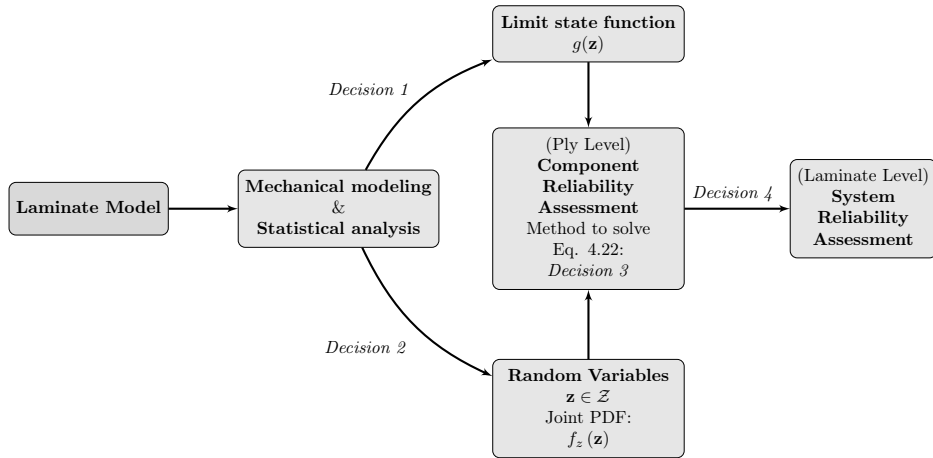


Figure 6.1: Schematic representation of a reliability problem in composites.

identifies results which evaluate the influence of such variability in the methodology.

In Table 6.1, additional information related to the decision topics is provided, that aims at helping the reader to derive a perspectival view for the reliability assessment in composites. The review work presented here focuses on reliability procedures and avoids transverse areas where reliability in composites is used as a methodological tool, like reliability based design and safety factor calibration. A review and discussion about these topics have been covered in [34].

6.1.1 Concept of failure.

Failure criteria used in probabilistic analysis are the same as that used in a deterministic approach, so the accuracy of reliability analysis is critically dependent on an appropriate criterion for the study conditions. A comprehensive review of failure theories at the ply level is given by Orifici *et al.* [170], where a classification for failure theories is proposed according to whether they are based on strength or fracture mechanics theories, whether they model failure in a general sense or are specific to a particular failure mode and whether they focus on in-plane or inter-laminar failure. Following this classification, the in-plane general strength failure criteria ranges almost all the literature in reliability, although important contributions have also been derived in reliability in composites based on other LSFs like damage based criteria [82], crack initiation over pipe surfaces [171, 172], buckling failure [166, 173], among others.

In relation to the scale level, although recent advances in multi-scale failure have been reported [174, 175], the body of reliability literature takes a mesoscale or macroscopic approach¹ to the failure as the phenomenological model to analytically describe the reliability of composites. An interesting approach, which seems to be a first step to multiscale reliability evaluation of composites, has been recently reported by [176]. In this study, a microscale and macroscale evaluations of the Tsai-Hill LSF are critically compared within a reliability framework showing good agreement and concluded that reliability analysis starting from microscale would help benchmarking corresponding macroscale analyses. In the reliability literature, due to the complexity of the failure concept, a step-by-step approximation to the subject is observed, from uniaxial tension reliability [87, 177] to a more general multiaxial case in recent years. In the latter multiaxial case, two main approaches have been proposed: the interactive and non-interactive, depending on the stress working or not collectively towards the failure of the element [78].

The non-interactive case considers reliability at each stress direction independently [78] or exclusively the most stressed direction [178, 179], in conjunction to Max Stress, Max Strain or Max Work criteria as LSF. This approach has not been extensively used in reliability due to its well-known insecure position for certain stress combinations [43]. Among the interactive failure criteria, *quadratic failure criteria*, are mostly used in reliability analysis mainly because the mature knowledge that has been achieved in considering quadratic functions as LSF for composites [72]. These criteria take into account the interactions between different stress components. The LSF for the quadratic failure criteria in the component orientation for one ply is expressed by:

$$g(\mathbf{z}) = (F_{ij}\sigma_i\sigma_j + F_i\sigma_i) - 1 = 0 \quad (6.1)$$

so that failure is represented when $g(\mathbf{z}) > 0$. In the last equation, $F_{ij} = F_{ij}(\mathbf{z})$, $F_i = F_i(\mathbf{z})$ are the strength parameters, $\sigma_i = \sigma_i(\mathbf{z})$ are the stresses in the tensor component i , with $i, j = 1, 2, 6$ being the tensor components [43]; and \mathbf{z} is the vector of random variables/parameters. Particularly, the quadratic Tsai's criterion has been fairly used in the literature motivated by being one of the existing mature theories today [180–182]. The main contributions in reliability have used the Tsai's criterion, although not exclusively, as shown in Table 6.1.

¹Mesoscale is related to the ply level whereas macroscale refers to the full laminate level.

Under such variability of failure criteria to define the LSF, certain authors [79, 81, 84, 169, 178] declined to prove with several possibles and compare to benchmark data when available. In [183] a quantitative trade-off for six different failure criteria was carried out from the viewpoint of reliability-oriented design of composite materials. This work yielded an important conclusion about the need to verify the criterion suitability under specific load combinations, which also agrees with Lin [83].

6.1.2 Analytical approaches for reliability in composites

In order to confer more simplicity in reliability calculations, some specialized analytical approaches have appeared for composites applications. Few of them have demonstrated good agreement in their range of application as compared to the standard MC method, taken as reference.

Edgeworth expansion method (EDW) and Pearson's empirical distribution (PRS)

In [184], two analytical approaches, namely, functional expansion technique and the introduction of Pearson's semi-empirical distribution function, were developed for the case of plane (2D) stress. Strength parameters were considered as random variables, each following a Weibull distribution. The purpose of these two analytical approaches was to determine the CDF of the failure condition $g(\mathbf{z}) > 0$ denoted by $F(g)$, whereby the failure probability P_f can be obtained.

The EDW, which was previously introduced for off-axis composites for the case of uniaxial tension [185, 186], was used to predict the cumulative probability of complex systems in terms of individual component moments [187]. The failure function in Equation 6.1 was expanded in a multivariable Taylor series in terms of central moments of the random variable $g(\mathbf{z})$. This is given by:

$$F(g) = \Phi(g) - \frac{1}{3!} \frac{\mu_3}{\mu_2^{3/2}} \Phi^3(g) + \frac{1}{4!} \frac{\mu_4}{\mu_2^2} \Phi^4(g) + \frac{10}{6!} \frac{\mu_3}{\mu_2^{3/2}} \Phi^6(g) + \dots \quad (6.2)$$

where μ_k are the central k -moments of the LSF $g(\mathbf{z})$ and $\Phi^n(g)$ is the n^{th} derivate of the normal CDF $\Phi(g)$. This method was further developed for the case of a laminate in a plane stress state considering the strength properties as stochastic variables [188], and more recently [86] by considering the elastic and thermal properties as random too. In the latter work, it was demonstrated over wind turbine blades application, that the stochastic nature of the material elastic properties drastically influences the failure locus, whereas, on the contrary, the influence of the material thermal properties is minimal within the temperature range met during operation of wind turbine rotor blades.

In PRS method the unknown CDF of the LSF is alternatively fitted by empirical statistical distributions once the central moments of $g(\mathbf{z})$ are calculated. The work by T.P. Philippidis *et al.* [184] provides several comparisons between analytical EDW, PRS, and MC method by considering different fiber angle and assumptions for the failure criteria. The results obtained with the analytical approaches were shown to be in excellent agreement with the MC method.

Generalization of LSF

Another relevant result in analytical methods for reliability in composites was proposed by Gurvich *et al.* [189]. This approach considers the LSF in the form of a random linear function of products of applied random stresses, in stead of the traditional consideration of the LSF as a random non-linear function of the stresses (see Equation 6.1). This approach allows us to obtain exact evaluation of the main statistical parameters (moments) of the LSF considered as a random function.

The possibility of considering all possible correlations between random variables is an important advantage of this method [189]. This analytical method only requires the adoption of any of the parametric distributions for the LSF $g(\mathbf{z})$: Gaussian, Weibull, Gamma Function, etc. In all of the remaining methods cited above, reliability calculation requires an assumption regarding the type of the distributions for strength and/or stress, i.e., for \mathbf{z} , whereas Gurvich's method requires those in the type of distribution $g(\mathbf{z})$. An interesting discussion between this analytical method in relation to the others is done at the end of Gurvich's work.

6.1.3 Recent numerical methods

In the specialized literature, there are a branch of methods for the evaluation of the probability integral in Equation 4.22 (others than the analytical approaches previously presented in Section 4.3), which are specially well-suited for composites. These are reviewed in the following paragraphs.

In a numerical scheme, particularly in the context of finite element modeling, the stochastic finite element modeling (SFEM) are receiving special attention for reliability, due to the significant advances in the available computational power nowadays [190]. SFEM involves finite elements whose properties are random so that response statistics can be generated from each node [191, 192].

There are three main variants of SFEM in the literature: a) the perturbation approach [193], which is based on a Taylor series expansion of the response vector; b) the spectral stochastic finite element method (SSFEM) [194], where each

response quantity is represented using a series of random Hermite polynomials; and c) Monte Carlo-SFEM [195–197], based on independent sampling of the response vector. In composites, Lin [83] used the stochastic finite element method (SFEM) to evaluate the reliability of angle-ply laminates with different types of buckling failure modes subjected to in-plane edge random loads. The results were compared with experimental FPF load data of centrally loaded composite plates with different lamination arrangements to study the accuracy of the method. Onkar *et al.* [84] used SFEM (perturbation approach) to generate statistics for the failure using Tsai-Wu and Hoffman as failure criterion in laminate plates with random material properties and random loads. In this case, the results were compared with analytical solutions. Ngah *et al.* [165] demonstrated an application of SSFEM in a composite panel subjected to random loads and constitutive properties. A comparative study of accuracy and computational effort of SSFEM versus MC method was presented. Recently, Noh *et al.* [198, 199] propose a formulation of SFEM based on perturbation techniques to determine the response variability in laminate composite plates considering the randomness of material parameters and different correlation states between them. In a more recent work by Noh [200], the SFEM formulation is derived by accounting the spatial randomness of Poisson's ratio for laminated composite plates. Both works, and particularly this latter proposal, confer efficient ways to obtain the response variability whereby to derive the probabilistic failure of composites.

6.1.4 Comparative review between reliability methods

Due to the wide range of reliability approaches and the lack of results coincidence when they are applied to composites, several authors have declined to contrast different well-accepted reliability methods to a specific composite application or to check one proposed method to failure data. The examples encountered in literature typically use at least MC method as reference.

In [75], the FPI methods and MC method was presented, and a comparison between them was done considering both Tsai-Wu and Tsai-Hill as failure criteria in different loading levels and ply angles. A sensitivity study was done to evaluate the influence of each stochastic variable in the reliability calculation. The comparisons were performed over three main fields: accuracy, conservatism and computational speed. For accuracy, FPI was observed to derive satisfactory accuracy in cases of low stresses and moderate fiber angle (it is pointed out the interval $30^\circ - 40^\circ$), when preferably using Tsai-Wu as failure criteria. In extremely low or

high orientation angles, near 0° and 90° , planar FPI were seem to be quite accurate. When studied the conservatism, the report concluded the need to consider the curvature in the MPP. Particularly, for planar FPI, independently of the accuracy, the conservatism would be depend upon whether the curvature is safe or unsafe. When considering computational speed, this work does not give substantial conclusions as compared to others like [85] cited in section 6.1.5. However, an interesting result about computational cost as compared to MC method was implicitly derived through reduction of variables to be sampled using IS by a sensitivity analyses, by the fact that depending on each specific case, the bulk of the reliability value depends upon several localized stochastic variables. That conclusion was later explicitly highlighted by Sciuva *et al.* [166], who compared FORM methods with MC method and explicitly pointed out for sensitivity analysis as an efficient method to reduce the stochastic variables to be sampled in MC without significant loss of accuracy. In this work, a laminated composite plate loaded by compressive distributed forces acting in its mid-plane was studied, with the LSF defined analytically for buckling loads. The results showed acceptable level of accuracy when FORM methods were used in this specific case, in which the buckling LSF fits well to linear.

In [83], three different methods, MC method, FORM and first-order second moment method were used to calculate the reliability and compared to experimental first-ply-failure data of centrally loaded laminated composite plates with different lay-ups. The LSF and baseline for load values, were also took as variables for comparison. As conclusion, this work also pointed out to FORM together with Tsai-Wu for obtaining reasonably good results. However according to Wetherhold *et al.* [169], this conclusion may be erroneous with different tensional ranges and fiber orientations than those used for the study.

In [86], the EDW previously introduced by Philippidis [184] was compared against MC and FORM using Tsai-Hahn as failure function concluding that the EDW estimation overrate the structural load carrying capacity of the laminated plate. More recently, Lopez *et al.* [201] perform a critical comparison between full characterization method (such as the polynomial chaos expansion) and FORM for laminated composite plates, using MC as reference method. The comparative exercise was carried out in terms of accuracy, convergence and computational cost, using the maximum stress and Tsai-Wu as failure criteria. The results show that the full characterization method gets similar, if not better results than MC when considering the computational cost, and outperforms FORM in terms of convergence irrespective the failure criterion chosen for the study.

6.1.5 Overview of recent computational techniques

The structural integrity analysis of composite laminates (and even more composite structures) based on probabilistic concepts is a time consuming process unless FPI methods were employed, and the problem can be exacerbated by the convergence difficulties associated to the non-linearity LSF. Other methods employing simulation procedures, such as MC or IS, may have a prohibitive computational cost in large structural systems even if the structural evaluation is accelerated by a vectorized manner, by techniques such as Neumann series expansion [192, 202], or by reducing the stochastic variables to be sampled through sensitivity analysis, as previously mentioned [166, 169].

In the literature, there have been advised two efficient ways to reduce the computational cost: a) by using new efficient algorithms for reliability and b) by reducing the effort of evaluation the LSF. In the former, new reliability algorithms have proved to save great amount of time of computation. Special attention require Subset Simulation method [62, 203] which confers large efficiency as compared to the standard MC, overall for small failure probabilities and high dimension problems. The ²SMART algorithm by Hurtado [204] uses a similar idea as in SS, i.e., the final failure probability is obtained as a product of higher conditional probabilities, although ²SMART algorithm hinges on the use of support vector machines [205] for classifying training points for producing the subsets. Both algorithms appear integrated on a OpenSees computational platform called FERUM, as acronym of Finite Element Reliability using Matlab[®] [206], which is a highly versatile reliability tool for practitioners. Unfortunately, these algorithms have not been sufficiently exploited in composites, precisely where these approaches may have significant impact since failure probabilities involved are very small due to restrictive fabrication standards.

In relation to the second approaches (b), the Response Surface Method (RSM), and more recently, Artificial Neuronal Networks (ANN), have also emerged as feasible alternatives. Heuristic algorithms like Genetic Algorithms [207] or Particle Swarm Optimization algorithms [208] are also fully employed nowadays in reliability, although they require higher computational resources. However, they are noticeably impacting in those cases of existence of multiple design points MPP in the LSF, especially when linking reliability and optimal design of composites (e.g. [209–215]). This topic is out of the scope of this thesis.

Response surface methods

In RSM, the LSF is substituted or sampled to improve the computational effort. The principle consists in the substitution of the actual LSF by approximate simple functions or sampled data, at the neighborhood of the design points where their contribution to the total failure probability is more important [216]. As a consequence, the computational cost is reduced with respect to the cost required when the full LSF is used or when it is necessary to evaluate the LSF by FEM runs.

When the LSF is substituted by simple functions, generally by explicit polynomial expressions, the method is called Polynomial-based Response Surface Method or simply RSM. Those methods that employ LSF approximation using training sampling data are called ANN-based response surface methods [179].

Polynomial based response surface. In the original conceptual form of the Response Surface technique, polynomials are used to approximate real LSF. Henceforth, an important requirement for the LSF is to be smooth around the area of interest. In order to obtain the RSM approximation, some regression analysis (for instance the least square method) may be required. As states in [202], one of the key factors resides in to effectively adjust the polynomials to the LSF by using fitting techniques such as a) the central composite design [217, 218] b) the fractional factorial design [219], c) the random design, d) the partially balanced incomplete box design [220] and e) Bucher and Bourgund's [221] proposal. In composites, Chen *et al.* [173] derived the longitudinal ultimate compressive strength of a composite stiffened ship's hull by a polynomial type with quadratic terms for RSM. The reliability analysis was carried out by FORM. In the same way, but in an effort to confer computational efficiency in a reliability-based design optimization problem, Young *et al.* [222] have recently proposed the polynomial RSM by regression analysis in a complex LSF considering fluid interaction of a Hexcel (IM7-8552) CFRP marine propeller. A FORM was also used to evaluate the influence of uncertainties in material and load parameters and thus to optimize the design parameters, obtaining in this case high accuracy contrasted to MC method. More recently, in [223] different types of polynomials were examined for RSM which was further used for reliability assessment of a composite stiffness panel.

ANN based response surface. As described in previous sections, when reliability analysis is applied to complicated structural systems, the response needs to be calculated by sophisticated numerical methods. In those cases, sampling the LSF by a trained ANN in substitution of MC or direct FEA sampling points, is

achieved conferring large efficiency [224]. ANN-based response surface emerges in reliability applications to solve the main limitation of polynomial-based response surface methods about the need to increase the number of deterministic analysis when the number of random variables is high, thus making them no as efficient as desirable [179]. Several authors have compared between both methods, showing that the ANN-based response surface method is more efficient than polynomial-based response surface method [202].

ANN are computational models based in parallel distributed processing with interesting properties such as the ability to learn, to generalize, to classify and to organize data. There are two main models developed for different specific computational tasks: a) those with a supervised training and b) networks without a supervised training. Networks may be also divided in feed forward, feedback architectures and a combination of both architectures. In reliability, Perceptron Multilayer Neural Networks and Neural Networks with Radial Basis Functions are mostly used. Both types of Networks have a supervised training, feed forward architecture and are universal tools for function approximation. To avoid duplication in the literature, a concise introduction of ANN for reliability by Elhewy *et al.* [179] is recommended. More details about different aspects of Neural Networks are given in [225].

In composites, ANNs are used in a wide range of applications like dynamic mechanical properties, processing optimization, numerical modeling, damage detection, delamination, among others [223, 226–229]. However, few works are encountered in reliability applications for composites, precisely where the computational efficiency of using ANNs can be fully amortized. More recently, Lopes *et al.* [85] use ANN to generate sample data for the LSF (Tsai-Wu) in stead of FEA, by which high computational efficiency is demonstrated, particularly for low failure probability values regardless the method employed for reliability evaluation. Two different ANNs were used for comparison: the Multilayer Perceptron Network and the Radial Basis Network. The results demonstrated that only 0.02% of CPU time is required for reliability calculation employing an ANN with high accuracy, using MC with samples from FEM as reference.

Excerpts from the reliability review.

Numerous studies have been conducted on the reliability of composite materials, the majority of them by focusing on static, i.e. non-progressive, loading conditions. The inherent statistical scatter in the material properties together with their complex mechanical performance, make reliability in composites a matter

of decisions, overall in regard to the adoption of the failure function. When large number of variables are involved in the mechanical description of composites, as compared to traditional materials, sensitivity analysis related to input parameters becomes a necessary exercise to reduce the dimensionality of the problem without significantly compromising on calculation performance (precision and accuracy of reliability calculation). Particularly important is the influence of fiber orientation as well as the stiffness parameters as recent results demonstrate.

It has been also shown that large composite structures require efficient techniques for reliability computation. Recent studies have proved Artificial Neural Networks (ANNs) as an advantageous technique. Genetic Algorithms (GA) are also relevant tools for those cases, where reliability is inside on a complex design optimization problem. New reliability algorithms available on OpenSees computation platforms like FERUM, should also be explored in composite reliability. These new algorithms together with ANNs for LSF evaluation, is a suggestion that may drastically reduce the computational cost for large composite structures systems and provide sufficient accuracy for small probabilities cases.

Through this up-to-date review presented in this section, it has been settled that very few works report about the progressive failure of composite laminates and its relationship with reliability calculation. Such a framework would help to derive a reliability formulation over the lifetime of composites.

In the next sections of this chapter, a novel approach to confer time-dependent reliability in composites under fatigue damage conditions is proposed. It is considered that a laminated composite panel has reached its failure point when any of its plies (upper-bound reliability formulation, recall the formulation in Section 4.3.2) is degraded by micro-cracks up to a certain threshold level and/or when the whole laminate stiffness has degraded up to a certain level. It is shown that the predicted reliability also serves to straightforwardly derive the CDF of the RUL, which is obtained as a by-product.

Table 6.1: Reliability bibliography Synoptic Table. Papers increasingly ordered by date of publication

Author	Failure Criteria	Methodology	Random Vars	Main Objective	Level
T.Y. <i>et al.</i> [87, 167]	TH	Others	Lds, Strn	Reliability	Ply
I. Cederbaum <i>et al.</i> [168]	H	FORM	Lds	Reliability	Ply
D.J. Thomas & R.C. Wetherhold [78]	Max Density Energy	MCM	Strn	Reliability	Laminate
T.Y. Kam <i>et al.</i> [178]	Max-S, Min-S, Max-W	Others	Lds, Strn	Reliability with damage	Laminate
T.L. Zhu [230]	Non-Interactive	FORM	Lds, Strn	Safety Factor Calibration	Ply
R.C. Wetherhold & A.M. Ucci [169]	TH,TW	Comparison	Lds, Strn	Reliability-Comparison	Ply
Y. Murotsu <i>et al.</i> [231]	TW	AFOSM	Lds, Str, Geo	Reliability	Laminate
M.R. Gurvich & R.B. Pipes [88]	Baseline based Criteria	MCM	Lds, Strn	Probabilistic Strn	Laminate
T.Y. Kam & E.S. Chang [79]	Max-S, TW	FORM	Strn	Validation PPF Reliability	Laminate
M. Miki <i>et al.</i> [232]	TW	AFOSM	Lds, Strn	RBDO	Laminate
C. Boyer <i>et al.</i> [81]	TH; TW, Max-S	FORM	Lds, Strn	Safety Factor Calibration	Laminate
H. Nakayasu & Z. Maekawa [183]	Comparison	Comparison	Lds, Strn	Reliability-Comparison	Laminate
C.G. Soares [77]	TH,TW	FORM	Lds, Strn	State of the Art	Laminate
T.P. Philippidis & D.J. Lekou [184]	TH	Analytical	Lds, Strn	Reliability	Ply
M.R. Gurvich & R.B. Pipes [189]	TW or any	Analytical	Lds, Strn	Reliability	Laminate
F. Richard and D. Perreux [82]	damage	FORM	Lds, Strn	Reliability and RBDO with damage	Laminate
F. Richard and D. Perreux [171]	damage strain criteria	FORM	Lds, Strn, Geo	Safety Factor Calibration	Laminate
S.C. Lin [83]	TW,TH,H,Max-S	Comparison	Lds, Strn, Geo	Reliability	Laminate
M. Di Sciuva & D. Lomario [166]	Buckling	Comparison	Lds, Strn, Stff, Geo	Reliability- Comparison	Laminate
D. M. Frangopol and S. Recek [80]	TW	MCM	Lds	Reliability- Comparison	Laminate
N.Z. Chen <i>et al.</i> [173]	Buckling	FORM	Lds, Str, Stff, Geo	Reliability	Laminate
A.K. Onkar <i>et al.</i> [84]	TW,H	SFEA	Lds, Strn	Reliability	Laminate
D.J. Lekou & T.P. Philippidis [86]	T-HN	Comparison	Ldd, Strn, Stff	Compare Methods	Laminate
S. Carillet <i>et al.</i> [233]	damage	FORM	Lds, Str, Stff, Geo	Safety factor Calibration	Laminate
P. Lopes <i>et al.</i> [85]	TW	Comparison	Lds, Geo	Reliability	Laminate
H.M. Gomes <i>et al.</i> [234]	TW	Comparison	Lds, Strn	Reliability	Laminate
R.H. Lopez <i>et al.</i> [201]	Max-S,TW	Comparison	Lds, Strn	Reliability-Comparison	Laminate
P.D. Gosling <i>et al.</i> [235]	Displacements, TW	Comparison	Geo	Reliability	Ply
V.M.K. Akula [223]	Others	Comparison	Stff, Strn, Str, Geo	Reliability-Comparison	Laminate

TW: Tsai-Wu, H: Hasin, TH: Tsai-Hahn, Max-S: Max. Stress, Min-S: Min. Strain, Max-W: Max. Work, Lds: Loads, Strn: Strngth, Str: Stress, Geo: Geometry, Stff: Stiffness

6.2 Long-term reliability assessment of composites

When the states of the system under study are time-dependent, then the temporal dimension is subsequently inherited to the reliability leading to the concept of *time-dependent reliability*. In this context, it is possible to obtain the formulation for the ℓ -step ahead prediction of reliability conditional on the most up-to date information of the system at time n , which is denoted here as $R_{n+\ell|n}$.

This section presents a reliability-based prognostics framework whereby the RUL is obtained as a probability from the predicted long-term reliability (as a particular case of time-dependent reliability), which is particularly useful for damage prognostics in composites where several degradation modes may co-exist, since reliability encapsulates information about the overall system performance as an unified indicator. The proposed reliability-based approach, which has been recently adopted in [7, 236], is specialized in this thesis for prognostics using PF. The multi-scale physics-based prognostics framework presented in Chapter 5, is adopted to sequentially predict the propagation of damage considering both matrix-cracks density and effective longitudinal Young's modulus as damage variables. Particle filters are employed to sequentially estimate the joint PDF for damage states and model parameters by fusing probability-based information from both, SHM data and damage models. Every time new data are collected, the *particles* are updated and further propagated forward in time whereby the time-dependent reliability is predicted. The long-term reliability is thus estimated as the sum of the normalized weights of the predicted particles that lie within a predefined *useful domain* at a particular time. As a by-product of the long-term reliability, an estimate of RUL of the composite laminate is obtained.

6.2.1 Formulation of long-term reliability

Recall that it is adopted the concept of *useful domain* $\mathcal{U} \subset \mathcal{Z}$ to denote the non-empty subset of "authorized" states of our system, and complementary, the *failure domain* $\bar{\mathcal{U}} = \mathcal{Z} \setminus \mathcal{U}$ as the subset of states that do not fulfill the design requirements even though the system could still work, i.e., the composite laminate might have not broken yet.

Next, for obtaining the long-term reliability of the system, it is necessary to evaluate the probability of the states to belong to the useful domain at general cycle $n + \ell$ using the most up-to-date information of the system at cycle n . In mathematical terms, it can be expressed as:

$$R_{n+\ell|n} \equiv P(\mathbf{z}_{n+\ell} \in \mathcal{U} | \mathbf{y}_{0:n}) = \int_{\mathcal{U}} p(\mathbf{z}_{n+\ell} | \mathbf{y}_{0:n}) d\mathbf{z}_{n+\ell} \quad (6.3)$$

where $p(\mathbf{z}_{n+\ell}|\mathbf{y}_{0:n})$ is the ℓ -step ahead predictive PDF of the system, as defined in Equation 4.4.3. Since the event $\{\mathbf{z}_{n+\ell} \in \mathcal{U}\}$ is the complementary of $\{\mathbf{z}_{n+\ell} \in \bar{\mathcal{U}}\}$, then $P(\mathbf{z}_{n+\ell} \in \mathcal{U}|\mathbf{y}_{0:n}) = 1 - P(\mathbf{z}_{n+\ell} \in \bar{\mathcal{U}}|\mathbf{y}_{0:n})$ so that the ℓ -step ahead reliability can also be obtained as:

$$R_{n+\ell|n} = 1 - \int_{\mathcal{Z}} \mathbb{I}_{(\bar{\mathcal{U}})}(\mathbf{z}_{n+\ell}) p(\mathbf{z}_{n+\ell}|\mathbf{y}_{0:n}) d\mathbf{z}_{n+\ell} \quad (6.4)$$

In the last equation, $\mathbb{I}_{(\bar{\mathcal{U}})}(\mathbf{z})$ is a *threshold function* that maps a given point in the joint state-parameter space \mathcal{Z} to the Boolean domain $\mathcal{Z} \rightarrow [0, 1]$ as follows:

$$\mathbb{I}_{(\bar{\mathcal{U}})}(\mathbf{z}) = \begin{cases} 1, & \text{if } \mathbf{z} \in \bar{\mathcal{U}} \\ 0, & \text{if } \mathbf{z} \in \mathcal{U} \end{cases} \quad (6.5)$$

By replacing $p(\mathbf{z}_{n+\ell}|\mathbf{y}_{0:n})$ by its approximation given by Equation 4.45, an approximation of the last multidimensional integral can be obtained as:

$$\begin{aligned} R_{n+\ell|n} &\approx 1 - \int_{\mathcal{Z}} \mathbb{I}_{(\bar{\mathcal{U}})}(\mathbf{z}_{n+\ell}) \left[\sum_{i=1}^N \omega_n^{(i)} \delta(\mathbf{z}_{n+\ell} - \mathbf{z}_{n+\ell}^{(i)}) \right] d\mathbf{z}_{n+\ell} \\ &= 1 - \sum_{i=1}^N \omega_n^{(i)} \mathbb{I}_{(\bar{\mathcal{U}})}(\mathbf{z}_{n+\ell}^{(i)}) \end{aligned} \quad (6.6)$$

Note that, as a particular case of the long-term reliability, the updated estimation of reliability can be obtained at time n when a new measurement is available as:

$$R_{n|n} = 1 - \sum_{i=1}^N \omega_n^{(i)} \mathbb{I}_{(\bar{\mathcal{U}})}(\mathbf{z}_n^{(i)}) \quad (6.7)$$

where $\{\mathbf{z}_n, \omega_n\}_{i=1}^N$ is the PF approximation of the updated PDF $p(\mathbf{z}_n|\mathbf{y}_{0:n})$, as shown in Equation 6.3.

6.2.2 Computation of RUL based on long-term reliability

In this section, the connection between RUL and long-term reliability is explored. Recall that the remaining useful life of an engineering component/system is the minimum time ℓ when the predicted state is expected to lie within the failure domain $\bar{\mathcal{U}}$. In mathematical terms:

$$RUL_n = \inf\{\ell \in \mathbb{N} : \mathbf{z}_{n+\ell} \in \bar{\mathcal{U}}\} \quad (6.8)$$

In the context of the fatigue problem investigated in this thesis, the RUL_n corresponds to the minimum amount of prospective fatigue cycles starting from n , such that the damage (matrix-cracks and stiffness loss) goes beyond a predefined set of thresholds.

In prognostics, RUL_n is typically expressed as a conditional probability denoted by $P(RUL_n = \ell | \mathbf{y}_{0:n})$. Note that, based on the definition provided in Equation 6.8, $P(RUL_n = \ell | \mathbf{y}_{0:n})$ is intuitively equivalent to the probability $P(\mathbf{z}_{n+\ell} \in \bar{\mathcal{U}} | \mathbf{y}_{0:n})$. In the literature, recent works have reported about such correspondence between probabilities [7, 236], basically accepting that $P(RUL_n = \ell | \mathbf{y}_{0:n}) \approx P(\mathbf{z}_{n+\ell} \in \bar{\mathcal{U}} | \mathbf{y}_{0:n})$ except for exhaustively monotonic latent processes where the equality holds. However, further insight is required to explore the underlined conditions behind such correspondence for a general latent process, i.e., not necessarily monotonic. In the next section, the equivalence between $P(RUL_n = \ell | \mathbf{y}_{0:n})$ and $P(\mathbf{z}_{n+\ell} \in \bar{\mathcal{U}} | \mathbf{y}_{0:n})$ is derived and examined under the axioms of Probability Logic.

6.2.3 Derivation of RUL as a probability using Probability Logic

In probability logic, $P(b|a)$ is interpreted as the degree of plausibility of proposition b based on the information in proposition a [128]; in other words, given the proposition a , then the proposition b holds with probability $P(b|a)$. Four axioms are defined in probability logic:

$$P(b|a) \geq 0 \tag{6.9a}$$

$$P(b|a) + P(\sim b|a) = 1 \tag{6.9b}$$

$$P(b|a \& b) = 1 \tag{6.9c}$$

$$P(c \& b|a) = P(c|b \& a)P(a|b) \tag{6.9d}$$

From these axioms, a number of properties can be derived. The first is that $P(b|a) \leq 1$, which can be readily derived from axioms (6.9a) and (6.9b). Now, suppose that the proposition a represents the data $\mathbf{y}_{0:n}$, b represents $[RUL_n = \ell]$ and c represents $[\mathbf{z}_{n+\ell} \in \bar{\mathcal{U}}]$. It is clear that the proposition $[RUL_n = \ell]$ implies the proposition $[\mathbf{z}_{n+\ell} \in \bar{\mathcal{U}}]$, i.e. $b \implies c$. Under the last postulate, the following inequality holds $P(b|a \& (b \implies c)) \leq P(c|a \& (b \implies c))$, which can be demonstrated using the axioms of Probability Logic as follows, where for the sake of clearness, the event $a \& (b \implies c)$ is grouped under d :

$$\begin{aligned}
& \underbrace{P(b|d\&c)P(c|d) = P(c\&b|d)}_{(6.9d)} = P(b\&(b \implies c)|d) \\
& = \underbrace{P(b|(b \implies c)\&d)P((b \implies c)|d)}_{(6.9d),(6.9c)} = P(b|d)
\end{aligned} \tag{6.10}$$

In the last equation the equivalence $b\&c \equiv b\&(b \implies c)$ is used in the last step. Given that $P(b|d\&c) \leq 1$, Equation 6.10 implies that $P(b|d) \leq P(c|d)$, thus the inequality

$$P(b|a\&(b \implies c)) \leq P(c|a\&(b \implies c)) \tag{6.11}$$

is formally demonstrated. Next, let the proposition e represents $(b \implies c)$ and let us multiply Eq. 6.11 by $P(e|a)$:

$$P(b|a\&e)P(e|a) \leq P(c|a\&e)P(e|a) \tag{6.12}$$

Based on axiom 6.9d, Equation 6.12 can be re-written as:

$$P(b\&e|a) \leq P(c\&e|a) \tag{6.13}$$

and equivalently as:

$$P(b\&(b \implies c)|a) \leq P(c\&(b \implies c)|a) \tag{6.14}$$

By the same reason that $P(b\&(b \implies c)|d) = P(b|d)$ in Equation 6.10, it can be easily accepted that $P(b\&(b \implies c)|a) = P(b|a)$ in Equation 6.14. Observe also that the event $c\&(b \implies c)$ is equivalent to c , thus $P(c\&(b \implies c)|a) = P(c|a)$, which finally leads to $P(b|a) \leq P(c|a)$, and equivalently $P(RUL_n = \ell | \mathbf{y}_{0:n}) \leq P(\mathbf{z}_{n+\ell} \in \bar{\mathcal{U}} | \mathbf{y}_{0:n})$, as we wanted to demonstrate. The last statement means that, in general, the event $[RUL_n = \ell]$ occurs with less or equal probability to the event $[\mathbf{z}_{n+\ell} \in \bar{\mathcal{U}}]$. In other words, $\ell \in \mathbb{N}$ might be an upper bound value for RUL_n when it is derived by focusing on the event $[\mathbf{z}_{n+\ell} \in \bar{\mathcal{U}}]$ for a general case.

In the case of exhaustively monotonic damage processes, $[RUL_n = \ell] \iff [\mathbf{z}_{n+\ell} \in \bar{\mathcal{U}}]$, i.e.: $b \iff c$. Then, the following property holds: $P(b|a\&(b \iff c)) = P(c|a\&(b \iff c))$, which can be readily demonstrated from Equations 6.10 to 6.11 by just considering that $P(b|d\&c) = 1$. The rest of steps from Equation 6.11 also apply here by considering identities instead of inequalities and also by considering that e in this case represents the event $b \iff c$, which finally lead to $P(RUL_n = \ell | \mathbf{y}_{0:n}) = P(\mathbf{z}_{n+\ell} \in \bar{\mathcal{U}} | \mathbf{y}_{0:n})$.

Notice that, by the reason given above, the implication $b \iff c$ also applies when considering the event $[RUL_n \leq \ell]$ instead of $[RUL_n = \ell]$, so that the equality $P(RUL_n \leq \ell | \mathbf{y}_{0:n}) = P(\mathbf{z}_{n+\ell} \in \bar{\mathcal{U}} | \mathbf{y}_{0:n})$ always holds irrespective to whether the process is monotonic or not.

6.2.4 Prognostics based on long-term reliability

The reasoning given above allows us to establish a rational connection between the RUL_n as a probability, and the time-dependent reliability, provided that events $[\mathbf{z}_{n+\ell} \in \bar{\mathcal{U}}]$ and $[RUL_n \leq \ell]$ occur with the same probability, i.e., $\mathbf{z}_{n+\ell} \in \bar{\mathcal{U}} \iff RUL_n \leq \ell$; hence the following identities hold:

$$\begin{aligned} F_{RUL_n}(\ell - n) &\equiv P(RUL_n \leq \ell | \mathbf{y}_{0:n}) = P(\mathbf{z}_{n+\ell} \in \bar{\mathcal{U}} | \mathbf{y}_{0:n}) \\ &= 1 - P(\mathbf{z}_{n+\ell} \in \mathcal{U} | \mathbf{y}_{0:n}) \\ &= 1 - R_{n+\ell|n} \end{aligned} \quad (6.15)$$

which makes use of the definition of long-term reliability given by Equation 6.3. In the last equation, F_{RUL_n} denotes the CDF of random variable $\ell - n \in \mathbb{N}$ defined for the RUL estimate. The last equation means in other words that the CDF of RUL at time of prediction n equals the threshold exceedance probability.

Next, the probability $P(RUL_n \leq \ell | \mathbf{y}_{0:n})$ can be approximated using Equation 6.6 as:

$$P(RUL_n \leq \ell | \mathbf{y}_{0:n}) \approx \sum_{i=1}^N \omega_n^{(i)} \mathbb{I}_{(\bar{\mathcal{U}})}(\mathbf{z}_{n+\ell}^{(i)}) \quad (6.16)$$

In Figure 6.3, a conceptual scheme of the proposed reliability-based prognostics framework is provided. Observe that it is possible to compute the entire CDF of RUL_n by evaluating Equation 6.16 for different values of $\ell > n$, until $R_{n+\ell|n} = 0$ is reached, which coincides when $F_{RUL_n}(\ell - n) = 1$ holds. This procedure for reliability update and prediction can be performed each time n new data are collected. The outcome of these steps are conceptually illustrated in Figure 6.2. In the top panel: the samples of \mathbf{z} -states along with their idealized sample trajectories are represented against time steps $\{n - 1, n, \dots, n + \ell\}$, where n is the last time when data are available. The horizontal line represents the boundary between the useful domain \mathcal{U} and its complementary region $\bar{\mathcal{U}}$. The curve of predicted reliability starting from time n is represented against time at the bottom panel. Observe the correspondence between predicted reliability $R_{n+\ell|n}$ and the $P(RUL_n \leq \ell | \mathbf{y}_{0:n})$, as showed in Eq. 6.15.

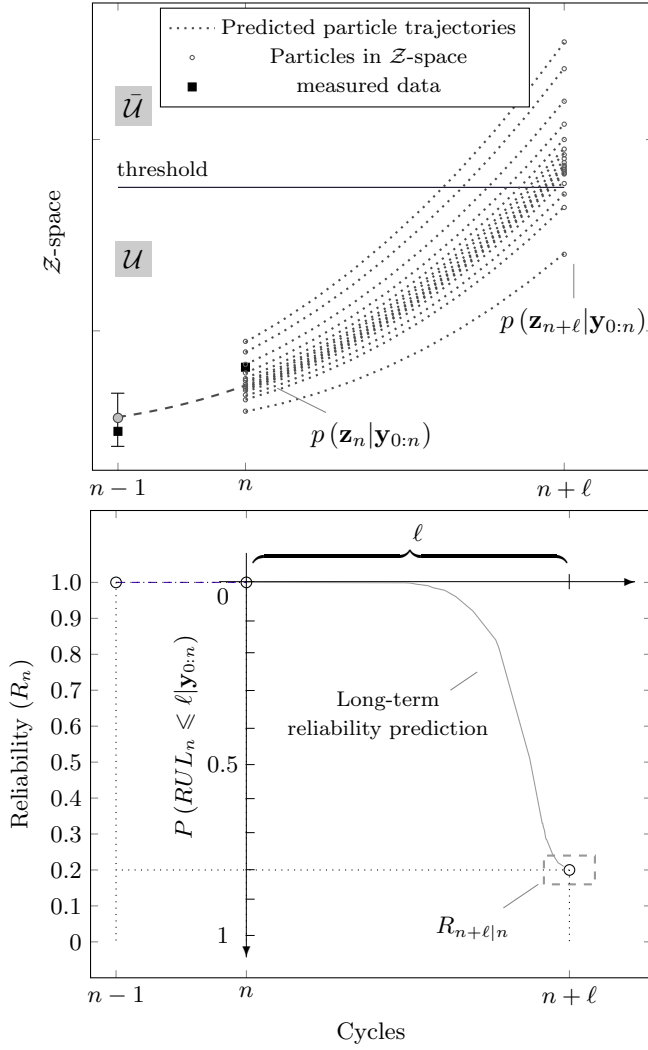


Figure 6.2: Illustration of the proposed framework for prognostics based on long-term reliability. Top panel: samples of \mathbf{z} -states along with their idealized sample trajectories represented against different time steps. Bottom panel: long-term reliability predicted from cycle n to $n + \ell$, where $\ell > 1 \in \mathbb{N}$.

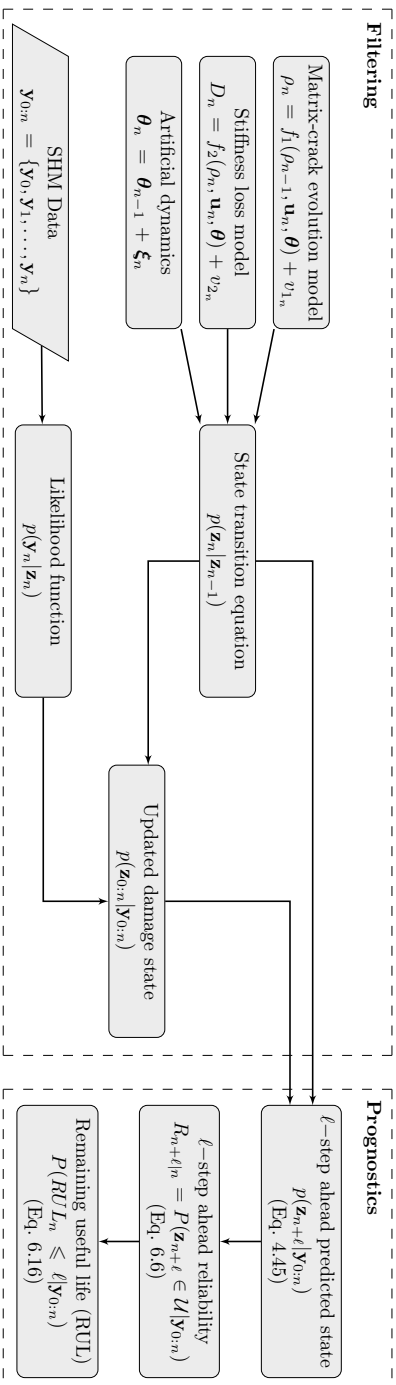


Figure 6.3: Conceptual scheme for prognostics based on long-term reliability.

7

New efficient algorithm for prognostics involving rare-events

This chapter presents an efficient computational framework for prognostics by combining the particle filter-based prognostics principles with the technique of Subset simulation, first developed in S.K. Au and J.L. Beck [62]. It has been named PFP-SubSim algorithm. The idea behind PFP-SubSim algorithm is to split the multi-step-ahead predicted trajectories into multiple branches of selected samples at various stages of the process, which correspond to increasingly closer approximations to the critical set of thresholds. A pseudocode implementation of PFP-SubSim algorithm is provided in this chapter along with a schematic description of the main blocks of computation, in order to help the reader to easily understand and implement the proposed algorithm for prognostics applications.

7.1 Introduction

One of the most important and challenging problems in prognostics is to accurately estimate the EOL/RUL of a system whose faulty behavior is highly unprovable or uncertain, as happens typically when predicting catastrophic failures of nuclear plants, collapse of materials under physical or chemical asymptotic degradation, abnormal discharge of batteries for critical systems, etcetera [237]. Model-based prognostics frameworks have attracted significant attention to the PHM community due to its better predictability. The aim of model-prognostics is to improve the predictability by capturing the underlying first principles behind the evolution of the fault indicator [9], hence reducing the *lack of knowledge* uncertainty, typically present in prognostics. Several examples can be found in the literature dealing with model-based prognostics for a widespread range of applications like fatigue crack growth in metals [10, 11], battery ageing and failure [12, 13], fatigue degradation in composite materials [134], just to name but a few.

However, there are additional sources of uncertainty, other than the model uncertainty, that are present in a typical prognostics problem like (a) uncertainty in future inputs to the system and (b) data uncertainty [22]. Further, it is added (c) the uncertainty that the prognostics algorithm introduces itself, since optimal closed-form solutions for prognostics are very limited and often intractable in real life applications [23]. Sampling-based algorithms (e.g. PF) [18, 19] are conventionally used in prognostics to efficiently approximate the continuous PDF of predicted states through a limited set of discrete particle paths representing random trajectories of system evolution in the state space [20–22]. Note that multi-step ahead state estimation is a prerequisite to prognostics, hence the statistical uncertainty that arises from the approximation error is propagated in time leading to an artificial increase of the final uncertainty for the prediction of system failure as well as for the EOL/RUL estimation [24]. The last is specially critical when prognostics involves rare-event simulation, as typically happens in prognostics of asymptotic processes where the set of thresholds are selected so high such that the vast majority of simulations are employed to simulate the model in the safe region (see Figure 7.1 for an illustrative representation). Higher-density sampling-based methods maybe employed achieving higher resolution for the estimations, however it is at the expense of a higher computational effort. To address this challenge, different algorithms have been proposed in recent years to achieve accuracy while maintaining a moderate computational burden [25].

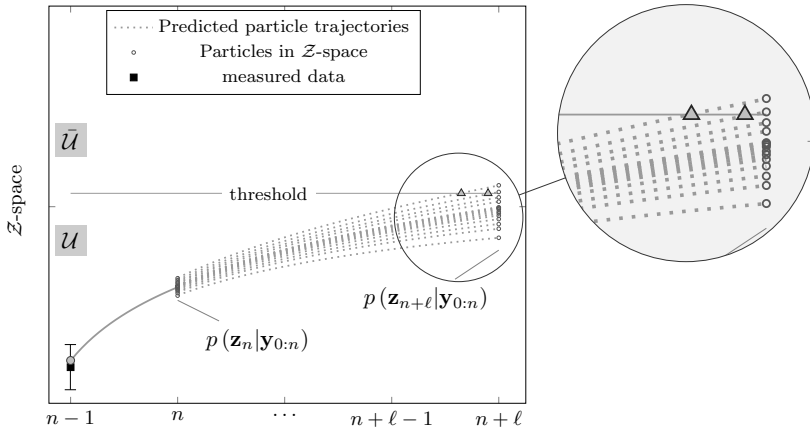


Figure 7.1: Schematic representation of a multi-step ahead prediction of an asymptotic process. Observe that only few particles reach the failure domain \mathcal{U} . Gray triangles represent the first-hitting points of the particles that reach threshold, whereby the time indexes for the EOL calculation can be derived.

Subset Simulation method [62] is an efficient simulation framework for simulation of rare-events in high-dimensional spaces which makes this method applicable to a broad range of areas of science and engineering where the simulation of a rare event is required [64, 203]. This chapter shows that for general prognostics problems where samples of the future states can be readily generated by means of Bayesian filtering methods, it is possible to implement Subset Simulation with significant gain in efficiency. The idea behind Subset Simulation method in application to prognostics is to split the multi-step-ahead predicted states into multiple branches of selected samples (seeds) at selected stages of the process. These seeds provide the starting points for reproducing offsprings of states by conditional sampling leading to a nested sequence of subsets (also referred to as simulation levels) which are produced adaptively until the final failure region is reached. At the higher simulation level, the samples are closely distributed in the vicinity of the final threshold achieving high resolution for the EOL estimate. The resulting computational framework is called PFP-SubSim and has been recently presented in [238] on behalf of the European Conference of the Prognostics and Health Management Society, 2014.

7.2 Prediction of system failure

The ℓ -step ahead prediction of states previously defined in Section 4.4.3 can be used for the forecasting of failure, which is defined here as the probability that

the system behaves unacceptably during a specific interval of future instants of time using the most up-to-date information about the system. The problem of interest regards the evaluation of the probability of expected performance of the stochastic system within the region $\bar{\mathcal{U}}$ during a prescribed time interval defined by $[n + 1, n + \ell] \subset \mathbb{N}$, as follows:

$$P(\bar{\mathcal{U}}) = \int_{\bar{\mathcal{U}}} p(\mathbf{z}_{n+1:n+\ell} | \mathbf{y}_{0:n}) d\mathbf{z}_{n+1:n+\ell} = \int_{\bar{\mathcal{U}}} \prod_{t=n+1}^{n+\ell} p(\mathbf{z}_t | \mathbf{y}_{0:n}) d\mathbf{z}_{n+1:n+\ell} \quad (7.1)$$

where we make the assumption that the model error term \mathbf{v} in Equation 4.34a is independent of time t , and therefore the joint PDF $p(\mathbf{z}_{n+1:n+\ell} | \mathbf{y}_{0:n})$ can be described by the product of independent PDFs like those previously defined in Equation 4.44. Equation 7.1 requires the evaluation of a multidimensional integral which can be approximated as a mathematical expectation using the samples from the PF approximation defined in Section 4.4.3 as follows:

$$\begin{aligned} P(\bar{\mathcal{U}}) &= \int_{\bar{\mathcal{U}}} \prod_{t=n+1}^{n+\ell} p(\mathbf{z}_t | \mathbf{y}_{0:n}) d\mathbf{z} = \int_{\mathcal{Z}} \mathbb{I}_{\bar{\mathcal{U}}}(\mathbf{z}) \prod_{t=n+1}^{n+\ell} p(\mathbf{z}_t | \mathbf{y}_{0:n}) d\mathbf{z} \\ &\equiv \mathbb{E}_{f_n} \left[\mathbb{I}_{\bar{\mathcal{U}}} \left(\{\mathbf{z}_t\}_{t=n+1}^{n+\ell} \right) \right] \approx \frac{1}{N_T} \sum_{i=1}^N \sum_{q=1}^{\ell} \mathbb{I}_{\bar{\mathcal{U}}}(\mathbf{z}^{(i,q)}) \end{aligned} \quad (7.2)$$

where $\{\mathbf{z}_t^{(n)}\}_{n=1}^{N_T}$ are N_T predictive samples simulated according to the dynamical model in Equation 4.34a and distributed with equally probability among N particle trajectories of fixed length ℓ , so that $N_T = N\ell$. The term $\mathbb{I}_{\bar{\mathcal{U}}}(\mathbf{z}^{(i,q)})$ is the value of the indicator function $\mathbb{I}_{\bar{\mathcal{U}}}$ evaluated for the q th sample of the i th Markov chain. The last approximation is unbiased as N_T approaches infinity.

7.3 Prognostics involving rare-events.

The method presented above has a serious drawback in cases of small values for $P(\bar{\mathcal{U}})$, due to the fact that a huge number of particles are required to achieve acceptable estimation accuracy which may increase the computational cost significantly. Hence, the research direction has been focused on developing a more efficient simulation method for the prognostics of rare events, which is described next. Afterward, a novel algorithm called PFP-SubSim for prognostics of rare-events is presented.

7.3.1 Subset Simulation for prognostics

By means of Subset Simulation the probability of the possibly rare event $P(\bar{\mathcal{U}})$ can be expressed as the product of larger conditional probabilities that can be obtained with much less computational effort. The conditional probabilities are efficiently estimated by means of conditional samples that correspond to specified levels of the performance function $g : \mathcal{Z} \rightarrow \mathbb{R}$ in a progressive manner.

To this end, it is assumed that $\bar{\mathcal{U}}$ in Equation 4.46 is defined as the intersection of m nested regions in \mathcal{Z} , i.e., $\bar{\mathcal{U}}_1 \supset \bar{\mathcal{U}}_2 \dots \supset \bar{\mathcal{U}}_{m-1} \supset \bar{\mathcal{U}}_m = \bar{\mathcal{U}}$, so that $\bar{\mathcal{U}} = \bigcap_{j=1}^m \bar{\mathcal{U}}_j$. Each subset $\bar{\mathcal{U}}_j$ is defined as $\bar{\mathcal{U}}_j \equiv \{\mathbf{z}_t \in \mathcal{Z} : g(\mathbf{z}_t) > b_j\}$, with $b_{j+1} > b_j$, such that $p(\mathbf{z}_t | \bar{\mathcal{U}}_j) \propto p(\mathbf{z}_t) \mathbb{I}_{\bar{\mathcal{U}}_j}(\mathbf{z}_t)$, $j = 1, \dots, m$. By definition of conditional probability, it follows that¹:

$$P(\bar{\mathcal{U}}) = P\left(\bigcap_{j=1}^m \bar{\mathcal{U}}_j\right) = P(\bar{\mathcal{U}}_1) \prod_{j=2}^m P(\bar{\mathcal{U}}_j | \bar{\mathcal{U}}_{j-1}) \quad (7.3)$$

where $P(\bar{\mathcal{U}}_j | \bar{\mathcal{U}}_{j-1}) \equiv P(\mathbf{z}_t \in \bar{\mathcal{U}}_j | \mathbf{z}_t \in \bar{\mathcal{U}}_{j-1})$, is the conditional failure probability at the $(j-1)^{th}$ intermediate failure domain, and is denoted here by P_j for simplicity. Equation 7.3 indicates that the probability $P(\bar{\mathcal{U}})$ may be relatively small, however it can be approximated by Subset Simulation as the product of larger conditional probabilities, thus avoiding prognostics of rare events.

To compute $P(\bar{\mathcal{U}})$ based on Equation 7.3, it is necessary to estimate the probabilities P_j , $j = 1, \dots, m$. P_1 can be readily estimated by the standard MC method as follows:

$$P(\bar{\mathcal{U}}_1) \approx \bar{P}_1 = \frac{1}{M} \sum_{i=1}^M \mathbb{I}_{\bar{\mathcal{U}}_1}(\mathbf{z}_t^{0,(i)}) \quad (7.4)$$

where $\mathbf{z}_t^{0,(i)}$, $i = 1, \dots, M$, are samples from identically distributed multi-step ahead predicted trajectories simulated according to the model given in Equation 4.34a. The superscript "0" here denotes that they are unconditional samples. The remaining factors are efficiently estimated using MCMC methods for sampling from the PDF $p(\mathbf{z}_t^{j-1} | \bar{\mathcal{U}}_{j-1})$ when $j \geq 2$ giving:

$$P(\bar{\mathcal{U}}_j | \bar{\mathcal{U}}_{j-1}) \approx \bar{P}_j = \frac{1}{M} \sum_{i=1}^M \mathbb{I}_{\bar{\mathcal{U}}_j}(\mathbf{z}_t^{j-1,(i)}) \quad (7.5)$$

¹The term $P(\bar{\mathcal{U}}) \equiv P(\mathbf{z} \in \bar{\mathcal{U}})$ is used for simpler notation.

where $\mathbf{z}_t^{j-1,(i)} \sim p(\mathbf{z}_t^{j-1}|\bar{\mathcal{U}}_{j-1})$. From this standpoint, several implementation issues immediately arises: (1) the establishment of the intermediate levels $\bar{\mathcal{U}}_j$, and (2) the selection of a suitable local proposal PDF for MCMC sampling.

Observe that the implementation issues about SS presented in Section 4.2.4 also apply here. In fact, the sample estimate of $P(\bar{\mathcal{U}}_j|\bar{\mathcal{U}}_{j-1})$ in Equation (7.5) is equal to a fixed value $P_0 \in (0, 1)$, preferably $P_0 = 0.2$, according to [62, 65]. This procedure gives MP_0 of these samples in $\bar{\mathcal{U}}_j$, which serve as seeds for generating more samples from $p(\mathbf{z}_t|\bar{\mathcal{U}}_j)$. The remaining $(1/P_0 - 1)$ samples are generated from $p(\mathbf{z}_t|\bar{\mathcal{U}}_j)$ by MCMC starting at each seed, giving a total of M samples in $\bar{\mathcal{U}}_j$. Figure 7.2 illustrates the generation of samples produced by PFP-SubSim algorithm using a two-dimensional example for ease of representation. Solid disks represent samples in the joint state-parameter space \mathcal{Z} . Disks with darker gray tones represent samples distributed according to decreasing intermediate regions. Circled disks are the Markov chain seeds for producing more samples according to the subsequent intermediate levels $p(\cdot|\bar{\mathcal{U}}_j)$, $j = 1, \dots, m$.

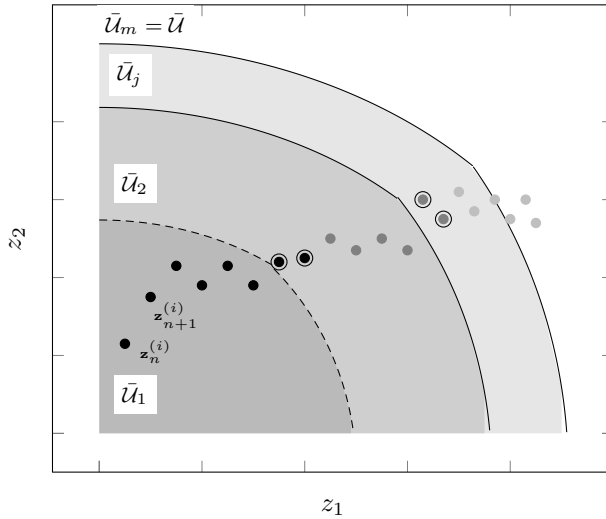


Figure 7.2: Schematic representation of two-dimensional samples produced by PFP-SubSim algorithm: solid disks represent samples in the joint state-parameter space. Disks with darker gray tones represent samples distributed according to decreasing intermediate regions. Circle disks are Markov chain seeds for $p(\cdot|\bar{\mathcal{U}}_j)$, $j = 1 \dots, m$.

7.3.2 The PFP-SubSim algorithm

See Algorithm 5 for a pseudocode implementation, which is intended to be sufficient for most cases of application. The algorithm is implemented such that a fixed amount of M samples are drawn per simulation level $\bar{\mathcal{U}}_j$, so that $N_T = mM$, with N_T the total amount of model evaluations required by the algorithm to reach the final threshold. It is important to remark that this choice is just to allow the computational burden to be controlled. In addition, the conditional probability is set to $P_0 = 0.2$, following the recommendation about Subset Simulation method in Section 4.2.4. Figure 7.3 provides an algorithm flow-chart to better understand the main steps of the algorithm. For simplicity, the time subscripts are dropped from Step 11 in Algorithm 5, since the time indexing information is implicitly contained in each sample. Observe also that the adaptive choice of the b_j -sequence guarantees that the estimated conditional probability $P(\bar{\mathcal{U}}_j|\bar{\mathcal{U}}_{j-1})$ is equal to P_0 .

Observe that the proposed methodology, and in particular the Steps 19 and 20 of the Algorithm 5, has anticipated that the multi-step ahead predicted trajectories simulated using the model in Equation 4.34a can be split into seeds (whereby subsequent states are generated), without artificially influencing the recurrence given by the stochastic process in Equation 4.34a. This is justified by the Markovian assumption for the transition equation in 4.34a, by which the probability of obtaining \mathbf{z}_t depends only on its preceding state \mathbf{z}_{t-1} and not on the history of past states. The last implies that the simulation of a sequence of states ℓ -steps ahead is essentially an uncoupled procedure given the information from the previous step.

Algorithm 5 Pseudocode implementation for PFP-SubSim

1: **Inputs:**
2: $P_0 \in [0, 1]$ {gives percentile selection, chosen so $NP_0, 1/P_0 \in \mathbb{Z}^+$; $P_0 = 0.2$ is recommended}.
3: M , {number of samples per intermediate level}; m , {maximum number of simulation levels allowed}; $\ell = M/N$.
4: $\{\mathbf{z}_n^{(i)}, \omega_n^{(i)}\}_{i=1}^N$; {e.g. use Algorithm 3.}
5: **Algorithm:**
6: **for** $i : 1, \dots, N$ **do**
7: **for** $t : n + 1, \dots, n + \ell$ **do**
8: Sample $\mathbf{z}_t^{0,(i)} \sim p(\mathbf{z}_t | \mathbf{z}_{t-1}^{(i)})$.
9: **end for**
10: **end for**
11: $[\mathbf{z}^{0,(1)}, \dots, \mathbf{z}^{0,(M)}]$
12: **for** $j : 1, \dots, m$ **do**
13: **for** $i : 1, \dots, M$ **do**
14: Evaluate: $g_j^{(i)} = g(\mathbf{z}^{j-1,(i)})$;
15: **end for**
16: Sort $\{\mathbf{z}^{j-1,(i)}\}_{i=1}^M$ so that $g_j^{(1)} \leq g_j^{(2)} \leq \dots \leq g_j^{(M)}$
17: Fix $b_j = \frac{1}{2} (g_j^{(MP_0)} + g_j^{(MP_0+1)})$
18: **for** $i = 1, \dots, MP_0$ **do**
19: Select as a seed $(\mathbf{z}_{(1)}^{j,(i)}) = (\mathbf{z}^{j-1,(i)}) \sim p(\mathbf{z} | \bar{U}_j)$
20: Run the model to generate $1/P_0$ states of a Markov chain lying in \bar{U}_j :
21: $[(\mathbf{z}_{(1)}^{j,(i)}), \dots, (\mathbf{z}_{(1/P_0)}^{j,(i)})]$
22: **end for**
23: Renumber $[(\mathbf{z}_{(k)}^{j,(i)})]_{i=1, \dots, MP_0; k=1, \dots, 1/P_0}$ as: $[(\mathbf{z}^{j,(1)}), \dots, (\mathbf{z}^{j,(M)})]$
24: **if** $b_j > b$ **then**
25: Record the times indexes of the first-passage points \rightarrow End Algorithm
26: **end if**
27: **end for**

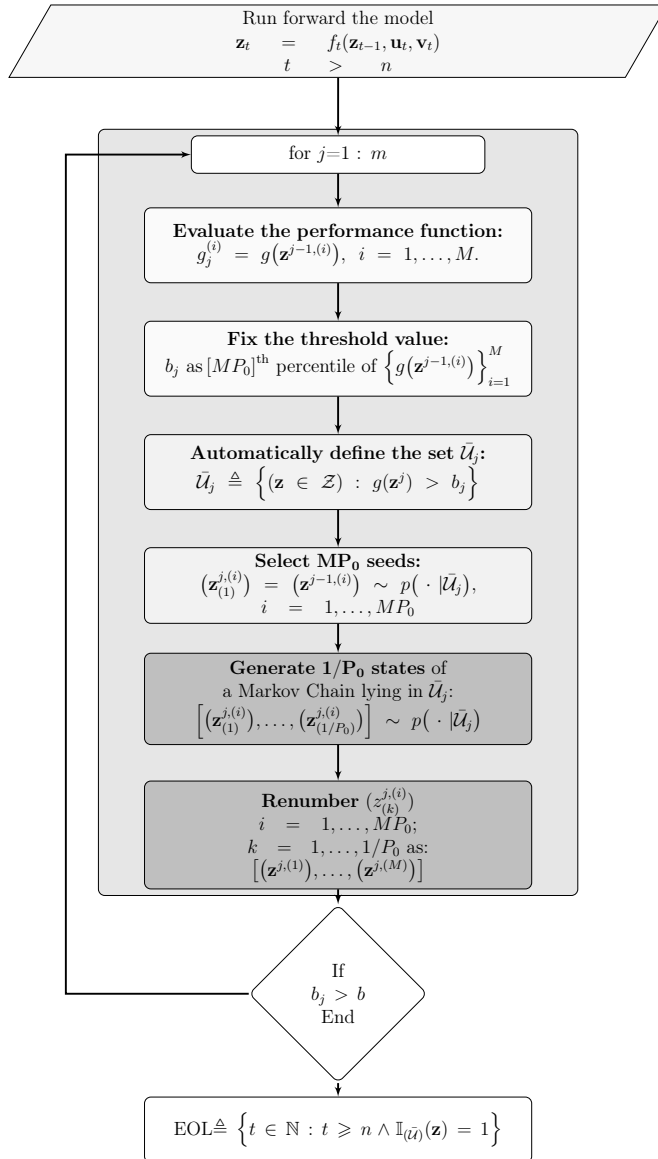


Figure 7.3: PFP-SubSim algorithm flowchart.

Part III

EXPERIMENTAL AND NUMERICAL VALIDATIONS

8

Fatigue damage dataset

This chapter is dedicated to present the fatigue damage data of composites used for calculations along with the methods followed for their acquisition and collection. Composite laminates material properties are also presented. It is important to remark that the data reported in this section correspond to the test of fatigue ageing on CFRP composites carried out by the Stanford Structures and Composites Laboratory (SACL) in collaboration with the Prognostic Center of Excellence (PCoE) at NASA Ames Research Center [239]. The resulting information from these tests has been recently uploaded as an open-access dataset distributed by NASA Ames Prognostics Data Repository [1]. The data organization and post-processing as well as the preparation of the open-access dataset were contributed by the author of this thesis.

8.1 Material and SHM system

The data presented in this section were collected from run-to-failure tension-tension fatigue experiments measuring the evolution of fatigue damage in CRFP laminates using PZT sensors for obtaining data of matrix micro-cracks density and delamination, along with strain gauges for measurements of normalized effective stiffness. The fatigue cycling data were obtained for graphite-epoxy laminates. Torayca T700G unidirectional pre-impregnated (typically termed as *prepreg*) material was used for $15.24 \text{ [cm]} \times 25.4 \text{ [cm]}$ coupons with dogbone geometry and a notch with dimensions $5.08 \text{ [mm]} \times 19.3 \text{ [mm]}$ to induce stress concentration. The coupons were subjected to a tension-tension fatigue test conducted under a controlled loop of cyclical loadings with a frequency of 5.0 [Hz] , a stress ratio of $R \simeq 0.14$ and a maximum applied load of 31.13 [KN] (which coincides with the 80% of the laminate ultimate stress). To account for the influence of ply orientation, three different symmetric layup configurations were considered to produce the coupons: *Layup 1*) $[0_2/90_4]_S$, *Layup 2*) $[0/90_2/45/-45/90]_S$, and *Layup 3*) $[90_2/45/-45]_S$.

The fatigue damage was monitored by a couple of six-PZT-sensors SMART Layer® from Acellent Technologies, Inc., which were attached to the surface of each coupon (see Figure 8.1 for a schematic view of sensors placement and configuration). This configuration allows six actuators and six sensors to monitor Lamb wave propagation through the samples defining a total of 36 actuator-sensor trajectories.

The tests were performed using a MTS machine following ASTM Standards D3039 and D3479 [240, 241]. The fatigue cycling tests were stopped at periodical cycles to collect PZT sensor data for all trajectories at different interrogation frequencies as well as strain-gauges data. X-rays images of the samples were taken using a dye-penetrant to enhance X-ray absorption. Further details about the fatigue testing can be found in [239].

8.1.1 Data acquisition for micro-cracks

Piezoelectric sensors (PZT) were employed since they have the capability of changing mechanical energy into electrical energy and vice versa. Thus, an electrical voltage acting as input in the i^{th} actuator, generates a mechanical excitation traveling across the specimen which can be sensed at the j^{th} sensor, $i, j = 1, \dots, 6$. The sensor response is further changed into an electrical signal that can be recorded. The system employed to generate and collect Lamb waves is the Scan Genie from Acellent Technologies, Inc.

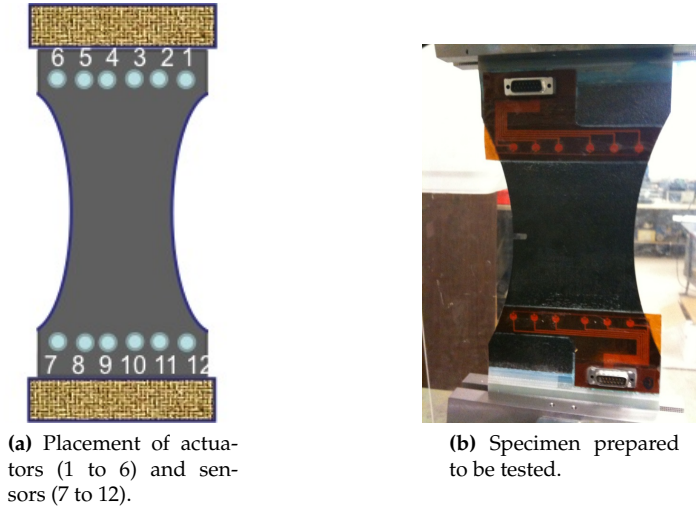


Figure 8.1: View of SMART® Layers location and coupon specimen. Both images are taken from [1], courtesy of NASA PCoE.

Since the likelihood of detecting damage increases by choosing the maximum set of trajectories sweeping the material surface as possible, the six actuators were connected to the six sensors defining a total number of 36 trajectories. By other hand, due to the dispersive nature of Lamb waves (group and phase velocity vary with frequency [242]), each trajectory was actuated at 7 different frequencies whose values range from 150 [Hz] to 450 [Hz], with an average input voltage of 50 volts and a gain of 20 [dB] [243]. Therefore, each collected data file corresponding to a specific fatigue cycle contains a total amount of $36 \times 7 = 252$ signals for the actuators and another 252 signals for the sensors, like those represented in Figure 8.2. It is represented the path 42 that corresponds to signal from actuator 1 and sensed by sensor 12 with a frequency 400 [Hz] and gain 25 [V]. This signal data were obtained at cycle 1.2×10^6 of the fatigue testing for a laminate with layup type 1. It is denoted by *path* to any of these 252 possible signal data. The path definition file includes the information about the path denomination (from 1 to 252), the pair actuator-sensor activated, input voltage, frequency and gain.

It is important to remark here that the fatigue data for each coupon were collected considering three different boundary conditions: *Type 1*) specimen loaded with the mean load, *Type 2*) specimen unloaded but clamped, and *Type 3*) coupon removed from the testing machine (absolute 0 loads). This information is attached to every data file collected as will be explained in the next section.

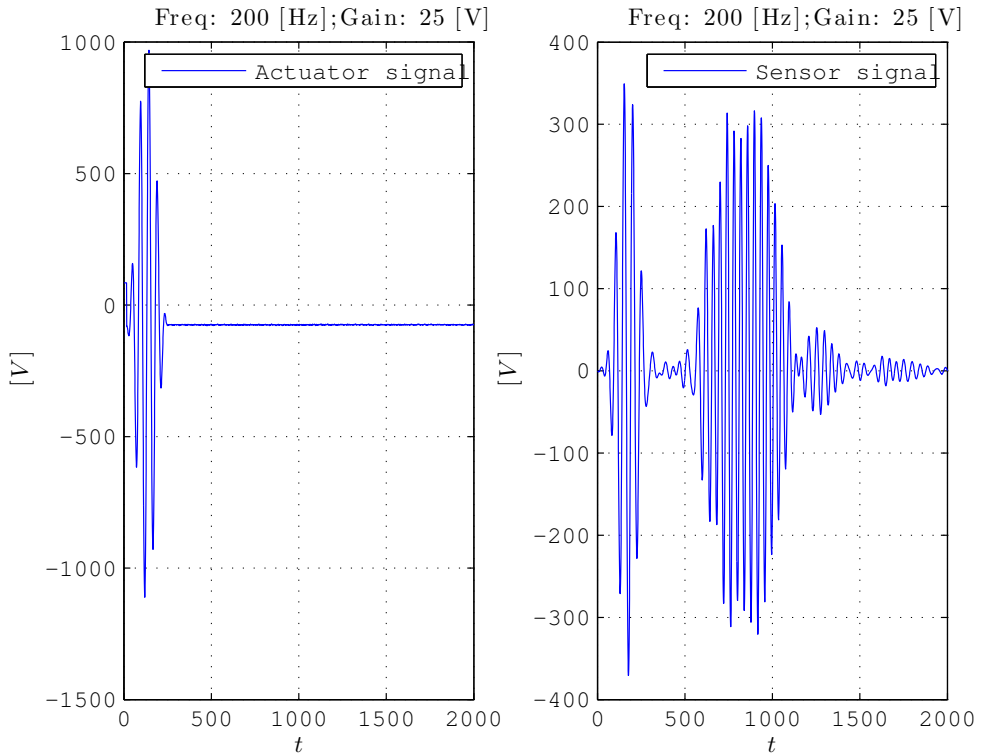


Figure 8.2: Plot of Lamb wave signals corresponding to path 42: actuator 1, sensor 12

In addition to this, and for the task of establishing a reference for identifying the progression of damage in the coupon, the first step was to collect data when the specimen was undamaged and without the presence of loads. By doing this, it was obtained baseline signals that serves as reference to detect the damage onset and propagation. Each of the folders (corresponding to each of the coupons) of the open-access composites dataset published by NASA Ames Data repository, contains one baseline data file along with graphical information (X-rays) for cross-validation of the initial conditions of damage.

8.1.2 Data organization

During the analysis of the fatigue dataset, it was highlighted the necessity of changing the data structure in order to make the information more accessible and intuitive for others. To this end, a set of Matlab® scripts were created by the author to automatically convert the initial data structure to a new structure for

each coupon. See Figure 8.3 for a schematic overview of the updated data structure finally published in [1]. The content of the variable "path.data(1,k)", where the Lamb signals for path k are located, $k = 1, \dots, 252$, is described in more detail in Table 8.1.

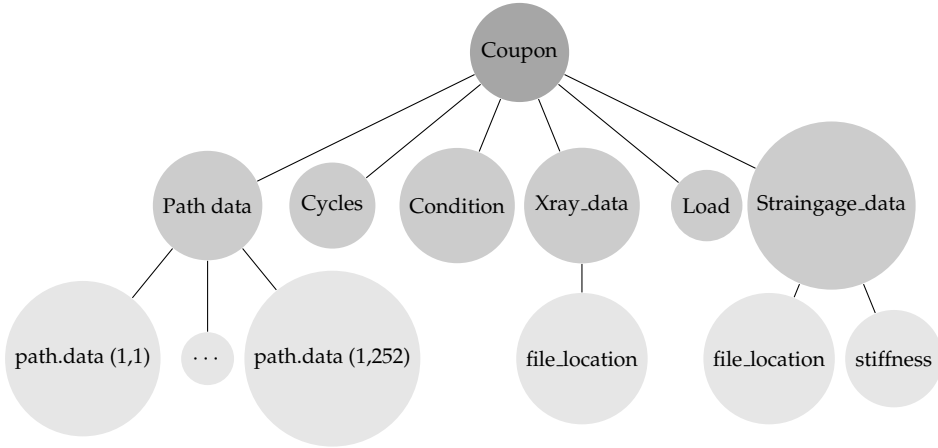


Figure 8.3: Schematic view of the new data structure from the Composite dataset, NASA Ames Prognostics Data Repository [1].

Field name	Field type
actuator	scalar
sensor	scalar
amplitude	scalar
sampling_rate	scalar
frequency	scalar
gain	scalar
signal_sensor	matrix
signal_actuator	matrix

Table 8.1: Structure of the variable "path.data(1,k)", $k = 1, \dots, 252$. Note that Lamb-wave signals are stored in "signal_sensor" and "signal_actuator" fields.

8.2 Damage feature extraction

The collected information from the Lamb wave signals along with the strain gauges were used to develop a method for on-line detecting, sizing and quantifying damage features in composites. It is important to remark that these issues, which are focused on SHM methods for on-line monitoring of composites under fatigue, were mainly contributed by Larrosa and Chang [243] and T. Peng *et al.* [244]. In [245] a mapping between PZT raw signals and micro-cracks density

is presented. In addition, a numerical method to obtain an approximation to the stiffness loss due to the estimation of micro-cracks by Lamb wave signals, is reported. The work by Peng and co-workers [244] is focused on detecting and sizing delaminations using Lamb wave signals. In this doctoral thesis, this information is taken as known since the focus here is on reliability and prognostics from real SHM data, and not on the SHM methods at all.

8.2.1 SHM-PHM connection

As previously mentioned in Section 4.5, making prognostics is a step forward from SHM methods that requires knowledge about the inherent qualities of the data, its structure and acquisition details. Thus, establishing a prognostic framework for fatigue in composites first requires to solve and understand the connection between the available SHM data within the prognostics formulation. Figure 8.4 provides an schematic overview of the connection between SHM and PHM in the context of the prognostic problem of composites presented in thesis. The SHM part together with the damage feature extraction done in [243, 245] are represented by the nodes rounded with dashed line. As has been explained in Section 5.4 and also justified in [113], the matrix micro-cracks are considered as damage signature for the prognostics framework. The delamination effects are considered through a systematic (and thus, updatable) modeling error within the prognostics formulation.

8.2.2 Summary of damage data used for calculations

The fatigue damage data used for calculations in Chapter 9 are summarized in Table 8.2. This damage data correspond to laminate L1S19 in the open-access dataset [1]. The stacking sequence of laminate L1S19 is $[0_2/90_4]_S$, (laminates with such stacking sequence are called as *cross-ply laminates* in the specialized literature). The data in Table 8.2 are presented for measured micro-crack density $\hat{\rho}_n$ and normalized effective stiffness \hat{D}_n . See the ply properties in Table 8.3.

Fatigue cycles, n	10^1	10^2	10^3	10^4	$2 \cdot 10^4$	$3 \cdot 10^4$	$4 \cdot 10^4$	$5 \cdot 10^4$	$6 \cdot 10^4$	$7 \cdot 10^4$	$8 \cdot 10^4$	$9 \cdot 10^4$	10^5
$\hat{\rho}_n$ [# cracks/m]	98	111	117	208	270	305	355	396	402	402	407	418	424
\hat{D}_n	0.954	0.939	0.930	0.924	0.902	0.899	0.888	0.881	0.896	0.872	0.877	0.885	0.880

Table 8.2: Experimental sequence of damage for cross-ply $[0_2/90_4]_S$ Torayca T700 CFRP laminate taken from the Composite dataset, NASA Ames Prognostics Data Repository [1].

Long. Modulus E_1	Trans. Modulus E_2	In-plane Poisson ν_{12}	Out-of-plane Poisson ν_{23}	Shear modulus G_{12}	Out-of-plane-Shear modulus G_{23}	Thickness t
$127.55 \cdot 10^9$	$8.41 \cdot 10^9$	0.309	0.49	$6.2 \cdot 10^9$	$2.82 \cdot 10^9$	$1.52 \cdot 10^{-4}$

Table 8.3: Ply properties used in the calculations (nominal values).

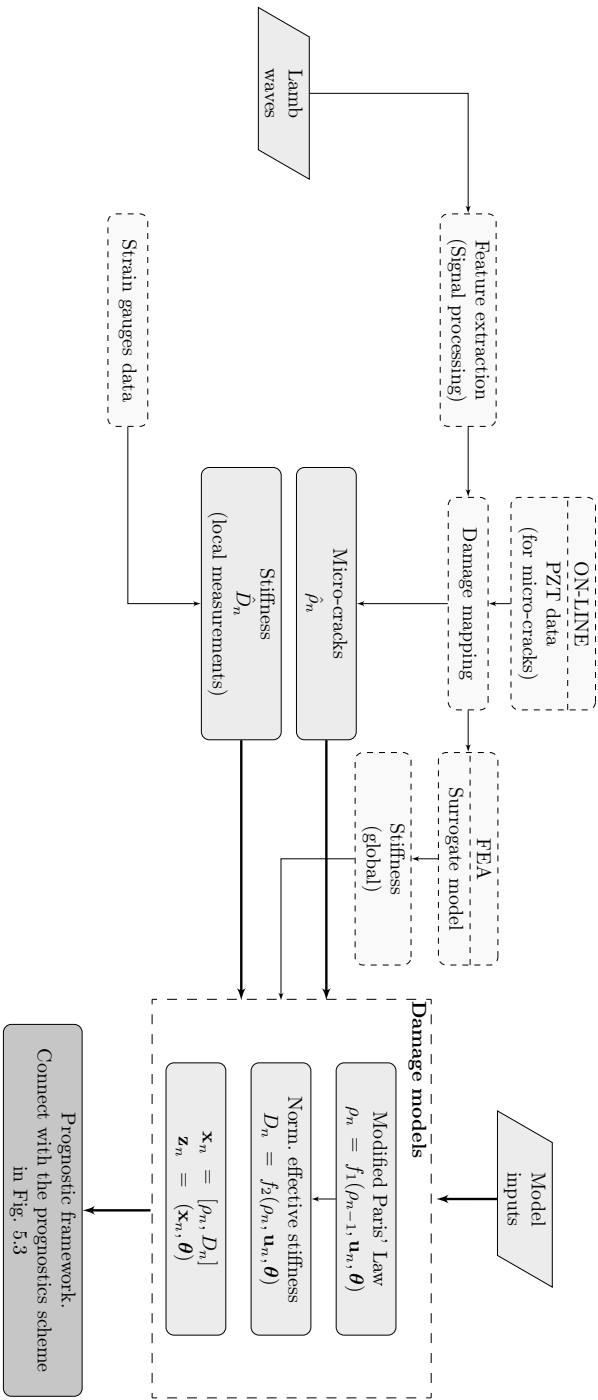


Figure 8.4: SHM-PHM connection in the context of the prognostics framework proposed.

9

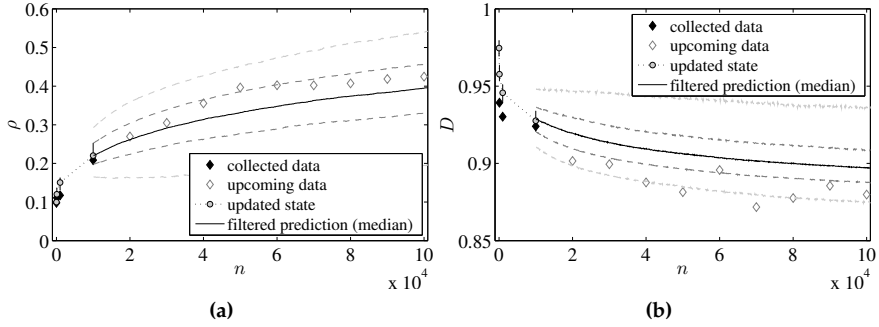
Case study of prognostics and long-term reliability assessment

In this chapter, the model-based prognostics framework proposed in Chapter 5 is demonstrated using structural health monitoring data collected from run-to-failure fatigue experiments in CRFP cross-ply laminates. Results are presented in Section 9.1 for the prediction of micro-cracks density and normalized effective stiffness for a specific composite laminate. In Section 9.2, the long-term reliability of the laminate is predicted and the RUL is derived following the methodology presented in Chapter 6. The results are discussed using prognostics metrics for prediction performance evaluation. In addition, the performance of the PFP-SubSim algorithm presented in Chapter 7 is investigated in Section 9.3 for the aforementioned case study. It is shown that PFP-SubSim algorithm is fairly accurate for making predictions of system failure as compared to the traditional particle filter-based prognostics approach, specially when predictions involve rare-event simulations.

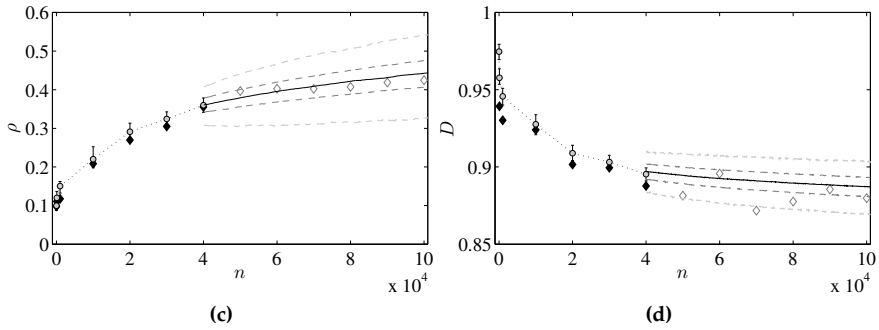
9.1 Results for EOL and RUL prediction

The model-based prognostics framework proposed in Chapter 5 is exemplified here to obtain predictions of RUL and EOL of a composite laminate subjected to fatigue loadings. Previously to this, sequential estimation of damage states by PF is required to incorporate the most up-to-date information about the system. Figure 9.1 shows the results for sequential state estimation as well as for multi-step ahead predictions for both quantities of interest, using SHM data from laminate L1S19 taken from NASA Ames Prognostics Data Repository (Composites dataset) [1]. Matrix micro-cracks density is expressed in cracks per millimeter whilst normalized effective stiffness is dimensionless.

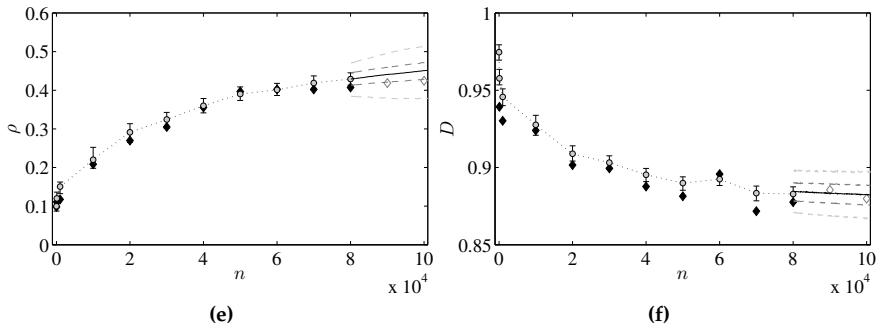
In Figure 9.1, the collected data up to fatigue cycles $n = \{1, 4, 8\} \times 10^4$ are represented along with the sequence of filtered damage states, which are estimated using Algorithm 3 with $N = 5000$ particles. For this example, the systematic importance resampling (SIR) version of the SIS algorithm is adopted, whereby the resampling step is run every time that new data is collected, hence $ESS = N$. Damage states are initialized at $\mathbf{x}_0 = (0.1, 1)$ and the standard deviation of measurement error parameters are set to $\sigma_{w_{1,n}} = 10^{-2}$ and $\sigma_{w_{2,n}} = 10^{-6}$, taking them as known. The scaling variables $RMAD_j^*$ and P_j^* are fixed to $0.3RMAD_{0,j}$ and 0.001 , respectively, where $RMAD_{0,j}$ is the RMAD of the prior PDF for the j th component of the model parameter vector θ , $j = 1, \dots, 6$. The diagonal elements of the covariance matrix $\Sigma_{\xi_{0,j}}$ are appropriately selected through initial test runs and set at 0.5% of the 5th-95th band of the prior PDFs for the j th component of θ . The probabilistic information of model parameters is given in Table 9.1. To reveal the uncertainty reduction in model parameters θ , the posterior mean (by the labels) of each j th component, $j = 1, \dots, n_\theta$, as well as their 25% – 75% and 5% – 95% probability bands are plotted against cycles in Figure 9.2.



($n = 1 \cdot 10^4$)



($n = 4 \cdot 10^4$)



($n = 8 \cdot 10^4$)

Figure 9.1: Sequential state estimation for matrix micro-cracks density (left panels), and normalized effective stiffness (right panels) up to a certain cycle n , where $n = 1 \times 10^4$ (a & b), 4×10^4 (c & d) and 8×10^4 (e & f). The distribution of multi-step ahead predicted damage states are represented using dashed lines for the 5% – 95% and 25% – 75% probability bands with increasing gray tones towards the region of higher probability.

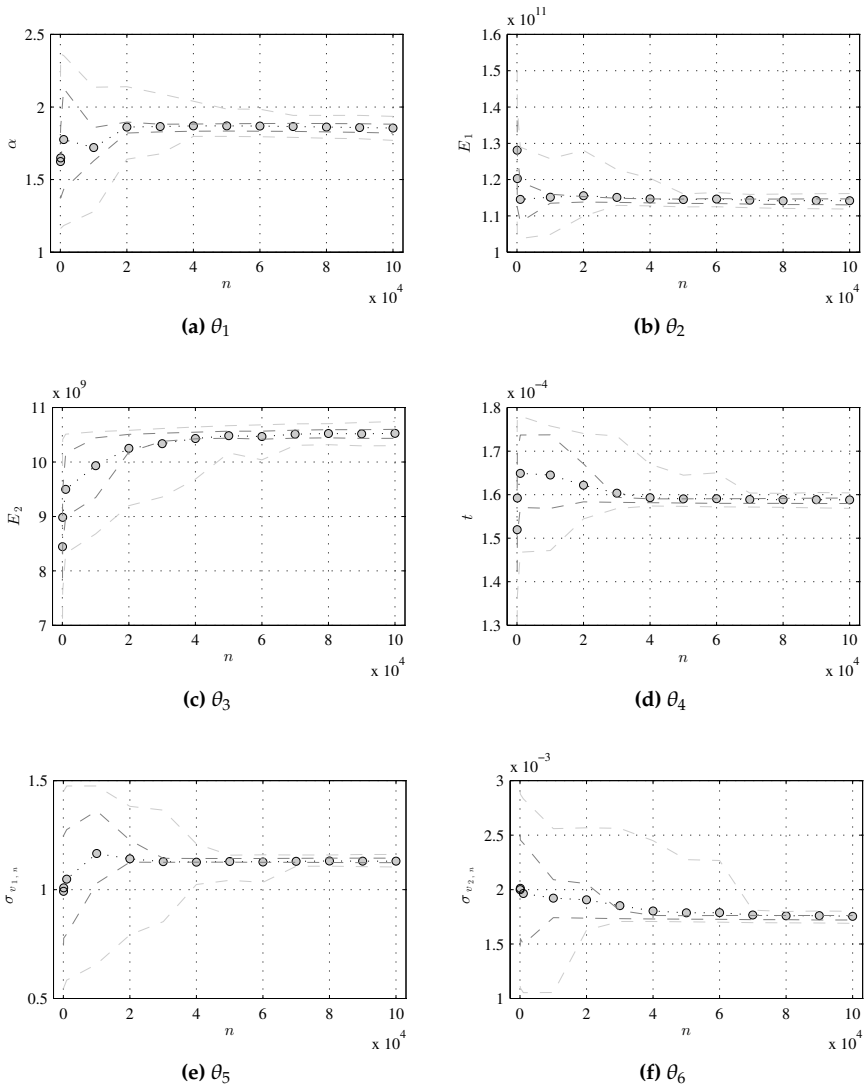


Figure 9.2: Trace of the mean values of model parameters θ against time. Dashed lines represent the 25% – 75% (darker color) and 5% – 95% probability bands, respectively.

Type	Parameter	Nominal value	Units	Prior PDF
Mechanical	E_1	$127.55 \cdot 10^9$	Pa	$\mathcal{LN}(\ln(127.55 \cdot 10^9), 0.1)$
	E_2	$8.41 \cdot 10^9$	Pa	$\mathcal{LN}(\ln(8.41 \cdot 10^9), 0.1)$
	G_{12}	$6.20 \cdot 10^9$	Pa	Not applicable
	ν_{12}	0.31	–	Not applicable
	G_{23}	$2.82 \cdot 10^9$	Pa	Not applicable
	t	$1.5 \cdot 10^{-4}$	m	$\mathcal{LN}(\ln(1.5 \cdot 10^{-4}), 0.1)$
Fitting	α	1.80	–	$\mathcal{LN}(\ln(1.80), 0.2)$
	A	$1 \cdot 10^{-4}$	–	Not applicable
	σ_{v_1}	–	$\frac{\# \text{cracks}}{m \cdot \text{cycle}}$	$\mathcal{U}(0.5, 8)$
	σ_{v_2}	–	–	$\mathcal{U}(0.001, 0.02)$

Table 9.1: Nominal values and prior uncertainty of model parameters used in calculations. The rest of parameters in damage mechanics models (Eq. 5.4 to 5.3) are obtained using the classical laminate plate theory [40, 41, 43] and the relations given in Appendix A. The nominal values for fitting parameters have been defined through initial fitting tests.

Algorithm 6 PF-based prognostics algorithm used for calculations

- 1: **inputs:**
 $\{ \mathbf{z}_n^{(i)} = (\mathbf{x}_n^{(i)}, \boldsymbol{\theta}_n^{(i)}) , \omega_n^{(i)} \}_{i=1}^N$, {updated particles at time n . Use Algorithm 3}
 - 2: Set $\mathcal{U} = \{ (\rho, D) \in [0, 0.418] \times [1, 0.875] \} \subset \mathcal{Z}$, {useful domain}
 - 3: **for** $i = 1$ to N **do**
 - 4: $t \leftarrow n$
 - 5: $\mathbf{z}_t^{(i)} \leftarrow \mathbf{z}_n^{(i)}$
 - 6: Evaluate $EOL_n^{(i)}(\mathbf{z}_t^{(i)})$
 - 7: **while** $\mathbb{I}_{(\mathcal{U})}(\mathbf{z}_t^{(i)}) = 0$ **do**
 - 8: Sample from Eq. 4.37: $\boldsymbol{\theta}_{t+1}^{(i)} \sim p(\boldsymbol{\theta}_{t+1} | \boldsymbol{\theta}_t^{(i)})$
 - 9: Sample from Eq. 5.11a: $\rho_{t+1}^{(i)} \sim p(\rho_{t+1} | \rho_t^{(i)}, \boldsymbol{\theta}_{t+1}^{(i)})$
 - 10: Sample from Eq. 5.11b: $D_{t+1}^{(i)} \sim p(D_{t+1} | \rho_n^{(i)}, \boldsymbol{\theta}_n^{(i)})$
 - 11: $t \leftarrow t + 1$
 - 12: Set $\mathbf{z}_t = (\rho_t^{(i)}, D_t^{(i)}, \boldsymbol{\theta}_t^{(i)}) \leftarrow \mathbf{z}_{t+1} = (\rho_{t+1}^{(i)}, D_{t+1}^{(i)}, \boldsymbol{\theta}_{t+1}^{(i)})$
 - 13: **end while**
 - 14: $EOL_n^{(i)} \leftarrow t$
 $RUL_n^{(i)} = EOL_n^{(i)} - n$
 - 15: **end for**
-

The updated damage states are further propagated into the future to compute the EOL and RUL following the methodology described in Section 5.5.3. The useful domain is defined here as $\mathcal{U} = \{(\rho, D) \in [0, 0.418] \times [1, 0.875]\} \subset \mathbb{R}^2$. A pseudocode implementation of the prognostics algorithm is provided as Algorithm 6, which is based on Algorithm 4 but particularized for the case study considered here.

Figures 9.3 and 9.4 show a sequence of histograms that correspond to estimations of the PDFs for EOL obtained at increasing times of prediction. The uncertainty reduction in the EOL prediction is clearly revealed by comparing consecutive PDFs, which makes sense since the predictions are periodically updated with incoming data. Observe also that from cycle $n = 6 \cdot 10^4$, the PDFs for EOL show increasingly higher density values at time of prediction n . An explanation to the last can be found in view of the asymptotic behavior of the damage process for both, micro-cracks density and normalized stiffness decrease (see Figure 9.1). Indeed, from cycle $n = 6 \cdot 10^4$ the model predicts an increasing amount of particles that already lie within the failure domain $\bar{\mathcal{U}}$. This leads to an increasing higher density concentrated at the predicting cycle n , as well as to a distributional tail corresponding to the cycle indexes of those particles that have not reached the failure region yet at cycle n .

The results of RUL estimates together with their quantified uncertainty by the 25% – 75% probability bands are plotted against time in Figure 9.5, where two shaded cones of accuracy at 10% and 20% of true RUL, denoted as RUL^* , are used to help evaluating the prediction accuracy and precision. Observe that the RUL prediction is appreciably inaccurate within the first stage of the fatigue process, that corresponds to the interval of cycles required for SHM data to train the model parameters. From this period, the prediction precision clearly improves with cycles. However, as fatigue cycles evolve, not only the prediction mean improves (values closer to RUL^* line) but also the prediction spread gets lower values. This visualization allows assessment of how prediction performance changes over time in terms of correctness (accuracy and precision). Also, one can assess how quickly performance converges within desired accuracy levels, whereby the prognostics horizon (PH) can be estimated. In this example, the PH for 0.2 as α -accuracy is $PH = 8 \cdot 10^4 - 1 \cdot 10^3 = 7.9 \cdot 10^4$ cycles.

Observe also that from cycle $n = 6 \cdot 10^4$, the estimated mean values for the RUL (labelled by the grey circles in Figure 9.5) get higher values with respect to the RUL^* line, leaving progressively the accuracy area as fatigue cycles evolve from $n = 6 \cdot 10^4$. This result is in accordance to the reasoning given above about

the asymmetry of the PDFs for EOL, as shown in Figure 9.4. In fact, it is an expected outcome for this problem since from $n \geq 6 \cdot 10^4$, there is a remaining set of particles of damage states whose hitting-points to the failure region occur at cycle values $\gg n$, so that producing a positive shift to the mean of EOL_n .

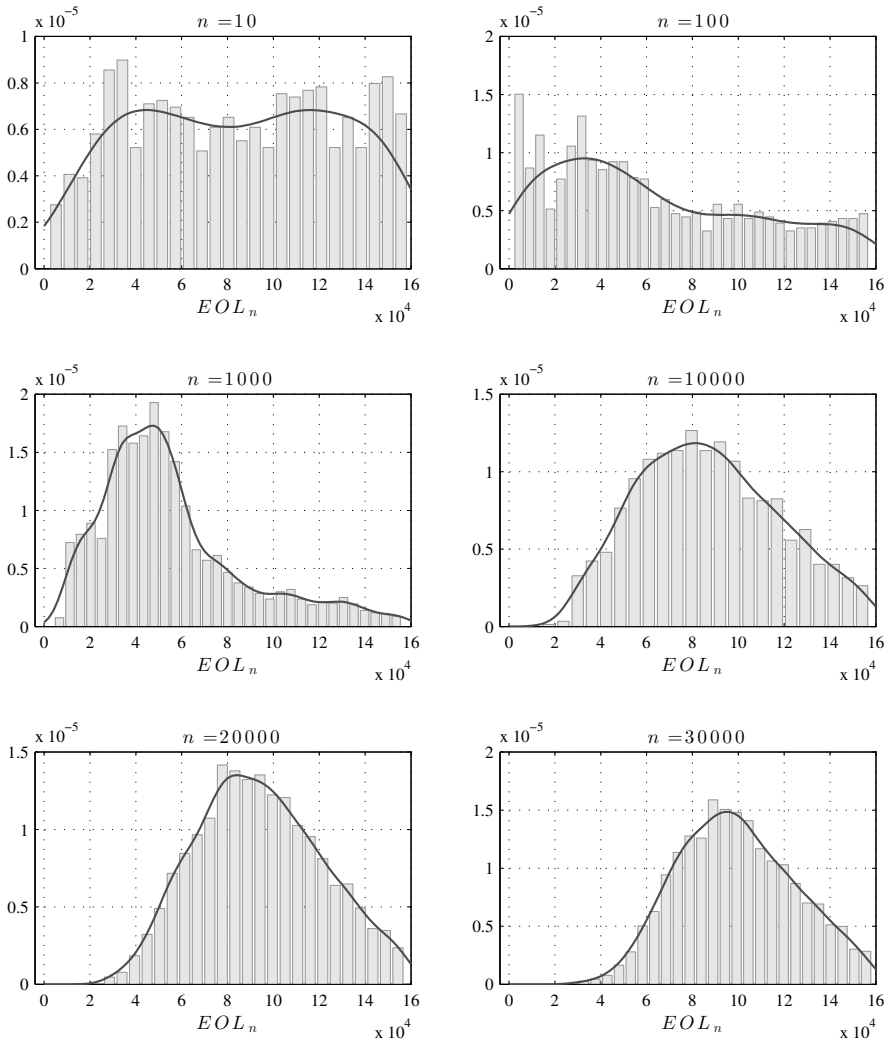


Figure 9.3: Normalized histograms for predicted EOL_n represented for fatigue cycles $n = \{10, 10^2, 10^3, 10^4, 2 \cdot 10^4, 3 \cdot 10^4\}$. Kernel density estimates of the PDFs of EOL_n are superimposed over the histograms using gray solid line for their representation.

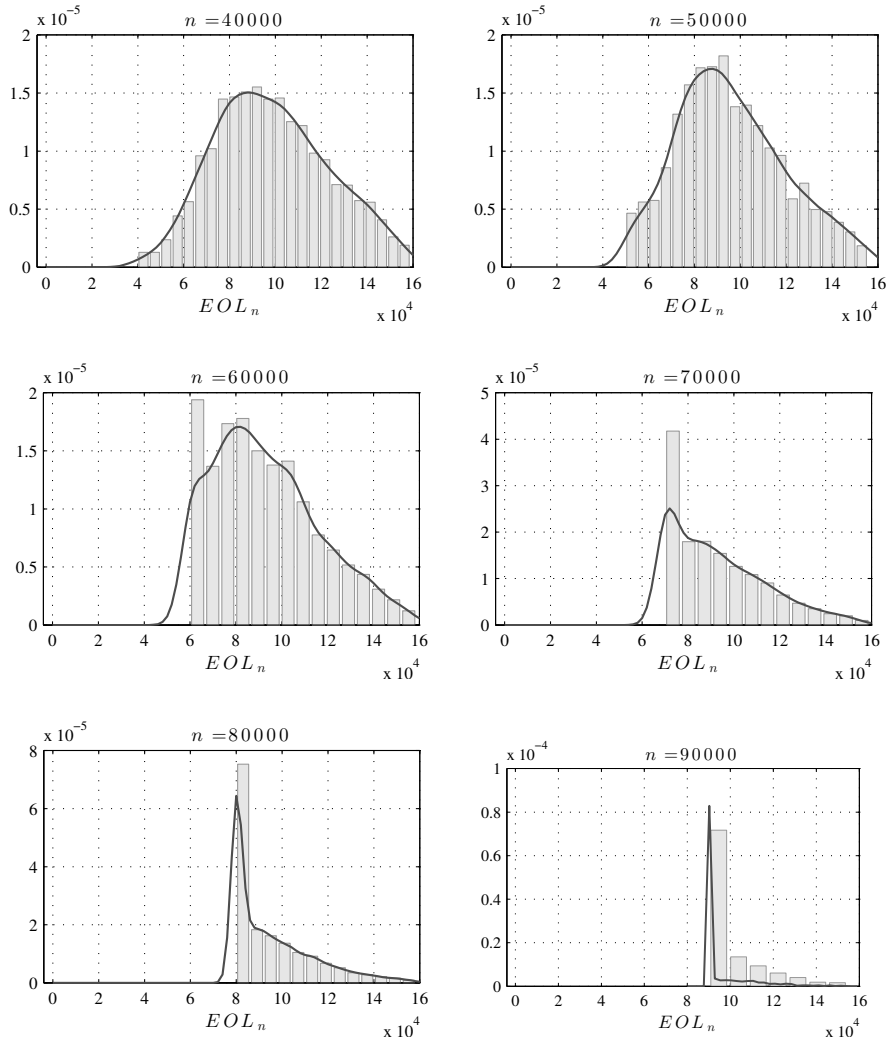


Figure 9.4: Normalized histograms for predicted EOL_n represented for fatigue cycles $n = \{4 \cdot 10^4, 5 \cdot 10^4, 6 \cdot 10^4, 7 \cdot 10^4, 8 \cdot 10^4, 9 \cdot 10^4\}$. Kernel density estimates of the PDFs of EOL_n are superimposed over the histograms using gray solid line for their representation. Note that for $n \geq 6 \cdot 10^4$, the histograms show increasingly higher values for $EOL_n = n$.

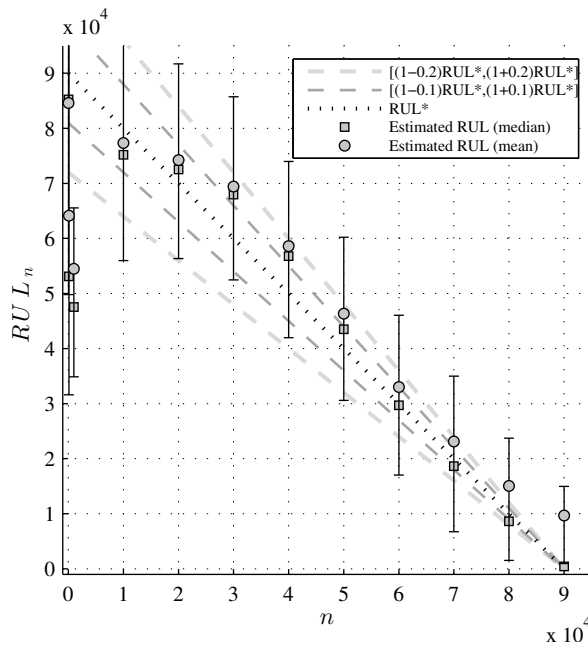


Figure 9.5: RUL vs. fatigue cycles plot to assess lifetime prediction performance for composites under fatigue ageing. Two cones of accuracy at 10% and 20% of true RUL are represented to help evaluating prognostics performance. Darker dashed lines represent the cone of accuracy at 10%. The true RUL, denoted as RUL^* , is represented using black dotted line.

9.2 Results for long-term reliability prediction

To obtain long-term reliability estimates, multi-step forward predictions of the damage states are computed every time new data arrive, using the methodology described in Section 6.2. The results are shown in Figure 9.6. The gray circles represent the updated reliability values up to prediction time n , whereas the solid curves correspond to the reliability prediction for upcoming fatigue cycles. By comparing the consecutive plots in Figure 9.6, one can observe that the reliability prediction gradually improves as more SHM data become available. Note that reliability values drop from cycle $n = 6 \cdot 10^4$, which makes sense since, according to what it was explained in the last section, $n \geq 6 \cdot 10^4$ is the cycle when the predictions are likelier to reach the failure region. Notice also that for $n = 9 \cdot 10^4$ (which corresponds to the cycle when measured damage reaches the failure region) the updated reliability is $R_{n|n} = 0.42$, i.e., the 42% of particles still lie in the useful domain at that cycle. This is again a manifestation of the asymptotic behavior of the latent damage process.

The RUL calculated from the predicted reliability is shown in Figure 9.7. Note that Figures 9.7 and 9.5 are essentially the same when, however, they are calculated from different methods.

9.3 Prognostics in composites using PFP-SubSim

In this section, the performance of the PFP-SubSim algorithm explained in Section 7 is exemplified. At each time of prediction, the standard PF-algorithm (Algorithm 3) is used to update the information about the system (damage states and model parameters), which is further employed to obtain ℓ -step ahead predictions of the damage states by PFP-SubSim algorithm. The results for both, micro-cracks density and normalized effective stiffness are presented in Figure 9.8, using¹ $P_0 = 0.5$ and $M = 2.4 \cdot 10^4$ samples per conditional level. For the sake of conciseness, only predictions at $n = \{1, 4, 8\} \times 10^4$ are presented, which corresponds to cycles from the beginning, middle and end of the fatigue process, respectively. Each subset is defined by samples (circles) in the \mathcal{Z} space. To illustrate how PFP-SubSim algorithm draws simulations by subsets, the intermediate predicted samples are superimposed in increasing gray tones, being the initial predicted samples those represented by brighter gray color. Observe that PFP-SubSim algorithm employs $m = \{2, 2, 1\}$ conditional levels for the predictions

¹ $P_0 = 0.5$ is adopted for this example to easily visualize how predicted samples are distributed in different subsets, since the recommended near-optimal value of $P_0 = 0.2$ (see 4.2.4) for Subset Simulation produced $m = 1$ for the majority of times of prediction.

at cycles $n = \{1, 4, 8\} \times 10^4$ respectively. These conditional levels are obtained automatically by the algorithm once P_0 is fixed, as explained in Section 4.2.4. In fact, given that $m = \log P(\vec{U}) / \log P_0$, the number of conditional levels employed by PFP-SubSim algorithm in Figure 9.8 can be easily verified in view of Figure 9.10a, which provides a plot of $P(\vec{U})$ against cycles. As a consequence, the total amount of samples N_T varies depending on the total amount of conditional levels used at each time of prediction.

The RUL predicted by PFP-SubSim algorithm is plotted against cycles in Figure 9.9. The results are satisfactory in the sense that PFP-SubSim algorithm is shown to be able to estimate the RUL with required precision, except in the first stage of the fatigue process, as also happened when using Algorithm 6 (see Figure 9.5). In addition, observe that, as well as in Figure 9.5, the mean predictive values of RUL depart from the true RUL at the final stage of the process by the same reason as that given in Section 9.1.

In Figure 9.10, an estimation of the system failure probability $P(\vec{U})$ is obtained at different cycles using comparatively PFP-SubSim algorithm and Algorithm 6. To avoid an excessive computational cost, the simulations are restricted to lie within the interval $(n, 10^5] \subset \mathbb{N}$, being n the time of prediction, as it is enough to highlight the differences between both algorithms. The results shown for Algorithm 6 were obtained using a large enough amount of samples for the approximation in Equation 7.2 to be sufficiently accurate. It is shown in Figure 9.10a that the estimations of $P(\vec{U})$ using PFP-SubSim algorithm agree well with the benchmark values given by Algorithm 6, although PFP-SubSim employs significantly less amount of samples. The total amount of samples required by each algorithm are plotted in Figure 9.10b. Note also that the estimated values for $P(\vec{U})$ are high (in comparison to P_0) and thus, a significant improvement in efficiency of PFP-SubSim algorithm would be expected in relation to Algorithm 6 if failure probability got lower values, as discussed further below.

9.4 Discussion of efficiency gained by PFP-SubSim

In this section, the quality of an estimator for $P(\vec{U})$ based on samples from the different competing algorithms, is examined. To this end, let $\tilde{P}(\vec{U})$ be an estimator for $P(\vec{U})$ as states in Equation 7.2. The expression for the c.o.v. of $\tilde{P}(\vec{U})$ when the standard PF-based prognostics algorithm (Algorithm 6) is employed is given by [62]:

$$\delta_{PF}(\tilde{P}(\vec{U})) = \sqrt{\frac{(1 - P(\vec{U}))}{P(\vec{U})N_{T2}}} [1 + \gamma] \quad (9.1)$$

where N_{T2} denotes the total amount of predictive samples used by Algorithm 6 and γ is the autocorrelation factor, which reveals the level of correlation between the samples of any of the N particle trajectories [62].

On the other hand, when PFP-SubSim algorithm is used, $\tilde{P}(\vec{U})$ can be readily obtained as $\tilde{P}(\vec{U}) = (P_0)^m$, where m is the total number simulation levels employed by the algorithm to reach the failure region. The c.o.v. of $\tilde{P}(\vec{U})$ can be calculated as (see [65] for a detailed demonstration):

$$\delta_{SS}(\tilde{P}(\vec{U})) = \sqrt{\left(\frac{\log(\gamma)}{\log(P_0)}\right)^2 \frac{(1-P_0)}{P_0 N_{T1}} [1+\gamma]} \quad (9.2)$$

where N_{T1} is the total amount of evaluations employed by PFP-SubSim algorithm. The objective here is to formally prove that PFP-SubSim algorithm is able to obtain the same or better quality for $\tilde{P}(\vec{U})$ (in the sense of lower c.o.v. of $\tilde{P}(\vec{U})$) but employing less model evaluations than Algorithm 6. For simplicity but no loss of generality, let us assume that both algorithms give samples with equal (or similar) level of correlation between them, hence γ is considered equal for both algorithms in this exercise. Next, it is reasonable to hypothesize that there exist a configuration for N_{T2} and N_{T1} where both algorithms give the same quality for $\tilde{P}(\vec{U})$. Then, the following equality holds:

$$\frac{(1-P_0)(\log P(\vec{U}))^2 P(\vec{U}) N_{T2}}{(1-P(\vec{U}))(\log P_0)^2 P_0 N_{T1}} = 1 \quad (9.3)$$

which is the result of dividing Equation (9.2) by Equation (9.1). From the last expression, it is easy to obtain the number of samples N_{T2} required by Algorithm 6 to obtain an estimate of $P(\vec{U})$ with the same level of accuracy as that obtained using PFP-SubSim Algorithm, provided that a total amount of N_{T1} samples are employed:

$$N_{T2} = N_{T1} \underbrace{\frac{(1-P(\vec{U}))P_0}{(1-P_0)P(\vec{U})} \left(\frac{\log P_0^2}{\log P(\vec{U})^2}\right)^2}_{\gg 1} \quad (9.4)$$

Observe that the factor that multiplies N_{T1} is always greater than unity, since by definition, $P_0 > P(\vec{U})$. In rare-event problems (like asymptotic processes with conservative thresholds), $P_0 \gg P(\vec{U})$, hence the last cited factor is fairly greater than 1, which demonstrates that significant computational savings can be gained when PFP-SubSim algorithm is employed for the prognostic of rare-events.

9.5 Numerical proofs for the computational efficiency gained

In this section, the computational improvement and accuracy that can be achieved using PFP-SubSim algorithm is investigated numerically. To this end, the performance of both algorithms, PFP-SubSim and Algorithm 6, are compared in a meaningful computational manner. For this exercise, the unit coefficient of variation² (c.o.v.) Δ is used since it provides a measure of efficiency that is inherent to the algorithm because it is invariant to the number of simulated samples [203]. This is of special interest for this comparative exercise since the total amount of samples required by PFP-SubSim algorithm varies depending on the system failure probability to be estimated, as explained before.

The computational efficiency is reported in Figure 9.11 for both algorithms in terms of the unit c.o.v. versus different threshold levels, which correspond to increasingly higher values for $P(\vec{U})$ (labelled by the text box). The numerical values of each plot are obtained considering the mean of 200 independent runs of the algorithms, in order to assess quantitatively the statistical properties for the prognostics estimates. The results are presented for the sample prediction time $n = 8 \times 10^4$. Observe that when the PFP-SubSim algorithm is employed, the unit c.o.v. increases slowly towards the region of thresholds that entail lower probability values (higher threshold values for matrix micro-cracks density), while for Algorithm 6, the unit c.o.v. grows steeply in that region. The performance of both algorithms is similar for higher values of $P(\vec{U})$, (say of the order of P_0). This confirms that PFP-SubSim algorithm gets its highest efficiency when predictions based on simulating rare-events are required.

To evaluate the performance of both algorithms for making RUL estimates, a comparison is carried out using the same total amount of samples per algorithm. Two metrics are considered: (a) the sample mean of the quadratic error between RUL_n and RUL_n^* , i.e., $\|RUL_n - RUL_n^*\|_2^2$ as an accuracy measure, and (b) the differential entropy³ of $p(RUL_n | \mathbf{y}_{0:n})$, as a measure quantifying the spread of the RUL, calculated as $1/2 \ln |(2\pi e) [var(RUL_n)]|$, being $var(RUL_n)$ the sample variance of RUL_n , which can be obtained drawing samples from $p(RUL_n | \mathbf{y}_{0:n})$. The results are plotted against cycles in Figure 9.12. Two threshold levels are considered for the comparison: (a & b) $\rho = 418$ micro-cracks per meter, $D = 0.875$; (c & d) $\rho = 600$ micro-cracks per meter, $D = 0.86$. For c & d cases, no SHM data

²Any stochastic algorithm for estimating $P(\vec{U})$ has a c.o.v. of the form $c.o.v. = \frac{\Delta}{\sqrt{N_T}}$

³This expression for the differential entropy is actually an upper-bound approximation to the actual differential entropy, where the exactness is achieved when the PDF $p(RUL_n | \mathbf{y}_{0:n})$ is Gaussian.

are available, thus the accuracy measure cannot be obtained. Instead, the comparative results of system failure probability between both algorithms are represented. The left-side panels show the differential entropy of $p(\text{RUL}_n | \mathbf{y}_{0:n})$. The right-side panels show the accuracy measure except for (d), where calculation of $P(\bar{U})$ is plotted against cycles. Observe that both algorithms perform fairly similar when considering a threshold value of $\rho = 418$ micro-cracks per meter (high probabilities of prediction, see Figure 9.10a). However, the same cannot be said when a higher threshold is adopted, which attain significantly lower values of failure probabilities. Observe in Figure 9.12d that only the first three values for the entropy measure are represented for Algorithm 6. Apart from these values, the rest of the estimations were obtained with significant level of numerical noise, so they are not represented. Figure 9.12d shows the estimated system failure probabilities when the threshold $\rho = 600$ is considered. Note that PFP-SubSim algorithm is able to estimate the values of $P(\bar{U})$ even though they are markedly low, whereas Algorithm 6 is unable to give any result different from 0 for the majority of times of prediction. These results suggest that high efficiency can be obtained by employing the PFP-SubSim algorithm for the prognostics of rare-events, at the same time that its performance is equivalent to the standard PF-based prognostics algorithm for the rest of cases.

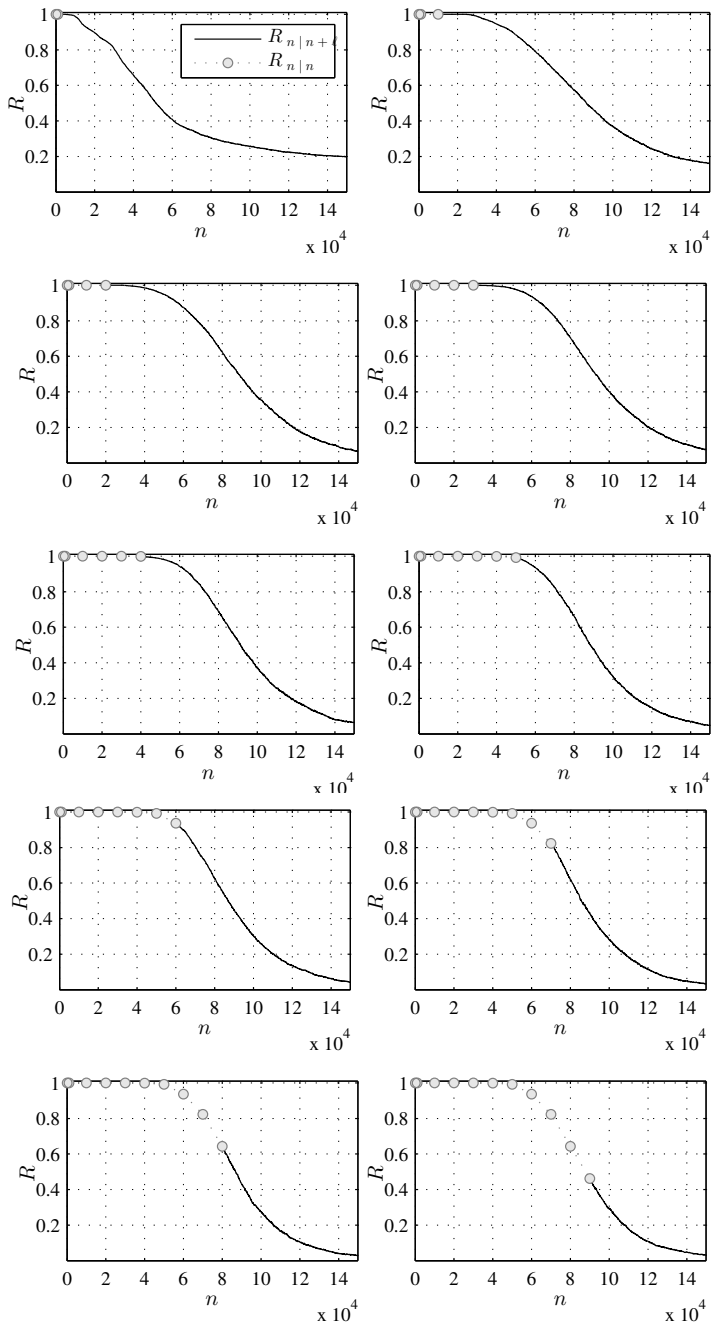


Figure 9.6: Reliability updation and long-term prediction at different cycles along the process.

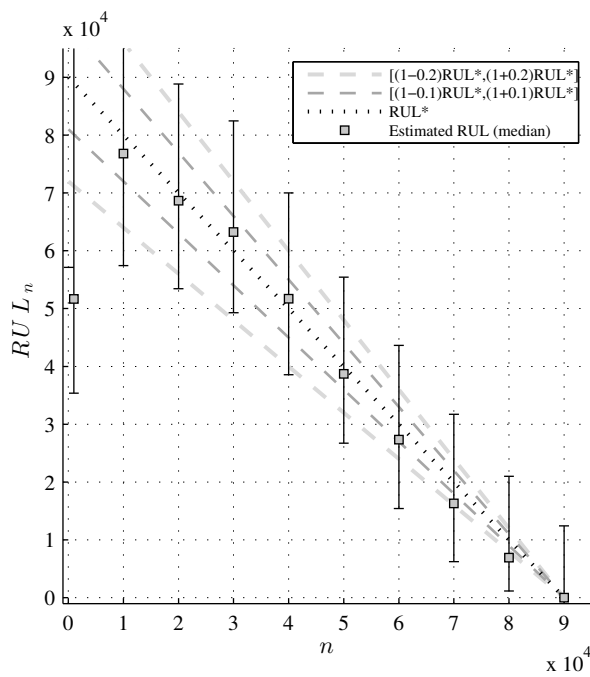


Figure 9.7: RUL vs. fatigue cycles plot obtained using the reliability-based prognostics framework. As in Figure 9.5, two cones of accuracy at 10% and 20% of true RUL, are represented using dashed lines (darker one corresponds to the cone at 10% of accuracy).

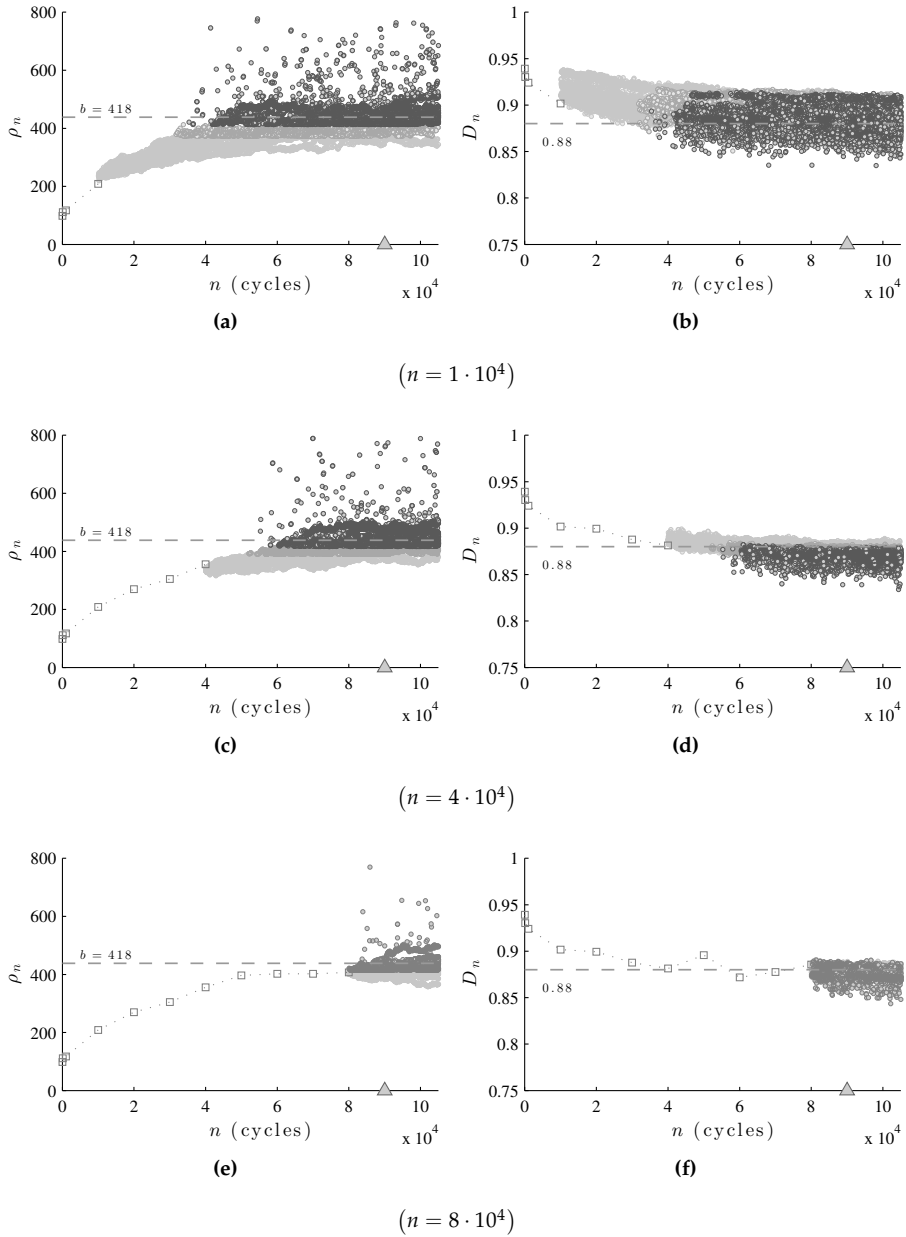


Figure 9.8: PFP-SubSim output for predicting matrix micro-cracks density and normalized effective stiffness. The triangles represent the experimental cycles for which matrix micro-cracks density and stiffness loss reach their respective thresholds, as observed from the data.

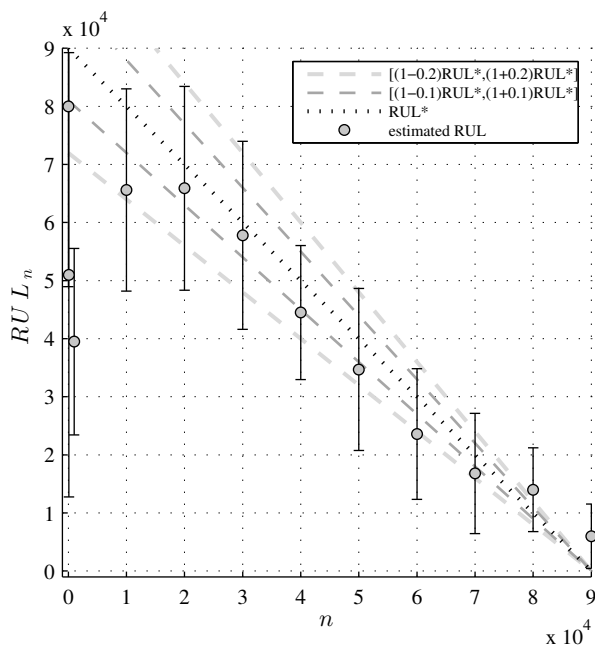


Figure 9.9: PFP-SubSim results for remaining useful life (RUL) predictions together with their quantified uncertainty by the 25% – 75% band.

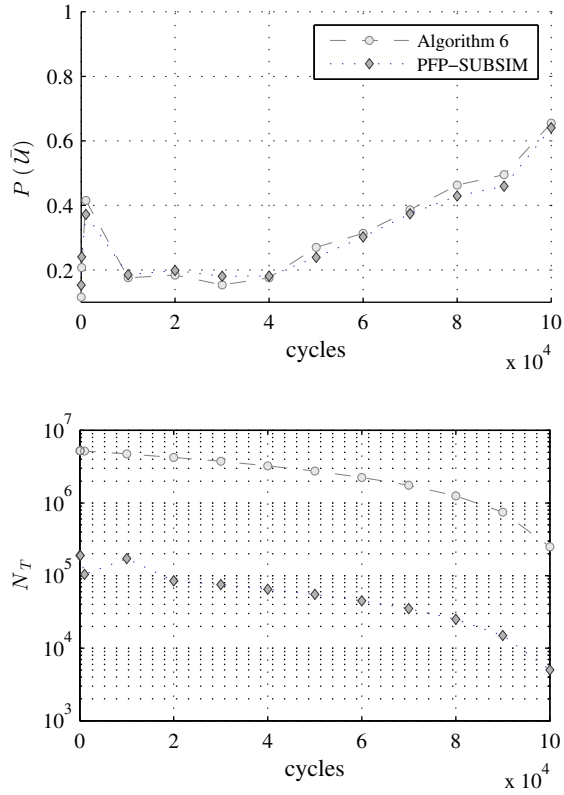


Figure 9.10: Plot for $P(\bar{U})$ estimation using PFP-SubSim algorithm in comparison to the standard PF-based prognostics algorithm used as benchmark.

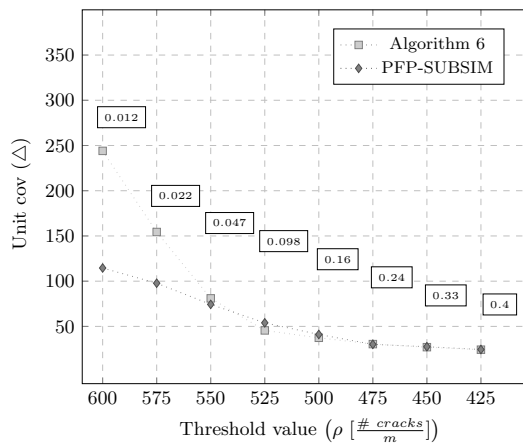
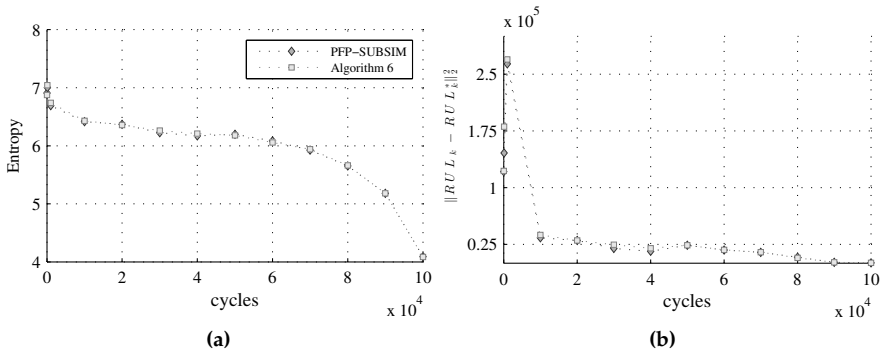
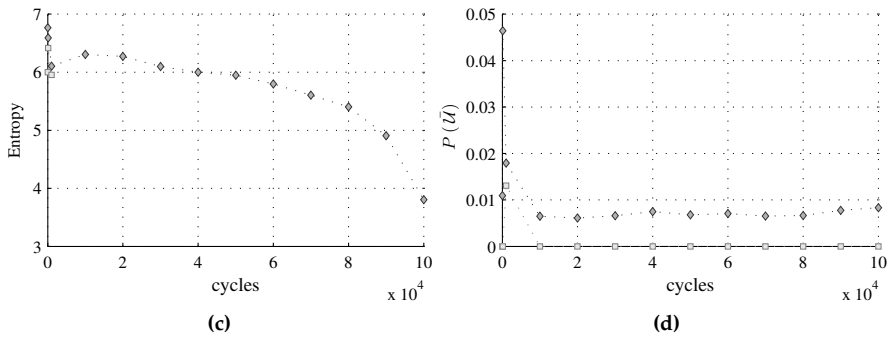


Figure 9.11: Results for the unit c.o.v. of $P(\bar{U})$ obtained using PFP-SubSim algorithm as compared to that obtained using Algorithm 6.



($b = 418$ [#cracks $\cdot m^{-1}$]; $D = 0.875$)



($b = 600$ [#cracks $\cdot m^{-1}$]; $D = 0.86$)

Figure 9.12: Results for the measures of accuracy and uncertainty of the RUL estimate using comparatively PFP-SubSim algorithm and Algorithm 6.

Part IV

CONCLUSIONS AND FUTURE WORKS

10

Conclusions and future works

In this chapter, the most relevant conclusions for the contributions presented in this thesis are extracted along with discussion about limitations and assumptions to be adopted. The open questions that arise from the development of this research work are outlined as future works.

Concluding remarks

This thesis reports on methods for fatigue damage prognosis and reliability in application to composite materials. First, in Chapter 5, a general architecture for prognostics was developed where prognostics was broken down into the three important problems about damage state estimation, future state prediction, and remaining useful life prediction, respectively. Bayesian filtering methods were used based on damage-mechanics models to represent the damage degradation that was in turn represented using micro-scale and macro-scale states of the system. These damage states were estimated by means of a filtering framework using SHM measurements of damage, so that they were further used to forecast the future health of the system.

A key feature of the proposed methodology was the systematic treatment of the various sources of uncertainty, that include system inputs (loading, environmental, operational conditions), system parameters, measurement noise, etc. The treatment of such uncertainty was accomplished through the use of a Bayesian state estimation framework, that allowed us to estimate the system damage states as a probability. Based on this estimation, the probability distribution of the EOL/RUL was obtained as an uncertainty propagation problem using the damage states estimated from the Bayesian state estimation problem.

The validity of the proposed methodology was demonstrated on SHM data collected from a tension-tension fatigue experiment using CFRP cross-ply laminates, outlined in Chapter 9. As a general comment, the results indicated that good accuracy can be obtained for EOL/RUL predictions after a first period of cycles, which corresponds to the interval of fatigue cycles required for SHM data to train the model parameters. In particular, it was shown that the proposed prognostic framework gives a prognostics horizon of about 87% of the lifetime with an accuracy level of 20%, following the methodology by Saxena *et al.* [110] to evaluate prognostics performance.

In Chapter 6, the proposed prognostics methodology was extended to consider the estimation of long-term reliability as a system-health indicator for prognostics. It was shown that the distribution of RUL can be readily obtained as a function from the long-term reliability prediction. Before presenting the methodology for long-term reliability prediction, an up-to-date and review of the reliability literature of composites was provided as an introductory section. This literature review was motivated by the lack of consensus that was observed in the composites reliability literature. One of the main conclusions from this review is the need for new methods that consider the progressive damage of composite laminates within the reliability formulation, which motivated the long-term reliability formulation proposed in Section 6.2.

As a difficulty encountered when predicting the matrix micro-cracks density saturation was the lack of confidence in the RUL estimations when using a filtering based prognostic algorithm (e.g., Algorithm 4), that requires a large enough amount of samples to get accuracy. This motivated a new algorithm called PFP-SubSim which combines the prognostics principles with the Subset Simulation method to efficiently achieve accuracy when predictions involve rare-event simulations, as stated in Section 7.3. It was demonstrated that PFP-SubSim gets efficiency by adaptively simulating samples over a nested sequence of subsets until the final prognostic threshold is reached. The sequence of subsets can be

adopted in an automated manner, which avoids tedious preliminary calibrations and allows its implementation for on-line prognostics architectures. The computational efficiency and accuracy that can be gained with the proposed algorithm was demonstrated in Section 9.3 with the fatigue damage dataset presented in Chapter 9, that illustrates some of the challenges that can be faced by the algorithm in a real-world application. It was demonstrated that the system failure probability (understood as the complementary of the long-term reliability) can be readily predicted with high accuracy using PFP-SubSim algorithm even when this failure probability is very small. In particular, it was shown by the numerical examples that PFP-SubSim algorithm was able to predict very small failure events (corresponding to extremely high levels of matrix micro-crack saturation for the laminate considered) with moderate computational effort. When the system failure probability is not so small, results showed that PFP-SubSim performs similar to the standard filtering-based prognostics algorithm, which indicates that PFP-SubSim can be considered as a general purpose prognostic algorithm, which is specially efficient for rare-event prediction.

Limitations

During the formulation of the various prognostics methods and algorithms proposed for this thesis, a number of assumptions were considered which, in certain manner, indicate the limitations of these methods. This section is intended to honestly highlight such assumptions and limitations.

First, it is important to remark that the Bayesian state estimation framework proposed in Chapter 5 was formulated by assuming that damage data are given in the form of matrix micro-cracks and normalized effective stiffness. However, today's SHM sensors hardly ever provide this information directly. Instead, raw signals are obtained which require further signal processing to capture the trend of degradation. Several works can be encountered in the literature reporting successful methods for signal processing that capture the degradation of composite materials by both, matrix micro-cracks and delamination (see for example C. Larrosa and F. K. Chang [243, 245]). The gap between raw signals from SHM sensors and processed data to be used for prognostics has been highlighted in Section 8.2.1 by the scheme in Figure 8.4, which indicates that certain off-line work is required previously to run a real-time prognostic experiment using the framework presented here.

To continue with the limitations, it is noticeable that the proposed framework was developed under the assumption that matrix micro-cracking is the dominant

damage mode and also the precursor of more severe damage modes in composites, which may be a reasonable assumption for cross-ply laminates [26], (as the laminate type considered in this thesis). Under such assumption, damage models were selected to account for matrix micro-cracks and stiffness reduction induced by micro-cracks and thus, other possible damage modes like delaminations and fiber-breakage, among others, were not physically modeled (although their uncertainty was considered and quantified through the model error terms). Since damage models were stochastically embedded to serve as transition/prediction kernels for the Bayesian state estimation formulation, the no consideration of other damage models may influence model predictability when other damage modes are present, with independence of how well the prognostics algorithm deals with long-term predictions. Therefore, if different laminate types were considered, other damage modes may be expected, therefore certain modifications to the damage models would be required to improve the predictability.

Finally, it is remarked that the proposed framework for fatigue damage prognosis has been designed, and validated by the numerical examples, at coupon level under laboratory conditions. Although this is the typical situation for most of the research programs on fatigue nowadays, it is worthy to indicate that an improvement of much interest, not only for researchers but also for practitioners, would be to deal with the fatigue behavior at component/subsystem level under realistic fatigue loads. This may require the development of ad hoc diagnostic technology for detecting, sizing and quantifying damage extent through built-in SHM sensors, as well as especially-designed prognostics frameworks that account for the particularities of the experimental setup.

Future works

The content of this section has been partially covered by the previous one, since facing any of the aforementioned limitations of this research with enough rigor may constitute a new prospective research objective to be considered for future work. However, the intention of the author with this section is to briefly highlight the most fruitful among them, which can be understood as the subsequent research steps of this thesis. In this sense, the consideration of other internal damage modes different from matrix micro-cracking is of special interest for further research. Different laminate lay-ups (like quasi-isotropic, angle-ply, etc) can also be adopted for validation.

In general, an ideal scenario for prospective research would be to jointly consider the development of on-board diagnostic SHM technology in conjunction

with a prognostic reasoner with decision-making capability about reliability and safety for composite structures.

11

Conclusiones y trabajos futuros

En este capítulo se presentan las conclusiones más relevantes, extraídas de las contribuciones aportadas en la tesis, junto con diversos comentarios sobre las limitaciones de la metodología e hipótesis a adoptar. Las preguntas abiertas que surgen del desarrollo de este trabajo de investigación se exponen finalmente como líneas futuras.

Comentarios concluyentes

Esta tesis proporciona métodos para el pronóstico de daño por fatiga y para fiabilidad en aplicación de materiales compuestos. En primer lugar, en el Capítulo 5 se desarrolló una metodología general para pronóstico de daño diferenciada en tres problemas clave, a saber: estimación de estados de daño, predicción de estados futuros, y predicción de vida útil remanente. Se utilizaron métodos de filtrado Bayesiano basados en modelos mecánicos de daño a distinta escala para obtener secuencialmente una estimación de los estados de degradación. El marco de filtrado Bayesiano usa la información disponible procedente de los sensores,

para posteriormente ser utilizada para pronosticar el estado de salud estructural futuro del composite. Una característica clave de la metodología propuesta fue el tratamiento sistemático de las distintas fuentes de incertidumbre, que incluyen valores futuros de las variables aleatorias (de carga y ambientales), los parámetros del sistema, la medición de ruido, etc. El tratamiento de la incertidumbre se llevó a cabo mediante un marco Bayesiano de estimación de estados, que permitió asociar los estados de daño del sistema a un valor de probabilidad. Sobre la base de esta estimación, las distribuciones de probabilidad de las variables *final de la vida útil* y *vida remanente*, fueron obtenidas como un problema de propagación de incertidumbre utilizando los estados de daño estimados mediante el filtro Bayesiano. La validez de la metodología propuesta se demostró usando los datos procedentes de la monitorización estructural del daño por fatiga del tipo tensión cíclica en laminados cross-ply de fibra de carbono, según se especifica en el Capítulo 9. Como comentario general, los resultados mostraron que una buena precisión de predicción puede ser obtenida tras un primer periodo de ciclos de fatiga, que corresponde con los ciclos requeridos por los datos para recabar suficiente información para los parámetros del modelo. En particular, se demostró que el marco de pronóstico propuesto proporciona un horizonte de pronóstico de un 87% del total de ciclos ensayados con un nivel de exactitud del 20%, según la metodología de Saxena *et al.* [110] para evaluación del pronóstico.

En el Capítulo 6, la metodología de pronóstico propuesta se amplió para considerar la estimación de la fiabilidad a largo plazo como un indicador unificado de salud estructural. Se ha demostrado que la distribución de la variable *vida remanente* se puede conseguir fácilmente como una función de la estimación de fiabilidad a largo plazo. Antes de presentar la metodología para la predicción de la fiabilidad a largo plazo se proporcionó un estado del arte y revisión de la literatura sobre fiabilidad de materiales compuestos como una sección introductoria al capítulo. Esta revisión de literatura fue motivada por la falta de consenso observado en la literatura fiabilidad de composites. Una de las principales conclusiones de esta revisión es la necesidad de desarrollo de metodología que tengan en cuenta el daño progresivo de composites dentro de la formulación de fiabilidad, lo que motivó la formulación de la fiabilidad a largo plazo propuesta en la Sección 6.2.

Una dificultad encontrada para la predicción de saturación de micro-grietas fue la inestabilidad en las estimaciones de vida remanente cuando se utiliza un algoritmo ordinario de pronóstico basado en filtrado Bayesiano (por ejemplo, Algoritmo 3), que requiere el empleo de una elevada cantidad de sampleos para

obtener exactitud en la predicción. Ello motivó un nuevo algoritmo llamado PFP-Subsim que combina los principios del pronóstico con el método de simulación Subset con objeto de obtener eficiencia cuando la predicción conlleva simulaciones de eventos raros, como se especifica en la Sección 7.3. Se demostró que PFP-Subsim consigue alta eficiencia mediante la simulación de muestreos distribuidos en subconjuntos anidados de forma secuencial hasta que se alcanza el umbral de pronóstico final. La secuencia de subconjuntos se establece de forma automatizada, lo que evita tediosas calibraciones preliminares y a su vez permite su implementación para aplicaciones de pronóstico en tiempo real. La eficiencia computacional y la precisión que se puede obtener con el algoritmo propuesto se demostró en la Sección 9.3 usando el conjunto de datos de daño por fatiga presentado en el Capítulo 9, ilustrándose así algunos de los problemas a los que pueden enfrentarse con eficiencia el algoritmo en una aplicación real. Se demostró que la probabilidad de fallo del sistema (entendida como la complementaria de la fiabilidad a largo plazo) se puede predecir fácilmente con alta precisión utilizando el algoritmo PFP-Subsim incluso cuando esta probabilidad es muy pequeña. En particular, se ha probado por los ejemplos numéricos que el algoritmo PFP-Subsim es capaz de predecir eventos de fallo muy pequeños (correspondientes a niveles extremadamente altos de saturación de la micro-grietas en la matriz para el laminado considerado) con un coste computacional moderado. Cuando la probabilidad de fallo del sistema no es tan baja, los resultados mostraron que PFP-Subsim se comporta de manera similar al algoritmo de pronóstico estándar, lo que indica que PFP-Subsim puede considerarse como un algoritmo de pronóstico de propósito general, con la particularidad de que es especialmente eficaz para el pronóstico de eventos raros.

Limitaciones

Una serie de hipótesis son consideradas en la formulación de los diversos métodos de pronóstico y algoritmos propuestos para esta tesis de modo que, en cierta manera, indican las limitaciones de la metodología propuesta. Esta sección pretende resaltar de forma honesta tales supuestos y limitaciones. En primer lugar, es importante señalar que el marco de estimación de estados Bayesiano propuesto en el Capítulo 5 fue formulado bajo el supuesto de que los datos viniesen dados en forma de densidad de micro-grietas en la matriz y rigidez efectiva normalizada. Sin embargo, los sensores actuales de monitorización estructural difícilmente proporcionan esta información de forma directa. En su lugar, las señales que se obtienen de los sensores requieren un procesamiento previo para

obtener los datos de degradación en sí. Varias contribuciones se pueden encontrar en la literatura sobre métodos válidos para procesamiento de señales procedentes de sensores del daño estructural en materiales compuestos (véase por ejemplo C. Larrosa y F. K. Chang [243, 245]). El trabajo intermedio que es necesario considerar para obtener los datos de daño desde las señales en bruto de los sensores, se ha presentado en la Sección 8.2.1, más concretamente mediante el esquema de la Figura 8.4. Ello indica que ciertos trabajos previos son requeridos para realizar un experimento de pronóstico en tiempo real utilizando el marco que aquí se presenta.

Para continuar con las limitaciones, es evidente que el marco propuesto se elaboró bajo el supuesto de que la micro-fisuración de la matriz es el modo dominante de daño y también el precursor de otros modos de daños más graves en el material compuesto, lo cual es una suposición razonable para laminados tipo cross-ply [26], (como el tipo de laminado considerado en esta tesis). Bajo tal supuesto, se seleccionaron modelos adecuados de fisuración por micro-grietas y de reducción de la rigidez inducida por micro-grietas. Por tanto, otros modos posibles daños como delaminación y rotura de fibra, entre otros, no quedan bien representados mediante los modelos considerados (aunque su efecto sí que se consideró como fuente de incertidumbre que es cuantificada a través de los términos de error del modelo). Dado que los modelos de daño son estocásticamente embebidos para servir como ecuaciones de transición/predicción en la formulación de filtrado Bayesiano, la no consideración de otros modos de daño en el modelo puede influir en la predictabilidad, con independencia de lo bien que predigan el algoritmo de pronóstico. Esto significa que si se consideran diferentes tipos de laminados, podría esperarse la aparición de otros modos de daño, por lo tanto, determinadas modificaciones a los modelos de daño serían requeridas para mejorar la capacidad de predicción. Por último, se señaló que el marco de pronóstico propuesto para daño por fatiga en composites ha sido diseñado, y también validado por los ejemplos numéricos, a nivel de cupón o especimen en condiciones de laboratorio.

Aunque esta es la situación habitual en la mayoría de los programas actuales de investigación sobre fatiga, es importante indicar que una mejora de mucho interés no sólo a nivel de investigación sino también para ingeniería, sería aquella que propusiera un programa de pronóstico de fatiga a nivel de componente estructural o subsistema bajo cargas de fatiga realistas. Esto puede requerir el desarrollo de tecnología específica de diagnóstico para la detección y la cuantificación de la extensión del daño a través de un sistema de sensores de monitorización de

salud estructural, así como un marco de pronóstico especialmente diseñado para ello.

Trabajos futuros

El contenido de esta sección ha sido parcialmente cubierto por la anterior, ya que el planteamiento con suficiente rigor de cualquiera de las limitaciones antes mencionadas, puede ser constitutivo de un nuevo objetivo potencial de investigación y por ende, una posible línea futura de trabajo. Sin embargo, la intención del autor con esta sección es la de destacar brevemente la más fructífera de entre las posibles que de esta manera surgen, entendiéndose así como las líneas de investigación más viables para trabajar tras esta tesis. En este sentido, la consideración de otros modos de daños internos diferentes del de micro-fisuración en la matriz sería de especial interés para futuras investigaciones. Es también de destacar que el estudio y validación del marco de pronóstico para diferentes tipos de secuencias de laminación (como quasi-isotropic, angle-ply, etc) también pueden ser considerado como línea de trabajo inmediata a seguir. En general, un escenario ideal para la investigación futura en esta materia estaría compuesto por una combinación adecuada entre desarrollo de tecnología de diagnóstico y detección de daño junto con un marco de pronóstico con capacidad de toma de decisiones sobre degradación y fiabilidad de estructuras complejas realizadas con materiales compuestos.

Part V

APPENDICES



Basic relations for ERR term formulation in composites

This appendix presents the expressions of some of the terms involved in the ERR term formulation for different damage mechanics models. Basis of the classical laminate theory is presented and used to derive the formulation of the ERR terms.

A.1 Shear-lag model nomenclature and basic relations of classical laminate theory

The function a in Equation 5.4 is defined as a function of the laminate and ply properties listed in Table 5.1, as follows:

$$a = \frac{E_2 t_{90}}{E_1 t_\phi} \left(1 - \nu_{xy}^{(\phi)} \frac{\frac{\nu_{xy}^{(\phi)} t_{90}}{E_y^{(\phi)}} + \frac{\nu_{12} t_\phi}{E_2}}{\frac{t_{90}}{E_y^{(\phi)}} + \frac{t_\phi}{E_1}} \right) \frac{1 - \nu_{12} \nu_{xy}^{(\phi)}}{1 - \nu_{12}^2 \frac{E_2}{E_1}} \quad (\text{A.1})$$

where properties with the superscript (ϕ) are referred to the outer $\left[\phi_{\frac{n_\phi}{2}}\right]$ -sublaminar

Notice that the subscripts $\{1, 2, 3\}$ refer to ply properties defined in local axis (material coordinate system) while the subscripts $\{x, y, z\}$ refer to sub-laminar or laminar properties defined in global axis, that corresponds to the laminar coordinate system. The first local direction "1" coincides with fibers direction at a given ply or lamina, while directions "2-3" are the in-plane and out-of-plane transverse directions. For global axis, "x" refers to the fatigue loading direction, while "y-z" refers to the in-plane and out-of-plane transverse directions, respectively. In addition, the superscript (ϕ) denotes: "property referred to the $\left[\phi_{\frac{n_\phi}{2}}\right]$ -sub-laminar".

The function a in Equation 5.4 is defined as a function of the laminar and ply properties listed in Table 5.1 where properties with the superscript (ϕ) are referred to the outer $\left[\phi_{\frac{n_\phi}{2}}\right]$ -sub-laminar. From the classical theory of laminates [41], these properties can be readily obtained as:

$$\frac{1}{E_x^{(\phi)}} = \frac{m^4}{E_1} + \frac{n^4}{E_2} + \left(\frac{1}{G_{12}} - 2\frac{\nu_{12}}{E_1} \right) m^2 n^2 \quad (\text{A.2a})$$

$$\frac{1}{E_y^{(\phi)}} = \frac{n^4}{E_1} + \frac{m^4}{E_2} + \left(\frac{1}{G_{12}} - 2\frac{\nu_{12}}{E_1} \right) m^2 n^2 \quad (\text{A.2b})$$

$$\frac{\nu_{xy}^{(\phi)}}{E_x^{(\phi)}} = \frac{\nu_{12}}{E_1} - \left(\frac{1 + 2\nu_{12}}{E_1} + \frac{1}{E_2} - \frac{1}{G_{12}} \right) m^2 n^2 \quad (\text{A.2c})$$

where $m = \cos(\phi)$, $n = \sin(\phi)$, and ϕ is the angle between the laminar x -axis and the fiber direction of $\left[\phi_{\frac{n_\phi}{2}}\right]$ -sublaminar. The rest of the parameters involved in Equations A.1 and A.2 are defined in Table 5.1. For a cross-ply laminar, which is the laminar type considered in the numerical experiments of this thesis, $\phi = 0^\circ$, hence, the laminar and sublaminar global axis $\{x, y, z\}$ coincide with ply local axis $\{1, 2, 3\}$. In this particular case, the following identities hold:

$$E_x^{(0)} = E_1; E_y^{(0)} = E_2; \nu_{xy}^{(0)} = \nu_{12}; G_{xy}^{(0)} = G_{12}; G_{xz}^{(0)} = G_{12} \quad (\text{A.3})$$

Regarding the undamaged longitudinal Young's modulus of the overall laminar, $E_{x,0}$, it is obtained as $E_{x,0} = \frac{1}{a_{11}^*}$, where a_{11}^* is the $(1, 1)^{th}$ element of the normalized compliance matrix of the laminar \mathbf{a}^* , obtained as the inverse of the

normalized laminate stiffness matrix \mathbf{A}^* . For the laminate considered in this thesis, the matrix \mathbf{A}^* can be readily calculated using the rule of mixtures [43] as $\mathbf{A}^* = \frac{t_\phi}{h} \bar{\mathbf{Q}}^{(\phi)} + \frac{t_{90}}{h} \bar{\mathbf{Q}}^{(90)}$, where $\bar{\mathbf{Q}}^{(\alpha)}$, $\alpha = \{\phi, 90\}$ is the corresponding stiffness matrix of the outer $\left[\phi \frac{n_\phi}{2}\right]$ -sub-laminates and 90 sub-laminate, respectively, defined as:

$$\bar{\mathbf{Q}}^{(\alpha)} = \begin{bmatrix} \bar{Q}_{11} & \bar{Q}_{12} & \bar{Q}_{16} \\ \bar{Q}_{21} & \bar{Q}_{22} & \bar{Q}_{26} \\ \bar{Q}_{61} & \bar{Q}_{62} & \bar{Q}_{66} \end{bmatrix} \quad (\text{A.4})$$

The elements of this matrix can be obtained as a function of the corresponding sub-laminate angle α as:

$$\begin{bmatrix} \bar{Q}_{11} \\ \bar{Q}_{22} \\ \bar{Q}_{12} \\ \bar{Q}_{66} \\ \bar{Q}_{16} \\ \bar{Q}_{26} \end{bmatrix} = \begin{bmatrix} U_1 & U_2 & U_3 & 0 & 0 \\ U_1 & -U_2 & U_3 & 0 & 0 \\ U_4 & 0 & -U_3 & 0 & 0 \\ U_5 & 0 & -U_3 & 0 & 0 \\ 0 & 0 & 0 & \frac{1}{2}U_2 & U_3 \\ 0 & 0 & 0 & \frac{1}{2}U_2 & -U_3 \end{bmatrix} \cdot \begin{bmatrix} 1 \\ \cos(2\alpha) \\ \cos(4\alpha) \\ \sin(2\alpha) \\ \sin(4\alpha) \end{bmatrix} \quad (\text{A.5})$$

where U_i , $i = 1, \dots, 5$ are invariants from the ply, whose values are defined regardless of the ply orientation as a function of the components of the "on-axis" ply stiffness matrix, as follows:

$$U_1 = \frac{3}{8}Q_{11} + \frac{3}{8}Q_{22} + \frac{1}{4}Q_{12} + \frac{1}{2}Q_{66} \quad (\text{A.6a})$$

$$U_2 = \frac{1}{2}Q_{11} - \frac{1}{2}Q_{22} \quad (\text{A.6b})$$

$$U_3 = \frac{1}{8}Q_{11} + \frac{1}{8}Q_{22} - \frac{1}{4}Q_{12} - \frac{1}{2}Q_{66} \quad (\text{A.6c})$$

$$U_4 = \frac{1}{8}Q_{11} + \frac{1}{8}Q_{22} + \frac{3}{4}Q_{12} - \frac{1}{2}Q_{66} \quad (\text{A.6d})$$

$$U_5 = \frac{1}{8}Q_{11} + \frac{1}{8}Q_{22} - \frac{1}{4}Q_{12} + \frac{1}{2}Q_{66} \quad (\text{A.6e})$$

where,

$$Q_{11} = \frac{E_1}{1 - \nu_{12}^2 \frac{E_2}{E_1}}, \quad Q_{22} = \frac{E_2}{1 - \nu_{12}^2 \frac{E_2}{E_1}}, \quad Q_{12} = \nu_{12} Q_{22}, \quad Q_{66} = G_{12} \quad (\text{A.7})$$

A.2 Energy release rate for micro-cracks interaction with local and global delamination (variational approach)

Expressions for $\chi(\bar{l})$ and its first derivate $\chi'(\bar{l})$ are given by:

$$\begin{aligned}\chi(\bar{l}) &= 2\alpha_1\alpha_2(\alpha_1^2 + \alpha_2^2) \frac{\cosh(2\alpha_1\bar{l}) - \cos(2\alpha_2\bar{l})}{\alpha_2 \sinh(2\alpha_1\bar{l}) - \sin(2\alpha_2\bar{l})} \\ \chi'(\bar{l}) &= 4\alpha_1\alpha_2(\alpha_1^2 + \alpha_2^2)^2 \frac{\sinh(2\alpha_1\bar{l}) \sin(2\alpha_2\bar{l})}{\alpha_2 \sinh(2\alpha_1\bar{l}) + \alpha_1 \sin(2\alpha_2\bar{l})}\end{aligned}\quad (\text{A.8a})$$

$$\begin{aligned}\chi(\bar{l}) &= \alpha_1\alpha_2(\alpha_1^2 - \alpha_2^2) \frac{\tanh(\alpha_2\bar{l}) \tanh(\alpha_1\bar{l})}{\alpha_2 \tanh(\alpha_2\bar{l}) - \alpha_1 \tanh(\alpha_1\bar{l})} \\ \chi'(\bar{l}) &= \alpha_1^2\alpha_2^2(\alpha_1^2 - \alpha_2^2) \frac{\frac{\tanh(\alpha_2\bar{l})}{\cosh^2(\alpha_1\bar{l})} - \frac{\tanh(\alpha_1\bar{l})}{\cosh^2(\alpha_2\bar{l})}}{(\alpha_2 \tanh(\alpha_2\bar{l}) - \alpha_1 \tanh(\alpha_1\bar{l}))^2}\end{aligned}\quad (\text{A.9a})$$

where $\alpha_1 = \sqrt{\frac{-p}{2} + \sqrt{\frac{p^2}{4} - q}}$ and $\alpha_2 = \sqrt{\frac{-p}{2} - \sqrt{\frac{p^2}{4} - q}}$. The Eq. A.8a applies when $\frac{4q}{p^2} > 1$ holds. Otherwise, Eq. A.9a should be consider. The terms p and q are relations of the ply properties and the stacking sequence defined by $p = (C_2 - C_4)/C_3$, $q = C_1/C_3$. The parameters C_i , $i : 1, \dots, 4$, are known functions of the laminate properties defined as:

$$C_1 = \frac{1}{E_1} + \frac{1}{\lambda E_2} \quad (\text{A.10a})$$

$$C_2 = \left(\lambda + \frac{2}{3}\right) \frac{\nu_{23}}{E_2} - \frac{\lambda \nu_{12}}{3E_1} \quad (\text{A.10b})$$

$$C_3 = (1 + \lambda) \left(3\lambda^2 + 12\lambda + 8\right) \frac{1}{60E_2} \quad (\text{A.10c})$$

$$C_4 = \frac{1}{3} \left(\frac{1}{G_{23}} + \frac{\lambda}{G_{12}}\right) \quad (\text{A.10d})$$

where λ is the ply-thickness ratio $\lambda = t_0/t_{90}$. Notice that ΔG_{LD} depends on the magnitude $(\bar{l} - \delta)$, which expresses the separation between the tips of two growing delaminations starting from the tips of the matrix micro-cracks. Without lack of generality, thermal stresses are not considered for the formulation of ERR in Tables 5.2 and 5.1, since the data used for this thesis, and also in most of fatigue experiments, are collected in a temperature controlled environment.

A.3 Energy release rate for micro-cracks interaction with local and global delamination (COD approach)

The normalized effective stiffness of a cracked laminate using a COD model can be stated using the formulation by Gudmundson and Weilin [148] as follows¹:

$$E_x^* = \frac{1}{((\mathbf{S}_0)^{-1} - \sum_{k=1}^T \nu^k t^k \rho^k (\mathbf{A}^k)^T \sum_{i=1}^N \beta^{ik} \mathbf{A}^i)_{(1,1)}^{-1}} \quad (\text{A.11})$$

where \mathbf{S}_0 is the in-plane compliance matrix of the intact laminate, T is the total amount of plies and, ν^k , t^k and ρ^k stand for the volume fraction, the thickness and the matrix-cracks density of the k th ply, respectively, $k = 1, \dots, T$. The term \mathbf{A}^k is a matrix determined by the compliance matrix and the orthonormal vector on the crack surface of the k th ply as follows:

$$\mathbf{A}^k = \mathbf{N}_I^k (\mathbf{S}^k)^{-1} \quad (\text{A.12})$$

where \mathbf{S}^k is the in-plane compliance matrix of the k th ply and \mathbf{N}_I^k is a matrix defined by the orthonormal vector to the surface of transverse cracks, \mathbf{n}^k , as:

$$\mathbf{N}_I^k = \begin{pmatrix} n_1^k & 0 & n_2^k \\ 0 & n_2^k & n_1^k \\ 0 & 0 & 0 \end{pmatrix}, \mathbf{n}^k = \begin{pmatrix} n_1^k \\ n_2^k \\ 0 \end{pmatrix} \quad (\text{A.13})$$

The terms β^{ki} are diagonal matrices used to account the average crack opening displacement of matrix cracks:

$$\beta^{ki} = 0, \forall k \neq i; \quad \beta^{kk} = \begin{pmatrix} \beta_1^k & 0 & 0 \\ 0 & \beta_2^k & 0 \\ 0 & 0 & \beta_3^k \end{pmatrix} \quad (\text{A.14})$$

¹The subscript (1, 1) in Equation A.11 denotes the first component of the resulting matrix.

where

$$\beta_1^k = \frac{4}{\pi} \gamma_1 \frac{\ln \left(\cosh \left(\frac{\pi t^k \rho^k}{2} \right) \right)}{(t^k \rho^k)^2} \quad (\text{A.15a})$$

$$\beta_2^k = \frac{\pi}{2} \gamma_2 \sum_{j=1}^{10} \frac{a_j}{(1 + t^k \rho^k)^j} \quad (\text{A.15b})$$

$$\beta_3^k = \frac{\pi}{2} \gamma_3 \sum_{j=1}^9 \frac{b_j}{(1 + t^k \rho^k)^{j-2}} \quad (\text{A.15c})$$

$$\gamma_1 = \frac{1}{2G_{12}} \quad (\text{A.15d})$$

$$\gamma_2 = \gamma_3 = \frac{1}{E_2} - \frac{\nu_{12}^2}{E_1} \quad (\text{A.15e})$$

The terms a_j and b_j are constants whose values are found in the literature (see for example Table 1 in [148] or Table 4.2 in [145]). It is important to remark that one should adopt different formulation for β_i^k , $i = \{1, 2, 3\}$ if surface cracks (e.g. global delaminations) are present (or expected) in the damage pattern of the laminate. See further insight in [148, 246].

B

Contributions

This thesis has given rise to the following scientific work which have been published or submitted for publication during the graduate program of the author. A list of talks at international conferences and selected technical seminars are also highlighted. Those pieces of work with close relation with the research objectives of this thesis (see Chapter 2) are highlighted using the items [O.1,O.2,O.3] which refer to research objectives 1, 2, and 3, respectively.

Journal articles

- Juan Chiachío, Manuel Chiachío, Abhinav Saxena, Shankar Sankararaman, Guillermo Rus, Kai Goebel. Bayesian model selection and parameter estimation for fatigue damage progression models in composites. *To appear in International Journal of Fatigue* (2014)
- Manuel Chiachío, James L. Beck, Juan Chiachío, Guillermo Rus. Approximate Bayesian Computation by Subset Simulation. *SIAM Journal on Scientific Computing* (2014), 36 (3), A1339-A1358
- Manuel Chiachío, Juan Chiachío, Guillermo Rus, James L. Beck. Predicting Fatigue in Composites. A Bayesian Framework. *Structural Safety* (2014), 51, 57-68.

- O.2 Manuel Chiachío, Juan Chiachío, Guillermo Rus. Reliability in composites- A selective review and survey of current development. *Composites Part B: Engineering* (2012), 43, 902-913.
- O.3 Manuel Chiachío, Juan Chiachío, Shankar Sankararaman, Abhinav Saxena, Guillermo Rus, Kai Goebel. An efficient algorithm for prognostics involving rare-events. *Submitted to SIAM Journal on Scientific Computing*.
- O.1 Juan Chiachío, Manuel Chiachío, Shankar Sankararaman, Abhinav Saxena, Guillermo Rus, Kai Goebel. A particle filtering approach for reliability-based prognostics in composites. *Submitted to Reliability Engineering and System Safety*
- Guillermo Rus, Juan Chiachío, Manuel Chiachío. Logical inference for inverse problems. *Submitted to Inverse Problems*.

Book chapters

- O.1 Juan Chiachío, Manuel Chiachío, Shankar Sankararaman, Abhinav Saxena, Kai Goebel. Prognostics Design for Structural Health Management, *To appear in: Emerging Design Solutions in Structural Health Monitoring Systems, Advances in Civil and Industrial Engineering Series (September 2014), Ed. IGI Global*.
- R. Muñoz, G. Rus, N. Bochud, D. Barnard, J. Melchor, J. Chiachío, M. Chiachío, S. Cantero, A. Callejas, L. Peralta. Nonlinear ultrasonics as an early damage signature, *To appear in: Emerging Design Solutions in Structural Health Monitoring Systems, Advances in Civil and Industrial Engineering Series (September 2014), Ed. IGI Global*.
- O.1 Kai Goebel, Manuel Chiachío, Juan Chiachío, Abhinav Saxena. An Energy-based Prognostic Framework to Predict Evolution of Damage in Aerospace Structures, *To appear in: Structural Health Monitoring (SHM) in Aerospace Structures (November 2014), Ed. Woodhead Publishing Limited*.

Conference proceedings (full-papers)

- O.3 Manuel Chiachío, Juan Chiachío, Abhinav Saxena, Guillermo Rus, Kai Goebel. An efficient simulation framework for prognostics of asymptotic processes-a case study in composite materials. *In Proceedings of the European Conference of the Prognostics and Health Management Society, 2014, ISBN-978-1-936263-16-5, pp. 202-214. (Nomination for Best-Paper Award)*
- O.2 Juan Chiachío, Manuel Chiachío, Abhinav Saxena, Guillermo Rus, Kai Goebel. A model-based prognostics framework to predict fatigue damage

evolution and reliability in composites. In *Proceedings of the European Conference of the Prognostics and Health Management Society, 2014*, ISBN-978-1-936263-16-5 pp. 732-742. (*Best-Paper Award*)

- O.3 Manuel Chiachío, Juan Chiachío, Abhinav Saxena, Shankar Sankaraman, Kai Goebel. Predicting remaining useful life in CRFP laminates under fatigue loads: A new efficient algorithm. In *Proceedings of the American Society for Composites 29th Technical Conference, 16th US-Japan Conference on Composites Materials, and ASTM D30 meeting, 2014*, pp. 1-20, (pending ISBN assignment).
- Juan Chiachío, Juan Chiachío, Abhinav Saxena, Shankar Sankaraman, Kai Goebel. A robust modeling approach for fatigue damage in composites based on Bayesian model class selection. In *Proceedings of the American Society for Composites 29th Technical Conference, 16th US-Japan Conference on Composites Materials, and ASTM D30 meeting, 2014*, pp. 1-18, (pending ISBN assignment).
- O.3 Manuel Chiachío, Juan Chiachío, Abhinav Saxena, Guillermo Rus, Kai Goebel. An efficient algorithm to predict the expected end-of-life in composites. In *Proceedings of the 16th European Conference on Composite Materials, 2014*, pp.1-8, (pending ISBN assignment).
- O.1 Juan Chiachío, Manuel Chiachío, Abhinav Saxena, Guillermo Rus, Kai Goebel. An Energy- Based Prognostic Framework to Predict Fatigue Damage Evolution in Composites. In *Proceedings of the Annual Conference of the Prognostics and Health Management Society, 2013*, ISBN-978-1-936263-06-6 pp. 363-371.
- O.1 Manuel Chiachío, Juan Chiachío, Abhinav Saxena, Guillermo Rus, Kai Goebel. Fatigue damage prognosis in FRP composites by combining multi-scale degradation fault modes in an uncertainty Bayesian framework. In *Proceedings of the Structural Health Monitoring, 2013*, ISBN: 978-1-60595-115-7, pp.1368-1376,
- Manuel Chiachío, Juan Chiachío, Guillermo Rus. Fatigue diagnosis in composites-A Robust Bayesian approach. In *Proceedings of the 15th European Conference on Composite Materials, 2012*, pp.1-8, ISBN: 978-88-88785-33-2.
- Juan Chiachío, Manuel Chiachío, Guillermo Rus, Nicolas Bochud, Laura Maria Peralta, Juan M. Melchor. A stochastic model for tissue consistence evolution based on the inverse problem. In *Proceedings of the ESB2012, Journal of Biomechanics, 45, Supplement 1, July 2012*, pp. S652.

- J. Chiachío, M. Chiachío, G. Rus. An Inverse-Problem Based Stochastic Approach to Model the Cumulative Damage Evolution of Composites. *Procedia Engineering, Volume 14, 2011, pp. 1557-1563.*

Patents

- Manuel Chiachio, Juan Chiachio, Guillermo Rus. Self-stressed structure for all-composite bridge (ES 2332442 B1). Spanish Bureau of Patents (OEPM).
- G. Rus, N. Bochud, J. Melchor, J. Chiachio, M. Chiachio. Petri-dish ultrasound-based monitoring device. (ES 2387770 B1). Spanish Bureau of Patents (OEPM).

International conferences

- O.3 **Manuel Chiachío**, Juan Chiachío, Abhinav Saxena, Guillermo Rus, Kai Goebel. An efficient simulation framework for prognostics of asymptotic processes-a case study in composite materials. 2nd European Conference of the Prognostics and Health Management Society, Nantes, France, July 7-10, 2014.
- O.1 **Manuel Chiachío**, Juan Chiachío, Abhinav Saxena, Guillermo Rus, Kai Goebel. Fatigue damage prognosis in FRP composites by combining multi-scale degradation fault modes in an uncertainty Bayesian framework. International Workshop on Structural Health Monitoring (IWSHM'13), Stanford University-Palo Alto, (USA) September 10-13, 2013.
- O.1 **Manuel Chiachío**, Juan Chiachío, Abhinav Saxena, Guillermo Rus, Kai Goebel. Connecting Microscale and Macroscale Damage Models in a Bayesian Framework for Fatigue Damage Prognostics of CFRP Composites. ASME 2013 International Mechanical Engineering Congress & Exposition, San Diego (USA), November 15-22, 2013.
- **Manuel Chiachío**, Juan Chiachío, Guillermo Rus. Cumulative Damage Reconstruction in Composites-Different Perspectives based on the Inverse Problem. 8th Solid Mechanics European Conference, Graz (Austria), July 9-13, 2012.
- **Manuel Chiachío**, Juan Chiachío, Guillermo Rus. Ultrasonic monitoring of artificial tissue mechanical properties in bioreactor. International Work Conference on Bioinformatics and Biomedical Engineering (IWBBIO 2014), 31th Annual Meeting, Granada (Spain), April 7-9, 2014.
- Juan Chiachío, **Manuel Chiachío**, Guillermo Rus. Tissue Consistence Evolution: A Statistical Approach. Tissue Engineering and Regenerative Medicine International Society, 31th Annual Meeting, Granada (Spain), June 7-10, 2011.

- O.3 **Manuel Chiachío**, Juan Chiachío, Abhinav Saxena, Guillermo Rus, Kai Goebel. An efficient algorithm to predict the expected end-of-life in composite under fatigue conditions. 16th European Conference on Composite Materials, Seville (Spain), June 22-26, 2014.
- **M. Chiachío**, J. Chiachío, G. Rus. Reliability Assessment of complex materials under mechanical degradation. 16th International Conference on Composite Structures (ICCS16), Porto (Portugal), June 21-26, 2011.

Technical seminars as invited speaker

- **Manuel Chiachío**. A Bayesian Framework in Cumulative Damage Diagnostic. Institute of Polymers and Composites. Technical University of Hamburg (TUHH-AIRBUS). By invitation of Prof. Dr. Ing. Karl Shulte.
- **Manuel Chiachío**. Predicting the Evolution of Damage in Composites Materials. Part 2: A Bayesian Approach. Graduate Aerospace Laboratories at California Institute of Technology (CALTECH). By invitation of Prof. Michael Ortiz.

References

- [1] A. Saxena, K. Goebel, C. Larrosa, and F.K. Chang. CFRP composites dataset, 2013. NASA Ames Prognostics Data Repository.
- [2] Valery V. Vasiliev and Evgeny V. Morozov. *Mechanics and Analysis of Composite Materials*. 2001.
- [3] Joris Degrieck and Wim Van Paepegem. Fatigue damage modeling of fibre-reinforced composite materials: Review. *Applied Mechanics Reviews*, 54(4):279, 2001.
- [4] Russell D Jamison, Karl Schulte, Kenneth L Reifsnider, and Wayne W Stinchcomb. Characterization and analysis of damage mechanisms in tension-tension fatigue of graphite/epoxy laminates. *Effects of defects in composite materials, ASTM STP*, 836:21–55, 1984.
- [5] Ramesh Talreja. Damage and fatigue in composites – A personal account. *Composites Science and Technology*, 68:2585–2591, 2008.
- [6] Charles R. Farrar and Nick A.J. Lieven. Damage prognosis: the future of structural health monitoring. *Philosophical Transactions of the Royal Society A: Mathematical, Physical and Engineering Sciences*, 365(1851):623–632, 2007.
- [7] Maurizio Gobbato, John B. Kosmatka, and Joel P. Conte. A recursive Bayesian approach for fatigue damage prognosis: an experimental validation at the reliability component level. *Mechanical Systems and Signal Processing*, 45(2):448–467, 2014.
- [8] Shankar Sankararaman, You Ling, Chris Shantz, and Sankaran Mahadevan. Uncertainty quantification in fatigue damage prognosis. In *Annual conference of the prognostics and health management society*, pages 1–13, 2009.
- [9] Matthew J Daigle and Kai Goebel. Model-based prognostics with concurrent damage progression processes. *Systems, Man, and Cybernetics: Systems, IEEE Transactions on*, 43(3):535–546, 2013.
- [10] F. Cadini, E. Zio, and D. Avram. Monte carlo-based filtering for fatigue crack growth estimation. *Probabilistic Engineering Mechanics*, 24(3):367–373, 2009.
- [11] Xuefei Guan, Ratneshwar Jha, and Yongming Liu. Model selection, updating, and averaging for probabilistic fatigue damage prognosis. *Structural Safety*, 33(3):242–249, 2011.

- [12] Mathew Daigle and Chetan Kulkarni S. Electrochemistry-based battery modeling for prognostics. In *Proceedings of the Annual Conference of the Prognostics and Health Management Society, 2013*, volume 1, pages 249–261, 2013.
- [13] Mathew Daigle, Abhinav Saxena, and Kai Goebel. An efficient deterministic approach to model-based prediction uncertainty estimation. In *Proceedings of the Annual Conference of the Prognostics and Health Management Society, 2013*, volume 1, pages 249–261, 2013.
- [14] J Celaya, Chetan Kulkarni, Gautam Biswas, Sankalita Saha, and Kai Goebel. A model-based prognostics methodology for electrolytic capacitors based on electrical overstress accelerated aging. In *Proceedings of Annual Conference of the PHM Society, September*, pages 25–29, 2011.
- [15] N. Patil, J. Celaya, D. Das, K. Goebel, and M. Pecht. Precursor parameter identification for insulated gate bipolar transistor (igbt) prognostics. *Reliability, IEEE Transactions on*, 58(2):271–276, 2009.
- [16] J.R. Celaya, A Saxena, C.S. Kulkarni, S. Saha, and K. Goebel. Prognostics approach for power mosfet under thermal-stress aging. In *Reliability and Maintainability Symposium (RAMS), 2012 Proceedings - Annual*, pages 1–6, 2012.
- [17] B. Saha, J.R. Celaya, P.F. Wysocki, and K.F. Goebel. Towards prognostics for electronics components. In *Aerospace conference, 2009 IEEE*, pages 1–7, 2009.
- [18] M Sanjeev Arulampalam, Simon Maskell, Neil Gordon, and Tim Clapp. A tutorial on particle filters for online nonlinear/non-Gaussian Bayesian tracking. *Signal Processing, IEEE Transactions on*, 50(2):174–188, 2002.
- [19] Arnaud Doucet, Nando De Freitas, and Neil Gordon. An introduction to sequential monte carlo methods. In Arnaud Doucet, Nando De Freitas, and Neil Gordon, editors, *Sequential Monte Carlo methods in practice*, pages 3–14. Springer, 2001.
- [20] Enrico Zio and Giovanni Peloni. Particle filtering prognostic estimation of the remaining useful life of nonlinear components. *Reliability Engineering & System Safety*, 96(3):403–409, 2011.
- [21] Eija Myötyri, Urho Pulkkinen, and Kaisa Simola. Application of stochastic filtering for lifetime prediction. *Reliability Engineering & System Safety*, 91(2):200–208, 2006.
- [22] Marcos Orchard, Gregory Kacprzyński, Kai Goebel, Bhaskar Saha, and George Vachtsevanos. Advances in uncertainty representation and management for particle filtering applied to prognostics. In *International conference on prognostics and health management*. IEEE, 2008.
- [23] Bhaskar Saha, Kai Goebel, and Jon Christophersen. Comparison of prognostic algorithms for estimating remaining useful life of batteries. *Transactions of the Institute of Measurement and Control*, 31(3-4):293–308, 2009.
- [24] Matthew Daigle and Kai Goebel. Multiple damage progression paths in model-based prognostics. In *Aerospace Conference, 2011 IEEE*, pages 1–10. IEEE, 2011.

- [25] Mathew Daigle and Kai Goebel. Model-based prognostics with fixed-lag particle filters. In *Proceedings of the Annual Conference of the Prognostics and Health Management Society, 2019*, volume 1, pages 249–261, 2009.
- [26] R.D. Jamison. The role of microdamage in tensile failure of graphite/epoxy laminates. *Composites Science and Technology*, 24(2):83–99, 1985.
- [27] Ramesh Talreja. Stiffness properties of composite laminates with matrix cracking and interior delamination. *Engineering Fracture Mechanics*, 25(5/6):751–762, 1986.
- [28] Enrico Zio and Francesco Di Maio. Fatigue crack growth estimation by relevance vector machine. *Expert Systems with Applications*, 39(12):10681–10692, 2012.
- [29] Dawn An, Joo-Ho Choi, and Nam Ho Kim. Prognostics 101: A tutorial for particle filter-based prognostics algorithm using matlab. *Reliability Engineering & System Safety*, 115:161–169, 2013.
- [30] M. Kamiński. On probabilistic fatigue models for composite materials. *International journal of fatigue*, 24(2):477–495, 2002.
- [31] D. Revuelta, J. Cuartero, A. Miravete, and R. Clemente. A new approach to fatigue analysis in composites based on residual strength degradation. *Composite Structures*, 48:183–186, 2000.
- [32] Shingo Nakanishi and Hidetoshi Nakayasu. Reliability design of structural system with cost effectiveness during life cycle. *Computers & Industrial Engineering*, 42:447–456, 2002.
- [33] T Kam. Fatigue reliability analysis of composite laminates under spectrum stress. *International Journal of Solids and Structures*, 34(12):1441–1461, 1997.
- [34] Manuel Chiachio, Juan Chiachio, and Guillermo Rus. Reliability in composites - A selective review and survey of current development. *Composites Part B*, 43(3):902–913, 2012.
- [35] Ravi Rajamani, Abhinav Saxena, Frank Kramer, Michael Augustin, John B Schroeder, Kai Goebel, Ginger Shao, Indranil Roychoudhury, and Wei Lin. Developing ivhm requirements for aerospace systems. Technical report, SAE Technical Paper, 2013.
- [36] S. Sankararaman and K. Goebel. Uncertainty in prognostics: Computational methods and practical challenges. In *Aerospace Conference, 2014 IEEE*, pages 1–9, 2014.
- [37] S. Sankararaman, M.J. Daigle, and K. Goebel. Uncertainty quantification in remaining useful life prediction using first-order reliability methods. *Reliability, IEEE Transactions on*, 63(2):603–619, 2014.
- [38] JR Celaya, A Saxena, and K Goebel. Uncertainty representation and interpretation in model-based prognostics algorithms based on kalman filter estimation. In *Proceedings of the Annual Conference of the PHM Society*, pages 23–27, 2012.
- [39] J.N. Reddy. *Mechanics of Laminated Composite Plates and Shells, Theory and Analysis, 2nd. Edition*. CRC Press, 2004.

- [40] S.W. Tsai and E.M. Wu. A general theory of strength for anisotropic materials. *Journal of composite materials*, 5(1):58, 1971.
- [41] S.W. Tsai. *Theory of composites design*. Think composites, 1992.
- [42] Duk-Hyun Kim. *Composite Structures for Civil and Architectural Engineering*. 1995.
- [43] Stephen W. Tsai. *Strength & Life of Composites*. Stanford University, USA, 2008.
- [44] Ramesh Talreja and Chandra Veer Singh. *Damage and failure of composite materials*. Cambridge University Press, 2012.
- [45] J.S. Liu. *Monte Carlo Strategies in Scientific Computing*. Springer Verlag, New York, 2001.
- [46] F. Liang, C. Liu, and J. Chuanhai. *Advanced Markov chain Monte Carlo methods*. Wiley Online Library, 2010.
- [47] N. Metropolis and S. Ulam. The monte carlo method. *Journal of the American Statistical Association*, 44(247):335–341, 1949.
- [48] G.L. Ang, AH-S Ang, and W.H. Tang. Optimal importance sampling density estimator. *Journal of Engineering Mechanics*, 118(5):1146–1163, 1992.
- [49] C.G. Bucher. Adaptive sampling—an iterative fast Monte Carlo procedure. *Structural Safety*, 5:119–126, 1988.
- [50] A. Karamchandani, P. Bjerager, and C Cornell. Adaptive importance sampling. In *5th International Conference on Structural Safety and Reliability, ICOSSAR, San Francisco*, pages 855–862, 1989.
- [51] A. Haldar and S. Mahadevan. *Probability, reliability, and statistical methods in engineering design*. 2000.
- [52] S.K. Au and J.L. Beck. First excursion probabilities for linear systems by very efficient importance sampling. *Probabilistic Engineering Mechanics*, 16:193–207, 2001.
- [53] W.R. Gilks. *Markov chain Monte Carlo*. Wiley Online Library, 2005.
- [54] C.P. Robert and G. Casella. *Monte Carlo statistical methods, 2nd Ed.* Springer-Verlag, New York, 2004.
- [55] N. Metropolis, A.W. Rosenbluth, M.N. Rosenbluth, A.H. Teller, and E. Teller. Equation of state calculations by fast computing machines. *The journal of chemical physics*, 21:1087–1092, 1953.
- [56] W.K. Hastings. Monte Carlo sampling methods using Markov chains and their applications. *Biometrika*, 57(1):97–109, 1970.
- [57] W.R. Gilks, S. Richardson, and D.J. Spiegelhalter. *Markov chain Monte Carlo in practice*. Chapman and Hall, 1996.
- [58] Christophe Andrieu. An Introduction to MCMC for Machine Learning. *Science*, pages 5–43, 2003.
- [59] J. Ching and Y. Chen. Transitional Markov chain Monte Carlo method for Bayesian model updating, model class selection and model averaging. *Journal of Engineering Mechanics*, 133(7), 2007.

- [60] A. Gelman, G. Roberts, and W. Gilks. Efficient Metropolis jumping rules. *Bayesian statistics*, 5:599–608, 1996.
- [61] G.O. Roberts and J.S. Rosenthal. Optimal scaling for various Metropolis-Hastings algorithms. *Statistical Science*, 16(4):351–367, 2001.
- [62] S.K. Au and J.L. Beck. Estimation of small failure probabilities in high dimensions by Subset Simulation. *Probabilistic Engineering Mechanics*, 16(4):263–277, 2001.
- [63] S.K. Au and J.L. Beck. Subset Simulation and its application to seismic risk based on dynamic analysis. *Journal of Engineering Mechanics*, 129(8):901–917, 2003.
- [64] J. Ching, S.K. Au, and J.L. Beck. Reliability estimation of dynamical systems subject to stochastic excitation using Subset Simulation with splitting. *Computer Methods in Applied Mechanics and Engineering*, 194(12-16):1557–1579, 2005.
- [65] K.M. Zuev, J.L. Beck, S.K. Au, and L.S. Katafygiotis. Bayesian post-processor and other enhancements of Subset Simulation for estimating failure probabilities in high dimensions. *Computers & Structures*, 93:283–296, 2011.
- [66] Manuel Chiachio, James L. Beck, Juan Chiachio, and Guillermo Rus. Approximate bayesian computation by Subset Simulation. *SIAM Journal on Scientific Computing*, 36(3):1339–1339, 2014.
- [67] S. Tavare, D.J. Balding, R.C. Griffiths, and P. Donnelly. Inferring coalescence times from DNA sequence data. *Genetics*, 145(2):505, 1997.
- [68] J.K. Pritchard, M.T. Seielstad, A. Perez-Lezaun, and M.W. Feldman. Population growth of human Y chromosomes: a study of Y chromosome microsatellites. *Molecular Biology and Evolution*, 16(12):1791–1798, 1999.
- [69] O. Ditlevsen and H.O. Madsen. *Structural reliability methods*, volume 315. 1996.
- [70] A.M. Hasofer and N.C. Lind. Exact and invariant second-moment code format. *Journal of the Engineering Mechanics Division*, 100(1):111–121, 1974.
- [71] M. Shinozuka. Basic analysis of structural safety. *Journal of Structural Engineering*, 109(3):721–740, 1983.
- [72] B. Fiessler, R. Rackwitz, and H.J. Neumann. Quadratic limit states in structural reliability. *Journal of the Engineering Mechanics Division*, 105(4):661–676, 1979.
- [73] M. Rosenblatt. Remarks on a multivariate transformation. *The Annals of Mathematical Statistics*, 23(3):470–472, 1952.
- [74] M. Hohenbichler and R. Rackwitz. Non-normal dependent vectors in structural safety. *Journal of the Engineering Mechanics Division*, 107(6):1227–1238, 1981.
- [75] A.M. Ucci. Probability techniques for reliability analysis of composite materials. Master’s thesis, State University of New York at Buffalo, 1992.
- [76] K. Dolinski. First-order second-moment approximation in reliability of structural systems: critical review and alternative approach. *Structural Safety*, 1(13):211–231, 1983.
- [77] C.G. Soares. Reliability of components in composite materials. *Reliability Engineering & System Safety*, 55(2):171–177, 1997.

- [78] D.J. Thomas and R.C. Wetherhold. Reliability analysis of continuous fiber composite laminates. *Composite Structures*, 17(4):277–293, 1991.
- [79] T.Y. Kam and E.S. Chang. Reliability formulation for composite laminates subjected to first-ply failure. *Composite Structures*, 38(1-4):447–452, 1997.
- [80] D.M. Frangopol and S. Recek. Reliability of fiber-reinforced composite laminate plates. *Probabilistic Engineering Mechanics*, 18(2):119–137, 2003.
- [81] C. Boyer, A. Béakou, and M. Lemaire. Design of a composite structure to achieve a specified reliability level. *Reliability Engineering & System Safety*, 56(3):273–283, 1997.
- [82] F. Richard and D. Perreux. A reliability method for optimization of $[+\varphi, -\varphi]_n$ fiber reinforced composite pipes. *Reliability Engineering & System Safety*, 68(1):53–59, 2000.
- [83] S.C. Lin. Reliability predictions of laminated composite plates with random system parameters. *Probabilistic Engineering Mechanics*, 15(4):327–338, 2000.
- [84] A.K. Onkar, C.S. Upadhyay, and D. Yadav. Probabilistic failure of laminated composite plates using the stochastic finite element method. *Composite Structures*, 77(1):79–91, 2007.
- [85] PAM Lopes, H.M. Gomes, and A.M. Awruch. Reliability analysis of laminated composite structures using finite elements and neural networks. *Composite Structures*, 92(7):1603–1613, 2009.
- [86] D.J. Lekou and T.P. Philippidis. Mechanical property variability in frp laminates and its effect on failure prediction. *Composites Part B: Engineering*, 39(7-8):1247–1256, 2008.
- [87] L. Yang and Z.K. Ma. A method of reliability analysis and enumeration of significant failure modes for a composite structural system. *Computers & Structures*, 33(2):337–344, 1989.
- [88] M.R. Gurvich and R.B. Pipes. Probabilistic analysis of multi-step failure process of a laminated composite in bending. *Composites Science and Technology*, 55(4):413–421, 1995.
- [89] E.M. Wu and C.S. Robinson. Computational micro-mechanics for probabilistic failure of fiber composites in tension. *Composites Science and Technology*, 58(9):1421–1432, 1997.
- [90] Geir Storvik. Particle filters for state-space models with the presence of unknown static parameters. *Signal Processing, IEEE Transactions on*, 50(2):281–289, 2002.
- [91] Jonathan R Stroud, Nicholas G Polson, and Peter Muller. Practical filtering for stochastic volatility models. In Andrew C Harvey, Siem Jan Koopman, and Neil Shephard, editors, *State space and unobserved component models*. Cambridge University Press, 2003.
- [92] Jane Liu and Mike West. Combined parameter and state estimation in simulation-based filtering. In Arnaud Doucet, Nando De Freitas, and Neil Gordon, editors, *Sequential Monte Carlo methods in practice*, pages 197–223. Springer, 2001.

- [93] Christian Musso, Nadia Oudjane, and Francois Le Gland. Improving regularised particle filters. In Arnaud Doucet, Nando De Freitas, and Neil Gordon, editors, *Sequential Monte Carlo methods in practice*, pages 247–271. Springer, 2001.
- [94] Matthew J Daigle and Kai Goebel. Model-based prognostics with concurrent damage progression processes. *Systems, Man, and Cybernetics: Systems, IEEE Transactions on*, 43(3):535–546, 2013.
- [95] O. Cappé, A. Guillin, J.M. Marin, and C.P. Robert. Population Monte Carlo. *Journal of Computational and Graphical Statistics*, 13(4):907–927, 2004.
- [96] JE Handschin and David Q Mayne. Monte carlo techniques to estimate the conditional expectation in multi-stage non-linear filtering. *International journal of control*, 9(5):547–559, 1969.
- [97] JE Handschin. Monte carlo techniques for prediction and filtering of non-linear stochastic processes. *Automatica*, 6(4):555–563, 1970.
- [98] NJ. Gordon, DJ Salmond, and AFM Smith. Novel approach to nonlinear/non-Gaussian Bayesian state estimation. *IEEE-Proceedings-F*, 140:107–113, 1993.
- [99] Jianye Ching, James L. Beck, Keith A Porter, and Rustem Shaikhutdinov. Bayesian state estimation method for nonlinear systems and its application to recorded seismic response. *Journal of Engineering Mechanics*, 132(4):396–410, 2006.
- [100] Genshiro Kitagawa. Monte carlo filter and smoother for non-gaussian nonlinear state space models. *Journal of computational and graphical statistics*, 5(1):1–25, 1996.
- [101] Augustine Kong, Jun S Liu, and Wing Hung Wong. Sequential imputations and bayesian missing data problems. *Journal of the American statistical association*, 89(425):278–288, 1994.
- [102] Juan Chiachio, Manuel Chiachio, Shankar Sankararaman, Abhinav Saxena, and Kai Goebel. Prognostics design for structural health management. In *Emerging Design Solutions in Structural Health Monitoring Systems*, Advances in Civil and Industrial Engineering Series (ACIE). IGI Global, 2014.
- [103] J.Z. Sikorska, M. Hodkiewicz, and L. Ma. Prognostic modelling options for remaining useful life estimation by industry. *Reliability Engineering & System Safety*, 25:1803–1836, 2011.
- [104] C. Papadimitriou, J.L. Beck, and S.K. Au. Entropy-Based Optimal Sensor Location for Structural Model Updating. *Journal of Vibration and Control*, 6(12):89–110, 2000.
- [105] Matthew Daigle, Abhinav Saxena, and Kai Goebel. An efficient deterministic approach to model-based prediction uncertainty estimation. In *Annual Conference of the Prognostics and Health Management Society*, pages 326–335, 2012.
- [106] Shankar Sankararaman and Kai Goebel. Remaining useful life estimation in prognosis: An uncertainty propagation problem. In *2013 AIAA Infotech@ Aerospace Conference*, pages 1–8, 2013.

- [107] Bhaskar Saha and Kai Goebel. Uncertainty management for diagnostics and prognostics of batteries using bayesian techniques. In *Aerospace Conference, 2008 IEEE*, pages 1–8. IEEE, 2008.
- [108] Abhinav Saxena, Indranil Roychoudhury, Jose Celaya, Bhaskar Saha, Sankalita Saha, and Kai Goebel. Requirement flowdown for prognostics health management. In *AIAA Infotech@Aerospace, Garden Grove, CA*, pages –. AIAA, 2012.
- [109] Abhinav Saxena, Jose Celaya, Bhaskar Saha, Bankalita Saha, and Kai Goebel. Metrics for offline evaluation of prognostic performance. *International Journal of the PHM Society*, 1(1):20, 2010.
- [110] Abhinav Saxena, Jose Celaya, Edward Balaban, Kai Goebel, Bhaskar Saha, Sankalita Saha, and Mark Schwabacher. Metrics for evaluating performance of prognostic techniques. In *Prognostics and Health Management, 2008. PHM 2008. International Conference on*, pages 1–17. IEEE, 2008.
- [111] Abhinav Saxena, Shankar Shankararaman, and Kai Goebel. Performance evaluation for fleet-based and unit-based prognostic methods. In *Prognostics and Health Management Society, Nantes, France 2014. EPHM 2014. 2nd European Conference of the*, pages –. IPHM, 2014.
- [112] Juan Chiachio Ruano. *A Bayesian approach to fatigue damage assessment in composite materials*. PhD thesis, Universidad de Granada, Spain, 2014.
- [113] Juan Chiachio, Manuel Chiachio, Abhinav Saxena, Shankar Shankararaman, and Kai Goebel. Bayesian model selection and parameter estimation for fatigue damage progression models in composites. *To appear in International Journal of Fatigue*, 2014.
- [114] Juan Chiachio, Manuel Chiachio, Shankar Shankararaman, Abhinav Saxena, and Kai Goebel. A robust modeling approach for fatigue damage in composites based on Bayesian model class selection. In *Proceedings of the American Society for Composites 29th Technical Conference, 16th US-Japan Conference on Composites Materials, and ASTM D30 meeting*, page paper No. 432. Destech Publications, Inc, 2014.
- [115] K.L. Reifsnider and A. Talug. Analysis of fatigue damage in composite laminates. *International Journal of Fatigue*, 2(1):3 – 11, 1980.
- [116] P.W.R. Beaumont, RA Dimant, and HR Shercliff. Failure processes in composite materials: getting physical. *Journal of Materials Science*, 41(20):6526–6546, 2006.
- [117] W.F. Wu and C.C. Ni. A study of stochastic fatigue crack growth modeling through experimental data. *Probabilistic Engineering Mechanics*, 18:107–118, 2003.
- [118] WF Wu and CC Ni. Probabilistic models of fatigue crack propagation and their experimental verification. *Probabilistic Engineering Mechanics*, 19(3):247–257, 2004.
- [119] J.T.P. Yao, F Kozin, Y.K. Wen, J.N. Yang, G.I. Schueller, and O Ditlevsen. Stochastic fatigue, fracture and damage analysis. *Structural Safety*, 3:231–267, 1986.
- [120] W.Q. Zhu and Y. Lei. A stochastic theory of cumulative fatigue damage. *Probabilistic Engineering Mechanics*, 6(3-4):222–227, December 1991.

- [121] YK Lin and JN Yang. On statistical moments of fatigue crack propagation. *Engineering Fracture Mechanics*, 18(2):243–256, 1983.
- [122] J.D. Rowatt and P.D. Spanos. Markov chain models for life prediction of composite laminates. *Structural Safety*, 20:117–135, 1998.
- [123] R Ganesan. A data-driven stochastic approach to model and analyze test data on fatigue response. *Computers & Structures*, 76(4):517–531, 2000.
- [124] Bo-Siou Wei, Shane Johnson, and Rami Haj-Ali. A stochastic fatigue damage method for composite materials based on Markov chains and infrared thermography. *International Journal of Fatigue*, 32(2):350–360, 2010.
- [125] J.L. Bogdanoff and F. Kozin. *Probabilistic models of cumulative damage*. John Wiley & Sons, 1985.
- [126] J. Chiachio, M. Chiachio, and G. Rus. An inverse-problem based stochastic approach to model the cumulative damage evolution of composites. *Procedia Engineering*, 14(0):1557 – 1563, 2011.
- [127] Manuel Chiachío, Juan Chiachío, Guillermo Rus, and James L. Beck. Predicting fatigue damage in composites. A Markov chain model. *Structural Safety*, 51(0):57–68, 2014.
- [128] J.L. Beck. Bayesian system identification based on probability logic. *Structural Control and Health Monitoring*, 17(7):825–847, 2010.
- [129] Sachin C. Patwardhan, Shankar Narasimhan, Prakash Jagadeesan, Bhushan Gopaluni, and Sirish L. Shah. Nonlinear bayesian state estimation: A review of recent developments. *Control Engineering Practice*, 20(10):933 – 953, 2012.
- [130] Eija Myotyrri, Urho Pulkkinen, and Kaisa Simola. Application of stochastic filtering for lifetime prediction. *Reliability Engineering and System Safety*, 91(2):200–208, 2006.
- [131] T.K. O’Brien, M. Rigamonti, and C. Zanotti. Tension fatigue analysis and life prediction for composite laminates. *International journal of fatigue*, 11(6):379–393, 1989.
- [132] W. Hwang and KS Han. Fatigue of composites-fatigue modulus concept and life prediction. *Journal of Composite Materials*, 20(2):154–165, 1986.
- [133] S Subramanian. A cumulative damage model to predict the fatigue life of composite laminates including the effect of a fibre-matrix interphase. *International Journal of Fatigue*, 17(5):343–351, 1995.
- [134] J. Chiach’io, M. Chiach’io, A. Saxena, G. Rus, and K. Goebel. An energy-based prognostics framework to predict fatigue damage evolution in composites. In *Proceedings of the Annual Conference of the Prognostics and Health Management Society, 2013*, volume 1, pages 363–371. Prognostics and Health Management Society, 2013.
- [135] Juan Chiachio, Manuel Chiachio, Abhinav Saxena, and Kai Goebel. A model-based prognostics framework to predict fatigue damage evolution and reliability in composites. In *Prognostics and Health Management Society, Nantes, France2014. EPHM 2014. 2nd European Conference of the*, pages 732–742. ISPHM, 2014.

- [136] Xiao-Sheng Si, Wenbin Wang, Chang-Hua Hu, and Dong-Hua Zhou. Remaining useful life estimation—a review on the statistical data driven approaches. *European Journal of Operational Research*, 213(1):1–14, 2011.
- [137] Mathew Daigle and Kai Goebel. A model-based prognostics approach applied to pneumatic valves. *International Journal of the PHM Society*, 2(8):16, 2010.
- [138] J.A. Nairn and S. Hu. The initiation and growth of delaminations induced by matrix microcracks in laminated composites. *International Journal of Fracture*, 57(1):1–24, 1992.
- [139] Olivier Cappé, Simon J Godsill, and Eric Moulines. An overview of existing methods and recent advances in sequential Monte Carlo. *Proceedings of the IEEE*, 95(5):899–924, 2007.
- [140] AL Highsmith and KL Reifsnider. Stiffness-reduction mechanisms in composite laminates. *Damage in composite materials, ASTM STP*, 775:103–117, 1982.
- [141] P Lundmark and J Varna. Constitutive relationships for laminates with ply cracks in in-plane loading. *International Journal of Damage Mechanics*, 14(3):235–259, 2005.
- [142] John A Nairn. The strain energy release rate of composite microcracking: a variational approach. *Journal of Composite Materials*, 23(11):1106–1129, 1989.
- [143] John A Nairn. In R Talreja and Manson J.A.E., editors, *Polymer Matrix Composites*, chapter Matrix Microcracking in Composites, pages 403–432. Elsevier Science, Amsterdam, 2000.
- [144] PF Paris, MP Gomez, and W. Anderson. A rational analytic theory of fatigue. *The Trend in Engineering*, 13:9–14, 1961.
- [145] Ramesh Talreja and Chandra Veer Singh. *Damage and Failure of Composite Materials*. Cambridge University Press, 2012.
- [146] KW Garrett and JE Bailey. Multiple transverse fracture in 90° cross-ply laminates of a glass fibre-reinforced polyester. *Journal of Materials Science*, 12(1):157–168, 1977.
- [147] Z Hashin. Analysis of cracked laminates: a variational approach. *Mechanics of Materials*, 4(2):121–136, 1985.
- [148] Peter Gudmundson and Zang Weilin. An analytic model for thermoelastic properties of composite laminates containing transverse matrix cracks. *International Journal of Solids and Structures*, 30(23):3211–3231, 1993.
- [149] Peter W Manders, Tsu-Wei Chou, Frank R Jones, and John W Rock. Statistical analysis of multiple fracture in 0/90/0 glass fibre/epoxy resin laminates. *Journal of Materials Science*, 18(10):2876–2889, 1983.
- [150] R Joffe and J Varna. Analytical modeling of stiffness reduction in symmetric and balanced laminates due to cracks in 90 layers. *Composites Science and Technology*, 59(11):1641–1652, 1999.
- [151] H.T. Hahn and R.Y. Kim. Fatigue behavior of composite laminate. *Journal of Composite Materials*, 10(2):156–180, 1976.

- [152] T.K. O'Brien, M. Rigamonti, and C. Zanotti. Tension fatigue analysis and life prediction for composite laminates. *International journal of fatigue*, 11(6):379–393, 1989.
- [153] N Post, J Bausano, S Case, and J Lesko. Modeling the remaining strength of structural composite materials subjected to fatigue. *International Journal of Fatigue*, 28(10):1100–1108, 2006.
- [154] J.W. Lee, DH Allen, and CE Harris. Internal state variable approach for predicting stiffness reductions in fibrous laminated composites with matrix cracks. *Journal of Composite Materials*, 23(12):1273–1291, 1989.
- [155] Nobuo Takeda and Shinji Ogihara. Initiation and growth of delamination from the tips of transverse cracks in cfrp cross-ply laminates. *Composites science and technology*, 52(3):309–318, 1994.
- [156] Henrik Schmutzler, Marko Alder, Nils Kosmann, Hans Wittich, and Karl Schulte. Degradation monitoring of impact damaged CFRP under fatigue loading with pulse phase thermography. *Composites Part A*, pages –, 2014.
- [157] Atsushi Hosoi, Narumichi Sato, Yasuyuki Kusumoto, Keita Fujiwara, and Hiroyuki Kawada. High-cycle fatigue characteristics of quasi-isotropic cfrp laminates over 10^8 cycles (initiation and propagation of delamination considering interaction with transverse cracks). *International Journal of Fatigue*, 32(1):29–36, 2010.
- [158] A. Hosoi, K. Takamura, N. Sato, and H. Kawada. Quantitative evaluation of fatigue damage growth in cfrp laminates that changes due to applied stress level. *International Journal of Fatigue*, 33(6):781–787, 2011.
- [159] JA Nairn. Fracture mechanics of composites with residual thermal stresses. *Journal of Applied Mechanics*, 64:804–815, 1997.
- [160] J.A. Nairn. Fracture mechanics of composites with residual thermal stresses. *J. Appl. Mech*, 64:804–810, 1997.
- [161] E.T. Jaynes. *Papers on probability, statistics and statistical physics*. (Ed. R.D Rosenkrantz), Kluwer Academic Publishers, 1983.
- [162] E.T. Jaynes. *Probability theory: the logic of science*. Ed. Bretthorst, Cambridge University Press, 2003.
- [163] A Papoulis. *Probability, Random Variables, and Stochastic Processes*. McGraw Hill, 1965.
- [164] Andrea Saltelli, Marco Ratto, Terry Andres, Francesca Campolongo, Jessica Cariboni, Debora Gatelli, Michaela Saisana, and Stefano Tarantola. *Global Sensitivity Analysis: The Primer*. Wiley-Interscience, 2008.
- [165] M.F. Ngah and A. Young. Application of the spectral stochastic finite element method for performance prediction of composite structures. *Composite Structures*, 78(3):447–456, 2007.
- [166] M. Di Sciuva and D. Lomario. A comparison between monte carlo and forms in calculating the reliability of a composite structure. *Composite Structures*, 59(1):155–162, 2003.

- [167] L. Yang. Reliability of composite laminates. *Mechanics of Structures and Machines*, 16(4):523–536, 1988.
- [168] I. Cederbaum et al. Reliability of laminated plates via the first-order second-moment method. *Composite Structures*, 15(2):161–167, 1990.
- [169] R.C. Wetherhold and A.M. Ucci. Probability methods for the fracture of composite materials. *Composite Structures*, 28(1):113–119, 1994.
- [170] A. Orifici, I. Herszberg, and R. Thomson. *Composite Structures*, 86(1-3):194–210, 2008.
- [171] F. Richard and D. Perreux. The safety-factor calibration of laminates for long-term applications: behavior model and reliability method. *Composites Science and Technology*, 61(14):2087–2094, 2001.
- [172] J. Rousseau and D. Perreux. *An experimental and theoretical study of the processing method influence on the performances of a composite structure: case of filament winding*. PhD thesis, Universit de Besanon, Besanon, FRANCE (Universit de soutenance), 1997.
- [173] N.Z. Chen, H.H. Sun, and C. Guedes Soares. Reliability analysis of a ship hull in composite material. *Composite structures*, 62(1):59–66, 2003.
- [174] Srinivas Sriramula and Marios K. Chryssanthopoulos. Quantification of uncertainty modelling in stochastic analysis of frp composites. *Composites Part A: Applied Science and Manufacturing*, 40(11):1673–1684, 2009.
- [175] F. Laurin, N. Carrere, and J.-F. Maire. A multiscale progressive failure approach for composite laminates based on thermodynamical viscoelastic and damage models. *Composites Part A: Applied Science and Manufacturing*, 38(1):198–209, 2007.
- [176] Andrew Shaw, Srinivas Sriramula, Peter D. Gosling, and Marios K. Chryssanthopoulos. A critical reliability evaluation of fibre reinforced composite materials based on probabilistic micro and macro-mechanical analysis. *Composites Part B: Engineering*, 41(6):446–453, 2010.
- [177] L. Yang and Z.K. Ma. Optimum design based on reliability for a composite structural system. *Computers & Structures*, 36(5):785–790, 1990.
- [178] T.Y. Kam, S.C. Lin, and K.M. Hsiao. Reliability analysis of nonlinear laminated composite plate structures. *Composite Structures*, 25(1-4):503–510, 1993.
- [179] A. Hosni Elhewy, E. Mesbahi, and Y. Pu. Reliability analysis of structures using neural network method. *Probabilistic Engineering Mechanics*, 21(1):44–53, 2006.
- [180] M. Hinton, A.S. Kaddour, and Soden P.D. A comparison of the predictive capabilities of current failure theories for composite laminates, judged against experimental evidence. *Composites Science and Technology*, 62(12-13):1725–1797, 2002.
- [181] M. Hinton, A.S. Kaddour, and Soden P.D. Evaluation of failure prediction in composite laminates: background to part b of the exercise. *Composites Science and Technology*, 62(12-13):1481–1488, 2002.

- [182] M. Hinton, A.S. Kaddour, and Soden P.D. Evaluation of failure prediction in composite laminates: background to part c of the exercise. *Composites Science and Technology*, 64(3-4):321–327, 2004.
- [183] H. Nakayasu and Z. Maekawa. A comparative study of failure criteria in probabilistic fields and stochastic failure envelopes of composite materials. *Reliability Engineering & System Safety*, 56(3):209–220, 1997.
- [184] T.P. Philippidis and D.J. Lekou. Probabilistic failure prediction for FRP composites. *Composites science and technology*, 58(12):1973–1982, 1998.
- [185] R.C. Wetherhold. Reliability calculations for strength of a fibrous composite under multiaxial loading. *Journal of Composite Materials*, 15(3):240, 1981.
- [186] Cramer H. *Mathematical Methods of Statistics*. Princeton University Press, USA, 1971.
- [187] G.J. Hahn and S.S. Shapiro. *Statistical Models in Engineering*. John Wiley & Sons. New York, NY, USA, 1994.
- [188] T.P. Philippidis and D.J. Lekou. A probabilistic approach to failure prediction of FRP laminated composites. *Mechanics of Advanced Materials and Structures*, 5(4):371–382, 1998.
- [189] M.R. Gurvich and R.B. Pipes. Reliability of composites in a random stress state. *Composites Science and Technology*, 58(6):871–881, 1998.
- [190] G. Stefanou. The stochastic finite element method: past, present and future. *Computer Methods in Applied Mechanics and Engineering*, 198(9-12):1031–1051, 2009.
- [191] T. Crestaux et al. Polynomial chaos expansion for sensitivity analysis. *Reliability Engineering & System Safety*, 94(7):1161–1172, 2009.
- [192] V. Papadopoulos and M. Papadrakakis. Stochastic finite element-based reliability analysis of space frames. *Probabilistic Engineering Mechanics*, 13(1):53–65, 1998.
- [193] M.Kleiber. *The Stochastic Finite Element Method*. 1992.
- [194] R.G Ghanem and P.D. Spanos. *Stochastic Finite Elements: A Spectral Approach*. 1991.
- [195] P.D. Spanos and A. Kotsos. A multiscale monte carlo finite element method for determining properties of polymer nanocomposites. *Probabilistic Engineering Mechanics*, (23):456–470, 2008.
- [196] Jin Guoliang, Chen Lilt, and Dong Jiamei. Monte carlo finite element method of structure reliability analysis. *Reliability Engineering & System Safety*, 40(1):77–83, 1993.
- [197] G Van Vinckenroy. The use of monte carlo techniques in statistical finite element methods for the determination of the structural behavior of composite materials structural components. *Composite Structures*, 32(1-4):247–253, 1995.
- [198] Hyuk-Chun Noh. Stochastic finite element analysis of composites plates considering spatial randomness of material properties and their correlations. *Steel and Composite Structures*, 11(2):115–130, 2011.
- [199] Hyuk-Chun Noh. A formulation for stochastic finite element analysis of plate structures with uncertain Poisson’s ratio. *Computer methods in applied mechanics and engineering*, 193:4857–4873, 2011.

- [200] Hyuk-Chun Noh and Taehyo Park. Response variability of laminate composite plates due to spatially random material parameter. *Computer methods in applied mechanics and engineering*, 200:2397–2406, 2011.
- [201] RH Lopez, LFF Miguel, IM Belo, and JE Souza Cursi. Advantages of employing a full characterization method over form in the reliability analysis of laminated composite plates. *Composite Structures*, 107:635–642, 2014.
- [202] H.M. Gomes and A.M. Awruch. Comparison of response surface and neural network with other methods for structural reliability analysis. *Structural safety*, 26(1):49–67, 2004.
- [203] S.K. Au, J. Ching, and J.L. Beck. Application of Subset Simulation methods to reliability benchmark problems. *Structural Safety*, 29(3):183–193, 2007.
- [204] J.E. Hurtado. Filtered importance sampling with support vector margin: A powerful method for structural reliability analysis. *Structural Safety*, 29(1):2 – 15, 2007.
- [205] J.S. Taylor and N. Cristianni. *An introduction to support vector machines and other kernel-based learning methods*. 2000.
- [206] A Der Kiureghian. Structural reliability software at the university of california , berkeley. *Structural Safety*, 28:44–67, 2006.
- [207] D.E. Goldberg. *Genetic algorithms in search, optimization, and machine learning*. Addison-Wesley Professional, 1989.
- [208] E. Elbeltagi, T. Hegazy, and D. Grierson. Comparison among five evolutionary-based optimization algorithms. *Advanced Engineering Informatics*, 19(1):43–53, 2005.
- [209] M. Gen and Y.S. Yun. Soft computing approach for reliability optimization: State-of-the-art survey. *Reliability Engineering & System Safety*, 91(9):1008–1026, 2006.
- [210] C.A Conceicao. A hierarchical genetic algorithm for reliability based design of geometrically non-linear composite structures. *Composite Structures*, 54(1):37–47, 2001.
- [211] F.S. Almeida and A.M. Awruch. Design optimization of composite laminated structures using genetic algorithms and finite element analysis. *Composite Structures*, 88(3):443–454, 2009.
- [212] Hossein Ghiasi, Damiano Pasini, and Larry Lessard. Optimum stacking sequence design of composite materials Part I: Constant stiffness design. *Composite Structures*, 90(1):1–11, 2009.
- [213] Hossein Ghiasi, Kazem Fayazbakhsh, Damiano Pasini, and Larry Lessard. Optimum stacking sequence design of composite materials Part II: Variable stiffness design. *Composite Structures*, 93(1):1–13, 2010.
- [214] R. Ge, J. Chen, and J. Wei. Reliability-based design of composites under the mixed uncertainties and the optimization algorithm. *Acta Mechanica Solida Sinica*, 21(1):19–27, 2008.
- [215] Jianqiao Chen, Yuanfu Tang, and Xiaoxu Huang. Application of surrogate based particle swarm optimization to the reliability-based robust design of composite pressure vessels. *Acta Mechanica Solida Sinica*, 26(5):480–490, 2013.

- [216] R.H. Meyers, A.I. Khuri, and W.H. Carter Jr. Response surface methodology: 1966-1988. *Technometrics*, 31(2):137–157, 1989.
- [217] G.E.P. Box and D.W. Behnken. Some new three level designs for the study of quantitative variables. *Technometrics*, 2(4):455–475, 1960.
- [218] L. Faravelli. Response-surface approach for reliability analysis. *Journal of Engineering Mechanics*, 115:27–63, 1989.
- [219] M. Kaufman, V. Balabanov, A.A. Giunta, B. Grossman, W.H. Mason, S.L. Burgee, R.T. Haftka, and L.T. Watson. Variable-complexity response surface approximations for wing structural weight in HSCT design. *Computational Mechanics*, 18(2):112–126, 1996.
- [220] K. Hinkelmann. *Design and analysis of experiments*. John Wiley & Sons. New York, NY, USA, 1994.
- [221] U. Bucher et al. A fast and efficient response surface approach for structural reliability problems. *Structural Safety*, 7(1):57–66, 1990.
- [222] Y.L. Young, J.W. Baker, and M.R. Motley. Reliability-based design and optimization of adaptive marine structures. *Composite Structures*, 92(2):244–253, 2010.
- [223] Venkata MK Akula. Multiscale reliability analysis of a composite stiffened panel. *Composite Structures*, 116:432–440, 2014.
- [224] Shao S. and Morutso Y. Structural reliability analysis using a neural network. *JSME International Journal, Series A*, 40(3):242–246, 1997.
- [225] S. Haykin. *Neural networks: a comprehensive foundation*. 1999. Printice Hall, New Jersey, USA, 1999.
- [226] A Vassilopoulos, E Georgopoulos, and V Dionysopoulos. Artificial neural networks in spectrum fatigue life prediction of composite materials. *International Journal of Fatigue*, 29(1):20–29, 2007.
- [227] M. Lefik, D.P. Boso, and B.A. Schrefler. Artificial Neural Networks in numerical modelling of composites. *Computer Methods in Applied Mechanics and Engineering*, 198(21-26):1785–1804, 2009.
- [228] H. El Kadi. Modeling the mechanical behavior of fiber-reinforced polymeric composite materials using artificial neural networks—A review. *Composite structures*, 73(1):1–23, 2006.
- [229] Z. Zhang and K. Friedrich. Artificial neural networks applied to polymer composites: a review. *Composites Science and technology*, 63(14):2029–2044, 2003.
- [230] T.L. Zhu. A reliability-based safety factor for aircraft composite structures. *Computers & Structures*, 48(4):745–748, 1993.
- [231] Y. Murotsu, M. Miki, and S. Shao. Reliability design of fiber reinforced composites. *Structural safety*, 15(1-2):35–49, 1994.
- [232] M. Miki, Y. Murotsu, T. Tanaka, and S. Shao. Reliability-based optimization of fibrous laminated composites. *Reliability Engineering & System Safety*, 56(3):285–290, 1997.

- [233] S. Carbillet, F. Richard, and L. Boubakar. Reliability indicator for layered composites with strongly non-linear behavior. *Composites Science and Technology*, 69(1):81–87, 2009.
- [234] Herbert Martins Gomes, Armando Miguel Awruch, and Paulo André Menezes Lopes. Reliability based optimization of laminated composite structures using genetic algorithms and Artificial Neural Networks. *Structural Safety*, 33:186–195, 2011.
- [235] PD Gosling, O Polit, et al. A high-fidelity first-order reliability analysis for shear deformable laminated composite plates. *Composite Structures*, 115:12–28, 2014.
- [236] Jianzhong Sun, Hongfu Zuo, Wenbin Wang, and Michael G Pecht. Prognostics uncertainty reduction by fusing on-line monitoring data based on a state-space-based degradation model. *Mechanical Systems and Signal Processing*, 45(2):396–407, 2014.
- [237] E Zio. Reliability engineering: Old problems and new challenges.
- [238] M. Chiach'ío, J. Chiach'ío, A. Saxena, G. Rus, and K. Goebel. A highly efficient simulation framework for prognostics of asymptotic processes- a case study in composite materials. In *Proceedings of the Annual Conference of the Prognostics and Health Management Society, 2014*, volume 1, pages –. Prognostics and Health Management Society, 2014.
- [239] A. Saxena, K Goebel, C Larrosa, V Janapati, S Roy, and FK Chang. Accelerated aging experiments for prognostics of damage growth in composites materials. In *The 8th International Workshop on Structural Health Monitoring, F.-K. Chang, Editor.*, volume 15, 2011.
- [240] ASTM International. *ASTM, Standard Test Method for Tension-Tension Fatigue of Polymer Matrix Composite Materials, in D3479/D3479M 96*, 2007.
- [241] ASTM International. *ASTM, Standard Test Method for Tensile Properties of Polymer Matrix Composite Materials, in D3039/D3039M 08*, 2008.
- [242] Nobuo Takeda, Yoji Okabe, Junichiro Kuwahara, Seiji Kijima, and Toshimichi Ogisu. Development of smart composite structures with small-diameter fiber Bragg grating sensors for damage detection: Quantitative evaluation of delamination length in CFRP laminates using Lamb wave sensing. *Composite Science and Technology*, 65:2575–2587, 2005.
- [243] Cecilia Larrosa and Fu-Kuo Chang. Real time in-situ damage classification, quantification and diagnosis for composite structures. In *Proceedings of the 19th International Congress on Sound and Vibration*, volume 15, 2012.
- [244] Tishun Peng, Abhinav Saxena, Kai Goebel, Yibing Xiang, Shankar Sankararaman, and Yongming Liu. A novel bayesian imaging method for probabilistic delamination detection of composite materials. *Smart Materials and Structures*, 22(12):125019, 2013.
- [245] Cecilia C. Larrosa. *Monitoring matrix cracking in composite laminates using built-in piezoelectric sensors*. PhD thesis, Stanford University, USA, 2013.
- [246] P. Gudmundson and S. Östlund. Prediction of thermoelastic properties of composite laminates with matrix cracks. *Composite Science and Technology*, 44:95–105, 1992.